

# The Many Deaths of Supercapacitors: Degradation, Aging, and Performance Fading

Emmanuel Pameté, Lukas Köps, Fabian Alexander Kreth, Sebastian Pohlmann, Alberto Varzi, Thierry Brousse, Andrea Balducci, and Volker Presser\*

High-performance electrochemical applications have expedited the research in high-power devices. As such, supercapacitors, including electrical double-layer capacitors (EDLCs) and pseudocapacitors, have gained significant attention due to their high power density, long cycle life, and fast charging capabilities. Yet, no device lasts forever. It is essential to understand the mechanisms behind performance degradation and aging so that these bottlenecks can be addressed and tailored solutions can be developed. Herein, the factors contributing to the aging and degradation of supercapacitors, including electrode materials, electrolytes, and other aspects of the system, such as pore blocking, electrode compositions, functional groups, and corrosion of current collectors are examined. The monitoring and characterizing of the performance degradation of supercapacitors, including electrochemical methods, in situ, and ex situ techniques are explored. In addition, the degradation mechanisms of different types of electrolytes and electrode materials and the effects of aging from an industrial application standpoint are analyzed. Next, how electrode degradations and electrolyte decompositions can lead to failure, and pore blocking, electrode composition, and other factors that affect the device's lifespan are examined. Finally, the future directions and challenges for reducing supercapacitors' performance degradation, including developing new materials and methods for characterizing and monitoring the devices are summarized.

## 1. Introduction

Electrification is an enabling technology for mobile computing, communication, and transportation and is essential for the large-scale implementation of renewable energy.<sup>[1]</sup> The ever-growing increase in energy demand has led to increased scientific research in electrochemical energy storage.<sup>[2]</sup> The primary focus was on the development of fresh technologies or innovative electrode materials for batteries and supercapacitors.<sup>[1,3]</sup> The latter represents an emerging class of energy storage systems that complement batteries in terms of power and conventional capacitors in terms of energy.<sup>[4]</sup> Supercapacitors find their use in various high-power applications like vehicles, memory backup, tramways, etc. Furthermore, their lifespan can be increased when combined in a hybrid system with high energy density components like fuel cells and batteries.<sup>[3,5]</sup>

The class of supercapacitors (or: ultracapacitors) can be sectioned into electrical double-layer capacitors (EDLCs) and

E. Pameté, V. Presser  
INM – Leibniz Institute for New Materials  
Campus D2 2, 66123 Saarbrücken, Germany  
E-mail: volker.presser@leibniz-inm.de

L. Köps, F. A. Kreth, A. Balducci  
Institute of Technical Chemistry and Environmental Chemistry and Center  
for Energy and Environmental Chemistry Jena (CEEC Jena)  
Friedrich-Schiller-University Jena  
Philosophenweg 7a, 07743 Jena, Germany

S. Pohlmann  
Skeleton Technologies GmbH  
Schücostraße 8, 01900 Großröhrsdorf, Germany


A. Varzi  
Helmholtz Institute Ulm (HIU)  
Helmholtzstrasse 11, 89081 Ulm, Germany

A. Varzi  
Karlsruhe Institute of Technology (KIT)  
P.O. Box 3640, 76021 Karlsruhe, Germany

T. Brousse  
Nantes Université  
CNRS  
Institut des Matériaux de Nantes Jean Rouxel  
IMN  
Nantes 44000, France

T. Brousse  
Réseau Sur Le Stockage Electrochimique de L'Energie (RS2E)  
CNRS FR 3459  
33 rue Saint Leu, Amiens Cedex 80039, France

V. Presser  
Saarland University  
Campus D2 2, 66123 Saarbrücken, Germany  
V. Presser  
Saarene – Saarland Center for Energy Materials and Sustainability  
Campus C4 2, 66123 Saarbrücken, Germany

 The ORCID identification number(s) for the author(s) of this article can be found under <https://doi.org/10.1002/aenm.202301008>

© 2023 The Authors. Advanced Energy Materials published by Wiley-VCH GmbH. This is an open access article under the terms of the Creative Commons Attribution License, which permits use, distribution and reproduction in any medium, provided the original work is properly cited.

DOI: 10.1002/aenm.202301008

pseudocapacitors.<sup>[6]</sup> EDLCs function by quickly and reversibly electrostatic accumulation of ions, forming an electrical double-layer at the interphase between the electrode and electrolyte.<sup>[7]</sup> Pseudocapacitors take advantage of redox reactions occurring on the surface of the electrode material to achieve electrochemical features similar to EDLCs.<sup>[8]</sup> However, since chemical reactions are not involved in the charging mechanism in EDLCs, the energy stored in these devices is lower than in lithium-ion batteries (LIBs).<sup>[9]</sup> Supercapacitors have several benefits, such as fast charge and discharge times, high specific power, and extended cycle life. Additionally, electrode materials with high electrical conductivity and a well-developed specific surface area can significantly improve their power density and charge storage capacity.<sup>[3]</sup>

Depending on the type of electrolyte and electrode materials, EDLCs have a lifetime of more than 1 000 000 cycles, while the cycle life of pseudocapacitors is generally less than 10 000 cycles.<sup>[10]</sup> These numbers, by themselves, are insufficient to judge the technology. The target cycle number largely depends on the target application and operation parameters, including the rate and temperature.<sup>[11]</sup> As the main symptoms during cell aging are the loss of their capacitance and the increase in their resistance, many authors diagnose the state of health of supercapacitors by monitoring only these two parameters at different periods during the operation of the system.<sup>[12]</sup> However, understanding supercapacitor failure modes and underlying mechanisms remains an ill-explored territory.

In this review, we assess supercapacitors' performance decay and failure mechanisms while paying particular attention to the general process of their degradation from the industrial point of view. First, appropriate methods and strategies for monitoring the performance degradation of EDLCs and pseudocapacitors are revised. Next, the reasons for the performance fading of supercapacitors are thoroughly examined for different types of electrolytes (aqueous, organic, ionic liquids, and solid-state) and electrodes (carbons, metal oxides, and 2D materials) materials. Beyond electrode degradations and electrolyte decompositions, we looked at many other factors affecting the lifespan of supercapacitors, such as pore blocking, electrode compositions (e.g., functional groups, binder), volume expansion of electrode materials during cell operation, materials dissolution, electrolyte interphase, and passivation/corrosion of the current collectors. Furthermore, the effects of aging from an industrial application standpoint are discussed. Finally, future directions and challenges for reducing supercapacitors' performance degradation are summarized.

## 2. Supercapacitors

### 2.1. General Processes of Supercapacitors

Supercapacitors generally consist of two physically separated electrodes immersed in an electrolyte. However, based on their material composition and the arising charge storage mechanism(s), they can be divided into EDLCs, pseudocapacitors, and hybrid capacitors.<sup>[7,13]</sup> With the charge storage mechanism of EDLCs relying on charge separation on the electrode surface, activated carbons with high surface area (up to 2000 m<sup>2</sup> g<sup>-1</sup>) are commonly used to achieve a high capacitance of the device.<sup>[14]</sup> Upon applying current to the system, charge carriers of the

ion-containing electrolyte migrate toward the oppositely charged electrode and form an electrical double layer.<sup>[15]</sup> While the formation of this electrical double layer is exploited to store energy electrostatically in the EDLC, redox reactions in this system are undesirable.<sup>[16]</sup>

In contrast, pseudocapacitors take advantage of redox reactions occurring on the surface of the electrode material to achieve electrochemical signatures similar to EDLCs.<sup>[8,17]</sup> Using different materials, for example, metal oxides like MnO<sub>2</sub> or RuO<sub>2</sub> redox processes lead to higher charge storage and enable higher energy density while keeping (ideally) EDLC-like power density.<sup>[18]</sup> With the same goal of combining battery-like energy density with EDLC-like power density, hybrid capacitors were designed with one electrode consisting of battery material and the other of activated carbon. Lithium-ion capacitors are their most prominent example among hybrid capacitors, usually applying graphite as the negative electrode material and activated carbon as material for the positive electrode.<sup>[19]</sup> While graphite-based lithium-ion capacitors enable higher energy densities, they struggle with lacking a Li-containing cathode requiring them to introduce lithium through sacrificial electrodes or salts, adding additional process or material costs.<sup>[20]</sup> Yet, the technology is not limited to lithium, with promising results also for sodium ion and potassium ions energy storage.<sup>[21]</sup> However, combining two different charge storage mechanisms in a single device requires careful tuning of the materials and voltage windows to ensure the high performance of the hybrid capacitor.

Naturally, different material compositions and charge storage mechanisms promote a variety of various aging mechanisms due to the different stability limits of the utilized compounds.<sup>[11]</sup> Additionally, supercapacitors storing charges by redox reactions tend to be less stable since redox processes are always less reversible than the pure movement of ions and the formation of an electrical double layer. This makes it challenging to describe universal aging processes occurring in EDLCs, pseudocapacitors, and hybrid capacitors. However, operating conditions such as temperature, voltage, or current all have comparable effects on the speed of aging of the various supercapacitors.<sup>[22]</sup> Higher temperatures improve molecular transport and faster reaction kinetics, increasing the available energy storage metrics.<sup>[23]</sup> This energy may be essential to overcome activation energy barriers and can therefore initiate a decomposition reaction that would not occur at lower temperatures. In addition, the cell voltage and electrode potentials have a comparable impact on electrochemical reactions.<sup>[24]</sup> Exemplary, when charging an EDLC, the cell voltage increases, which leads to the occupation of higher energy levels of the molecules by charges.<sup>[25]</sup> Subsequently, electrochemical decomposition of the respective compound is initiated as soon as enough energy for the decomposition process is provided.

Temperature and voltage deliver energy to reach the necessary activation energy and thus initiate similar electrochemical decomposition reactions.<sup>[26]</sup> Conversely, this means that the aging of a supercapacitor, which would occur at a specific temperature and cell voltage, cannot occur if one of these parameters is decreased. Furthermore, in addition to inducing electrochemical reactions, increasing the cell voltage results in a proportionally stronger electric field.<sup>[27]</sup> This leads to a higher attraction of the oppositely charged ions to the respective electrodes and thus accelerated aging processes. Last, the current rate strongly

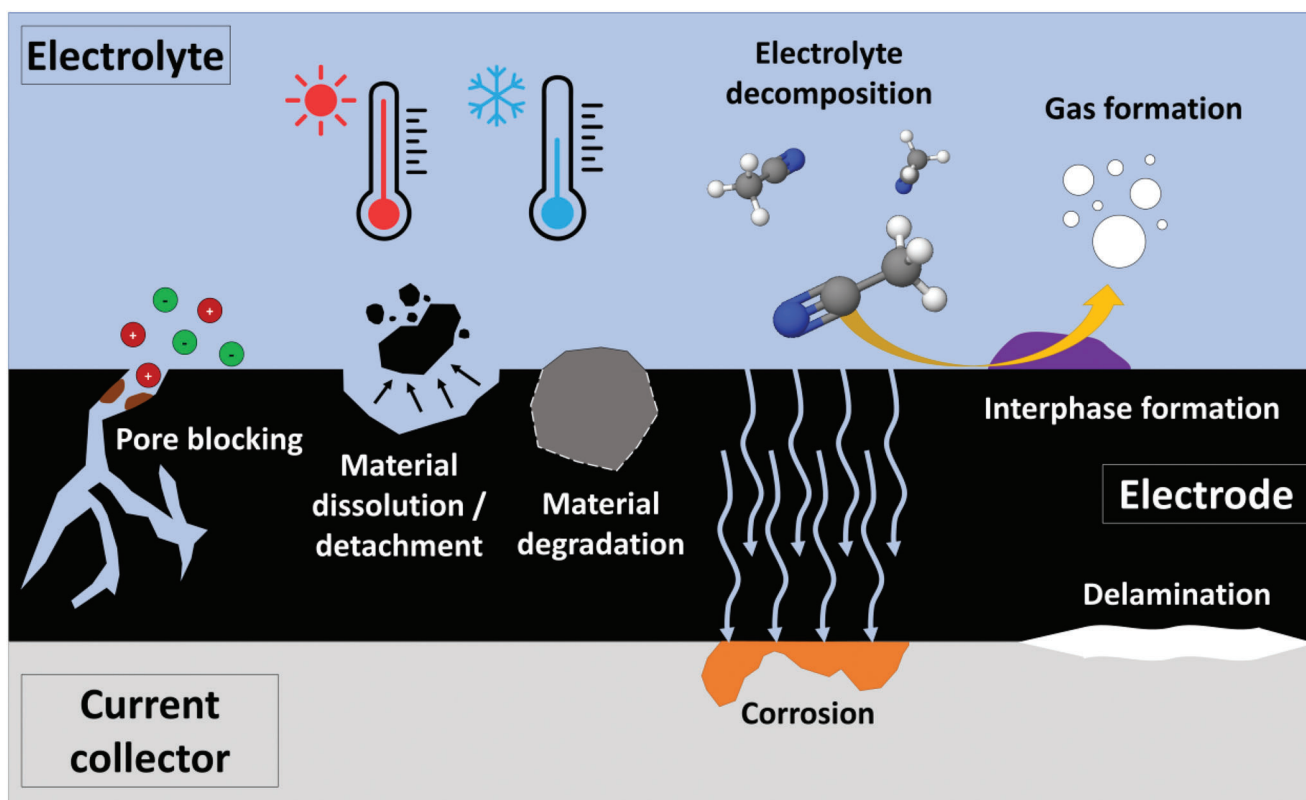


**Figure 1.** Overview over common degradation pathways and failure mechanisms in supercapacitors. Electrolyte decomposition can occur due to factors such as high temperatures, high voltages, and prolonged cycling, resulting in the formation of gases, solids, or other degradation products that can clog the pores of the electrode or lead to the formation of a passivating layer on the electrode surface. The active materials used in supercapacitors can undergo structural and chemical changes during charge/discharge cycles, leading to a decrease in their capacitance and/or stability. The performance and stability of supercapacitors can also be affected by the operating conditions such as temperature, humidity, and voltage. Elevated temperatures can cause chemical reactions in the supercapacitor, leading to electrolyte decomposition and a decrease in capacitance. Conversely, low temperatures can cause the electrolyte to freeze, resulting in mechanical stress and possible damage to the supercapacitor. The interphase between the electrode and electrolyte can also degrade over time due to factors such as electrochemical reactions, charge/discharge cycling, and mechanical stress. When exposed to the electrolyte the metal current collectors can undergo corrosion upon cell operation, which is a significant failure mechanism in supercapacitors.

influences all processes in the supercapacitors, including the charge storage mechanisms and aging processes, kinetically.<sup>[28]</sup> Thus, a high current rate might reduce decomposition reaction rates but can stress and degrade the active material at the same time. Especially redox-based systems, which feature naturally slower charging mechanisms than EDLCs, are somewhat limited in performance by higher current rates and show accelerated aging since thermodynamically not preferred reaction products might be formed. Therefore, these reaction pathways might be less reversible than intended and strongly contribute to cell aging.

In addition to these environmental conditions, the chemical purity of the utilized materials plays a crucial role in the aging of supercapacitors. Since impurities might introduce less stable compounds to the system, their decomposition could occur under less harsh conditions than the actual cell materials (Figure 1). While these parasitic redox reactions consume charges, formed decomposition products can undergo further reactions with cell components, leading to additional cell degradation. Exemplary, in the case of EDLCs, the carbon's surface functions strongly influence the device's stability and lifetime since functional groups are more prone to reduction

or oxidation than pure carbon, especially at elevated electrode potentials.<sup>[29]</sup>

All this indicates the complexity of aging processes in supercapacitors. The immense number of different material combinations enables many possible decomposition mechanisms, and the operating conditions can influence that. Thus, it is incredibly challenging to describe aging by universal aging processes. However, aging processes occurring in specific supercapacitors can be investigated in detail to understand their impact on the device and design a tailor-made solution to overcome this aging process. Experimental methods and known failure mechanisms (Table 1) from the literature will be summarized in the following.

## 2.2. How to Monitor the Degradation of Supercapacitors?

The degradation of supercapacitor performance (Figure 2A) can be described by an electrical model consisting of two branches of parameterized capacitor-resistor (RC) networks.<sup>[30]</sup> Classically, the main assessment methods consist of measuring the changes in electric parameters, mainly the equivalent series resistance (ESR) responsible for the electrical losses and the capacitance

**Table 1.** Summary of commonly used aqueous, non-aqueous, ionic liquid, and solid-state electrolytes with their failure mechanisms.

Electrolyte	Failure mechanisms
Aqueous	
NaCl; KCl; Na <sub>2</sub> SO <sub>4</sub> ; Li <sub>2</sub> SO <sub>4</sub> ; NaHCO <sub>3</sub> ; NaNO <sub>3</sub>	Corrosion of electrode materials, gas evolution, water decomposition. Low conductivity due to dissociating only a tiny fraction of the salt molecules into ions.
NaOH; KOH; LiOH	Corrosion of metal electrodes due to the formation of metal hydroxides and metal oxide layers, low voltage window due to water electrolysis, water decomposition., gas evolution,
H <sub>2</sub> SO <sub>4</sub>	Corrosion of electrode materials and dendrite formation, gas evolution, low voltage window, water decomposition.
ZnCl <sub>2</sub> ; NH <sub>4</sub> Cl	Corrosion of current collectors; Corrosion of metal electrodes due to the formation of metal chlorides and low voltage window due to water electrolysis, low conductivity.
Organic	
Acetonitrile-based organic electrolytes	Formation of a passivation layer on the electrode surface due to the oxidation of acetonitrile at high voltages, which reduces the effective surface area of the electrodes and leads to capacity fading. Electrolyte decomposition: hydrolysis, (cyclo-)polymerization, Hofmann elimination, and fluorination reactions.
Propylene carbonate and Ethylene carbonate-based organic electrolytes	Reductive decomposition of PC or EC at high voltages, resulting in the formation of SEI on the electrode surface, which increases the cell resistance and reduces the effective surface area of the electrodes; gas evolution.
Non-conventional organic electrolytes	Electrolyte breakdown, formation of SEI, dendrite formation, gas evolution
Ionic liquids	
1-ethyl-3-methylimidazolium tetrafluoroborate; 1-butyl-3-methylimidazolium hexafluorophosphate; N-butyl-N-methylpyrrolidinium bis(trifluoromethylsulfonyl)imide; N-methyl-N-propylpiperidinium bis(trifluoromethylsulfonyl)imide	Ion transport limitations due to low ionic conductivity and/or high viscosity, which can limit ion transport and increase internal resistance; electrode/electrolyte interface instability caused by changes in the surface chemistry of the electrodes; electrolyte decomposition under certain conditions (such as high temperatures or high potentials); electrochemical window limitations, water absorption.
Solid and quasi-solid state	
Poly(ethylene oxide)-based	Low ionic conductivity, limited electrochemical stability window, formation of SEI, dendrite formation
Gel polymer electrolytes; Inorganic solid-state electrolytes	Limited ionic conductivity, formation of SEI, dendrite formation, gas evolution

(C) of the interphase between the conductive electrode and the electrolyte.<sup>[31]</sup> Accordingly, capacitance must be a constant value all over the investigated potential window. Thus, the decrease in capacitance leads to decreasing energy density, whereas the power density decreases as the ESR increases.<sup>[32]</sup> Accordingly, a supercapacitor is considered degraded when its initial capacitance decreases by 20% and/or its ESR increases by 100% compared to its initial value.<sup>[31,33]</sup> Therefore, precisely evaluating these two parameters is essential, and the measurement methods must respect a rigorous protocol to avoid uncertainty in the parameter's characterization.<sup>[34]</sup>

Nevertheless, since supercapacitors are very sensitive to temperature, significant temperature changes may also influence their lifespan. As their degradation is generally evaluated at high rates, considerable temperature variations may arise due to the heat generated inside the cell. The heat generations occur from an irreversible Joule heat generation and an irreversible heat generation from the ion motion during discharging and charging.<sup>[35]</sup> Hence, supercapacitors' cycle life should be assessed at controlled thermal conditions, and their thermal behaviors should not be neglected.

The degradation of supercapacitors is often evaluated by recording several thousands of galvanostatic charge/discharge (GC/GD) cycles.<sup>[9,31,36]</sup> Although the cycling stability test is straightforward, it is highly time-consuming, mainly because a

20% capacitance loss is generally observed for commercial supercapacitors after 500 000 to 1 000 000 cycles. For example, Rizoug et al. reported 560 000 cycles recorded in almost one year (325 cumulated days) of continuous charge/discharge cycling.<sup>[37]</sup> Such long cycling is sometimes because most authors perform the cycling test at low specific currents to keep the IR voltage drop small. Consequently, the delay of a single cycle of some reported GC/GD is in the range of minutes, corresponding to relatively mild operation conditions, which limits the monitoring of potential degradation caused by stress and fatigue resulting from the alternating charge/discharge processes. Therefore, to conduct practical and effective cycling tests, the length of one galvanostatic charge/discharge cycle of supercapacitors should be in the order of seconds. Hence, realistic and meaningful cycling tests should be performed at currents adapted to the use of supercapacitors, recommended at relatively high specific currents of at least 1 A g<sup>-1</sup>. Nevertheless, the resulting Ohmic drop at such high rates is relatively high.

A more accurate lifespan of carbon/carbon supercapacitors can be determined in potentiostatic mode by performing the so-called floating test, consisting of holding the cell at the nominal voltage and determining the capacitance and ESR as a function of time by occasional GC/GD.<sup>[36,38]</sup> The floating test offers the advantage of requiring a much shorter time than galvanostatic charge/discharge cycling while giving the proper maximum

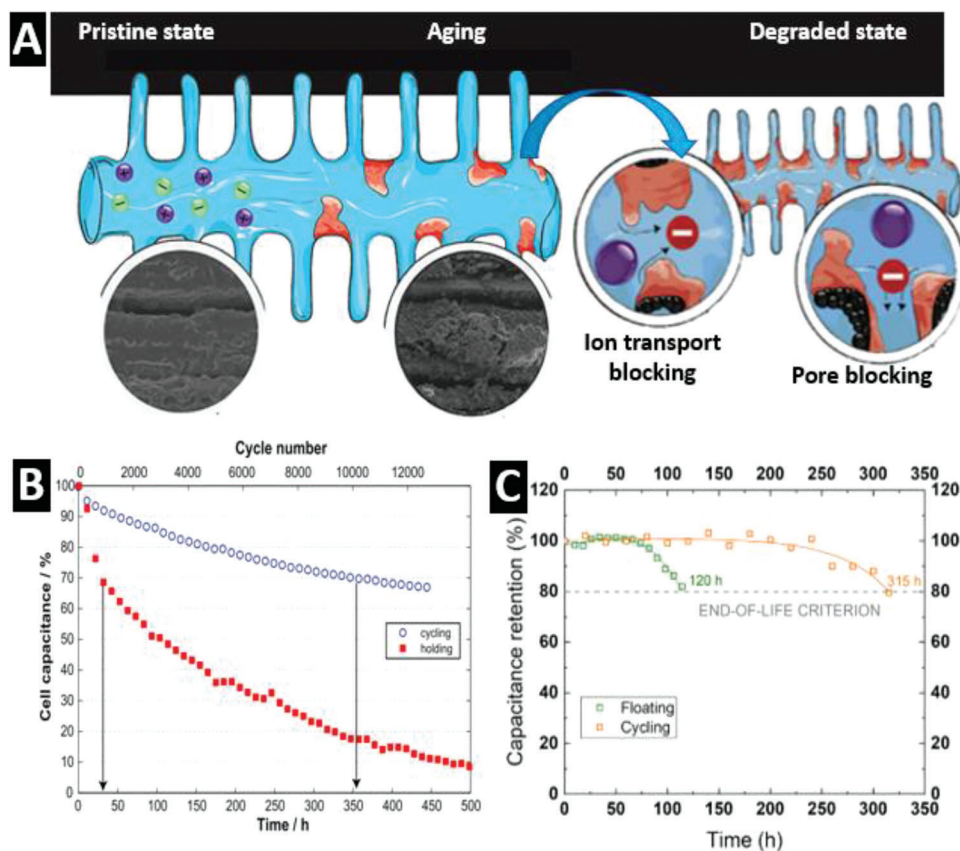


**Figure 2.** A) Schematic representation of pristine and the degrading states of supercapacitor electrodes. Cross-section high-resolution scanning electron microscopy micrographs of pristine and aged carbon electrode. Ion transport and pore blocking on a supercapacitor electrode held cumulatively for 30 d at 5 V. Reproduced with permission.<sup>[12]</sup> Copyright 2017, Elsevier. Galvanostatic charge/discharge cycling and floating (holding) test of supercapacitors utilizing activated carbon electrodes in organic B) and aqueous C) electrolytes. Reproduced with permission.<sup>[31,36]</sup> Copyright 2013 and 2019, Elsevier.

operating voltage value, owing to the very low leakage current and, consequently, negligible ohmic drop. Weingarth et al. reported a comparative study of both cycling and floating tests on supercapacitors utilizing a standard organic electrolyte (1 M TEABF<sub>4</sub> in acetonitrile) (Figure 2B).<sup>[36]</sup> For the device tested in potentiostatic mode, 30% of capacitance loss was observed after only 30 h of floating, whereas 350 h (corresponding to 10 000 GC/GD cycles) was needed to monitor the same capacitance loss using the cycling test (Figure 2B). Later work confirmed that the floating test is much aging-effective for capacitors in aqueous media as its time of operation for reaching the same end-of-life (20% capacitance drop) is about three times shorter than in cycling test (Figure 2C).<sup>[31]</sup>

Though the above-listed methods help to quantify performance decay, they provide indirect information on the degradation mechanism. Thus, advanced in situ/operando techniques and post-mortem methods are essential tools for understanding (during cell operation) how supercapacitors degrade. Many in situ/operando techniques are being used under cell operation to evaluate the structural and morphological degradation process over extended cycles. The set of methods includes electrochemical dilatometry, electrochemical quartz crystal microbalance, scanning electrochemical microscopy, electrochemical mass spectrometry, X-ray diffraction, atomic force mi-

croscopy, small-angle X-ray scattering, X-ray absorption spectroscopy, X-ray photoelectron spectroscopy (XPS), nuclear magnetic resonance spectroscopy, electron microscopy, and Raman spectroscopy.<sup>[39]</sup> Each technique has its unique way of providing a comprehensive understanding of the relationship between the electrode material and electrolyte and the charge storage mechanism during the electrochemical operation of supercapacitors. The primary information under in situ/operando conditions includes the Faradaic and non-Faradaic mechanism, the electrode-electrolyte reaction, the electrolyte ion transport behavior, and the structural and morphological evolution of the cell. More detailed information on the in situ/operando techniques in supercapacitors research can be found in ref. [40], where the authors reviewed recent advances in these techniques and provided insights on computational simulations to model supercapacitor systems and predict their degradation process during long-term cycling.<sup>[40]</sup>

The main factors reducing the capacitance and ESR of supercapacitors primarily stem from electrode oxidation, electrolyte decomposition products blocking the pores, ionic starvation in the electrodes, and weakening of the adhesion between the electrode active mass and the current collector. Thus, postmortem analyses are essential to identify (and quantify) the degradation mechanisms. Many post-mortem experimental methods include X-ray photoelectron spectroscopy, Fourier-transform

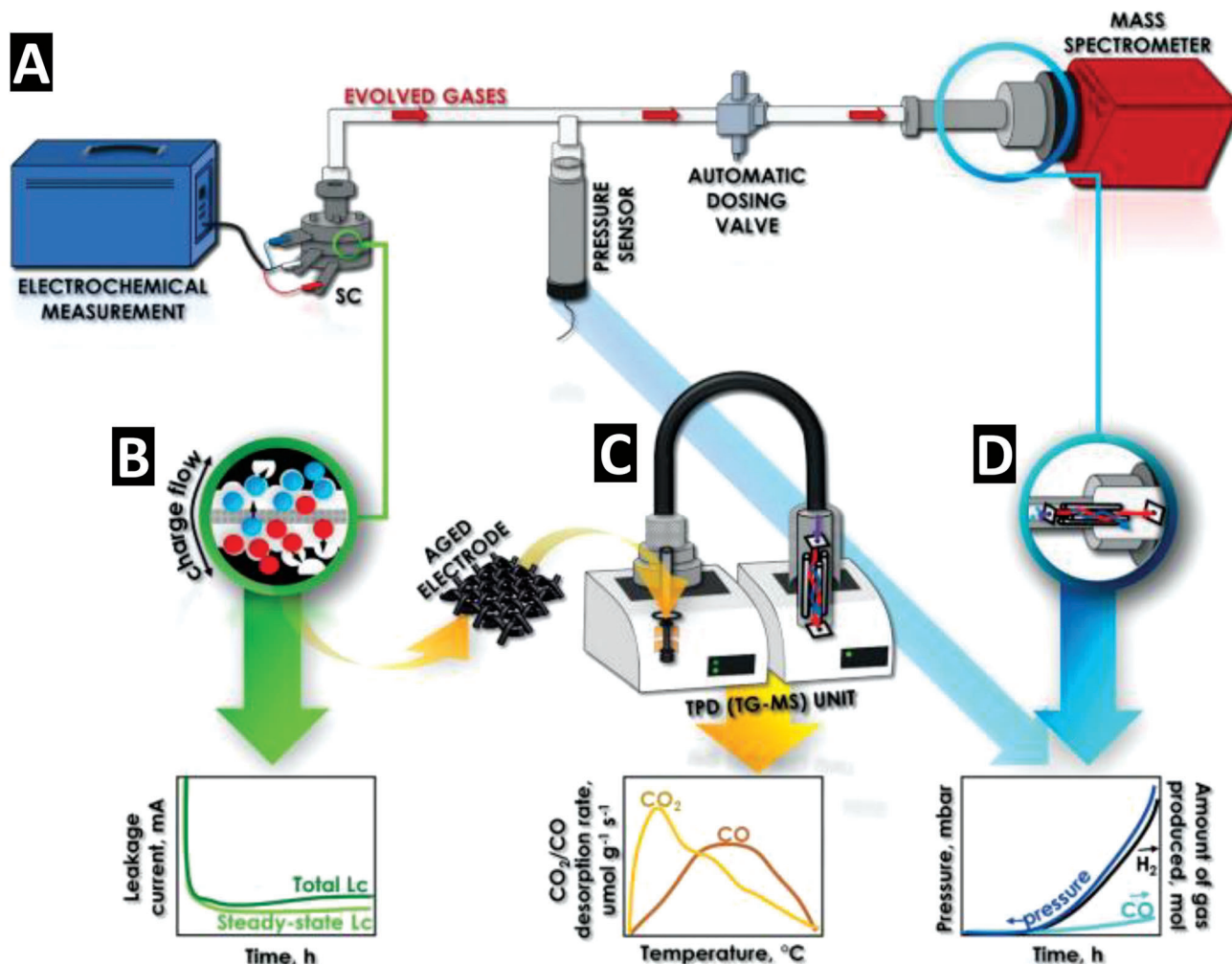


**Figure 3.** Schematic concept of the approach used for assigning the charge passing through a carbon-based supercapacitor in the aqueous electrolyte under aging by prolonged potentiostatic floating: A) Simplified scheme of the EMS system; B–D) Illustration of the analysis realized for determining the processes taking place during high voltage performance of the supercapacitor: B) electrochemical measurement of the leakage current, C) post-mortem surface functionality analyses realized by TPD on aged AC electrodes, D) operando EMS analysis and pressure records. Reproduced with permission.<sup>[41]</sup> Copyright 2019, Wiley-VCH GmbH.

infrared spectroscopy, and temperature-programmed desorption (TPD), which is the most used. The combination of EMS and TPD was also proposed to obtain quantitative and qualitative information on all mechanisms of supercapacitors during and after aging (Figure 3).<sup>[41]</sup> While the in situ technique was used to monitor the gas evolution in the cell during its cycling, the post-mortem analysis (TPD coupled with MS) was implemented after its death to measure oxygenated surface functionalities on the electrodes.

### 2.3. Degradation from an Industrial Perspective: What Metrics Count?

Supercapacitors are considered aged when they degrade in capacitance, exhibit increased internal resistance,<sup>[42]</sup> or are otherwise affected by any condition that results in a deformed, opened, or otherwise damaged cell or energy storage module.<sup>[43]</sup>

End-of-life can also be considered from an application perspective: End-of-life conditions for any industrial energy storage device are deemed to be reached when the device cannot provide enough energy or power for the application in question.

Three metrics need to be considered for the industrial relevance of supercapacitor device degradation: Energy, power, and device integrity.<sup>[43]</sup> It depends on the application profile on which metric is the most relevant. While most applications relate to short-term energy storage for a charge or discharge pulses shorter than 30 s, the actual performance requirements are generally defined by the lowest acceptable power the system can provide at the lowest adequate voltage. Studies of industrial supercapacitor applications in different systems (tram kinetic energy recuperation<sup>[44]</sup> and wave power peak shaving<sup>[45]</sup>) show that the application power profile alone decides the difference in performance between a beginning-of-life and end-of-life supercapacitor system.

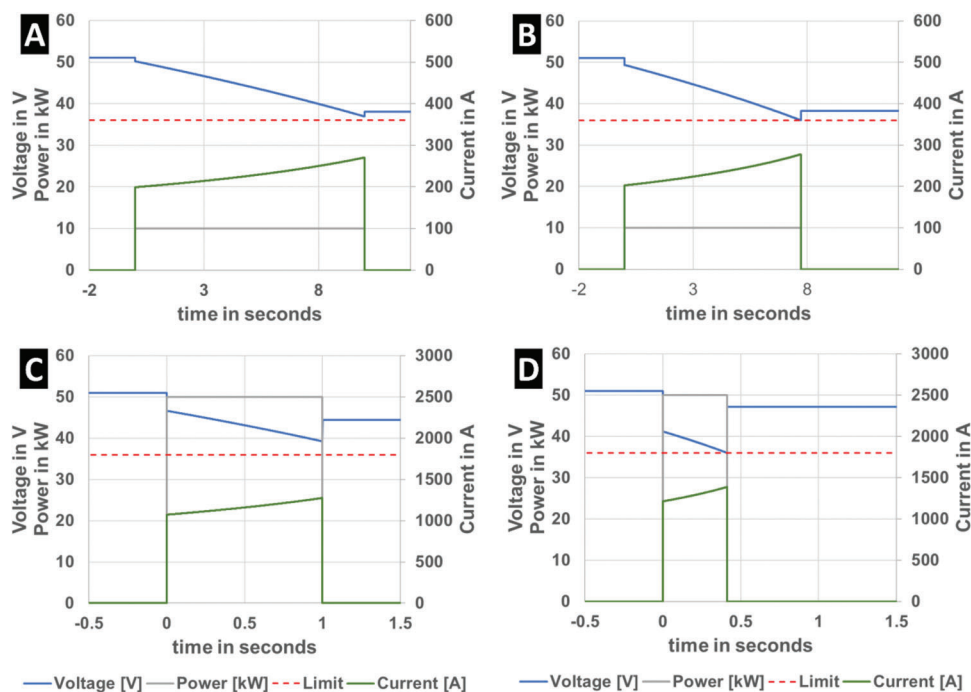


**Figure 4.** Constant power discharge profile simulation data for a 51 V. Supercapacitor pack consisting of 18 industrial 3200 F cells in series. The discharge power is set to 10 kW for A,B) 10 s or 50 kW for C,D) 1 s . Pack current (red) and pack voltage (blue) develop over the constant power pulse as the pack discharges. A,C) The left sides of the image shows simulation data for the beginning of life with 4 mΩ ESR and 177 F capacitance. B,D) Right side of the image shows simulation data for end-of-life with 8 mΩ ESR and 141.6 F capacitance. A pale red dotted line indicates the application voltage limit. Simulations have been carried out using Skeleton Technologies' model for industrial Supercapacitor cells.

**Figure 4A,B** shows the simulated behavior of a 51 V supercapacitor cell pack under a 10 s, constant 10 kW discharge pulse within the voltage boundaries of a common 48 V system (51 to 36 V). To keep the power constant over 10 s, the current needs to increase throughout the power pulse due to the decreasing voltage over time. Consequently, reduced capacitance and increased resistance, both encountered in aged supercapacitors, influence application performance. The decreased capacitance will impact the slope of the voltage decay when drawing constant power, meaning that decreased system capacitance will result in higher peak currents, as seen by reaching a current of 250 A after 5 s of pulse time for an aged cell pack (80% of initial capacitance, 141.6 F; 200% of initial ESR, 8 mΩ) in comparison to reaching 250 A after 8 s for a pristine cell pack (177 F, 4 mΩ).

An increased equivalent series resistance will increase the voltage drop upon current switching, as seen by the increased voltage drop for the aged cell pack at the start of the test. This increased voltage drop contributes to the voltage loss over time but is less relevant for longer pulses such as the 10 s pulse seen in Figure 4A,B. To illustrate the effect of aging on higher power pulse applications, Figure 4C,D considers a 1 s 50 kW pulse for both a pristine and an aged cell pack. Although this pulse contains only 50% of the energy contained in the 10 kW, 10 s pulse described in Figure 4A,B, the high voltage drop at the onset of the pulse results in a similar overall voltage drop after the pulse has ended, indicating that much of the energy is lost in the resistive heating of the cell pack. For the aged cell pack (Figure 4D), the doubled ESR results in most of the supercapacitor pack's energy being dissipated into heat during the pulse onset, not allowing

it to fulfill the same 1 s pulse length before passing the lower voltage limit.

The comparison of simulated behavior of both a pristine and an aged supercapacitor cell pack yields the conclusion that while both the decay in capacitance and the increase in ESR need to be considered for the performance of the supercapacitor cell pack under end-of-life conditions, their impact is much different depending on the nature of the application use case. ESR plays a more critical role in performance than capacitance for short, high-power pulses. For longer pulses, the capacitance and, thus, the overall energy content of the pack becomes more dominant in impacting the cell pack performance. In turn, the importance of different degradation metrics heavily depends on the envisioned application: An excellent capacitance retention is very relevant to low-power pulses with a limited voltage drop. In contrast, a high-power pulse application benefits more from reduced ESR increase over the device lifetime.

From the mechanical stability and device integrity perspective, it is essential to consider that supercapacitors can develop gaseous decomposition products when aged.<sup>[46]</sup> As these products accumulate within the cell, internal pressure builds up. To prevent the cell from rupturing uncontrollably, industrial supercapacitor designs comprise an overpressure breakpoint that opens at a predefined pressure and releases the accumulated gases in a controlled manner. This event renders most supercapacitor cells unusable as the cells' integrity is damaged.<sup>[44]</sup> In turn, the evolution of gases for different voltages and temperatures must be understood in detail when providing supercapacitor aging models relevant to industrial cell designs.

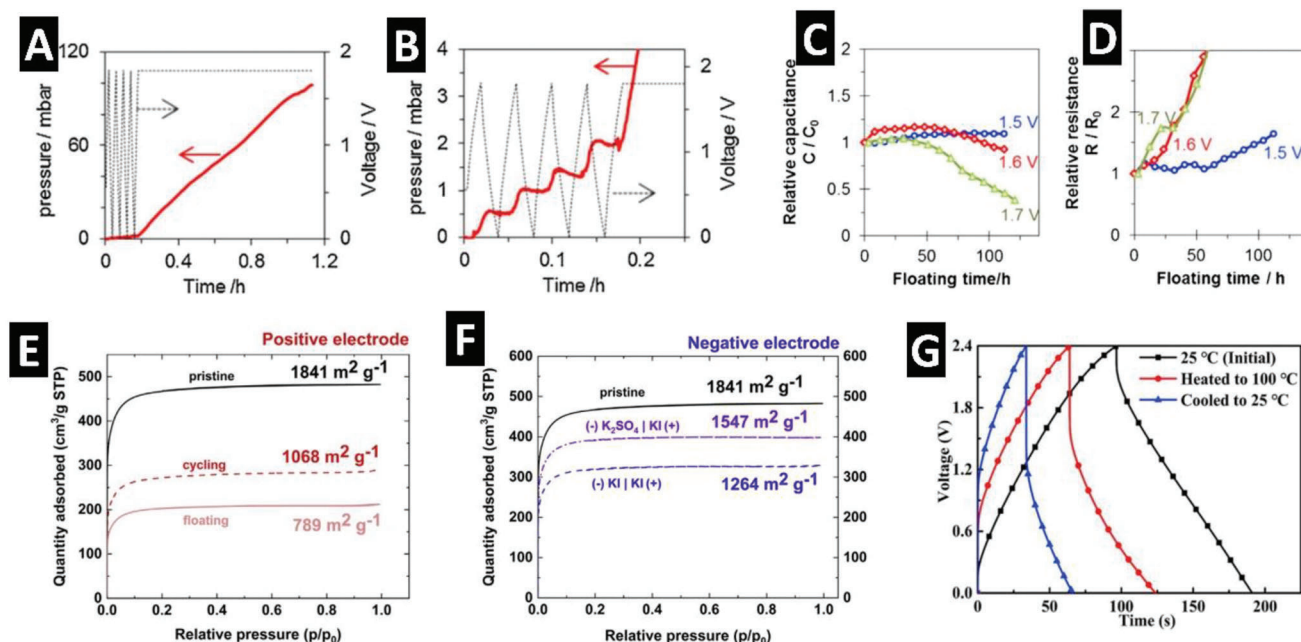


**Figure 5.** A) Cell internal overpressure evolution at 24 °C during galvanostatic cycling of an AC/AC electrochemical capacitor with 1 M  $\text{Li}_2\text{SO}_4$  electrolyte followed by floating at 1.8 V and B) magnification of the pressure evolution during galvanostatic cycling. Effect of the floating voltage on C) the relative capacitance and D) the relative resistance of the same type of capacitor. Reproduced with permission.<sup>[38]</sup> Copyright 2014, Elsevier. Postmortem  $\text{N}_2$  adsorption/desorption isotherms with surface area values of E) positive AC electrodes after cycling and floating tests in 1 M KI electrolyte and F) of negative AC electrodes after the same tests performed in a hybrid electrolyte system ( $\text{K}_2\text{SO}_4/\text{KI}$ ). Reproduced with permission.<sup>[31]</sup> Copyright 2019, Elsevier. G) Voltage profiles of a supercapacitor with 20 M LiTFSI WISE a cycle of heating and cooling cycle from 25 °C to 100 °C and backward. Reproduced with permission.<sup>[68]</sup> Copyright 2019, Elsevier.

### 3. Failure Mechanisms of Electrolytes

#### 3.1. Aqueous Electrolytes

Aqueous solutions are a natural choice when developing electrolytes for electrochemical energy storage devices. The appeal of water-based electrolytes mainly arises from their intrinsic safety (non-flammability and non-toxicity) and reduced cost (of both materials and manufacturing process). The high ionic conductivity, which can exceed  $1 \text{ S cm}^{-1}$  (i.e., at least one order of magnitude higher than organic electrolytes), is a further feature particularly sought after in supercapacitors applications as it enables high capacitance, good rate capability and, thus, excellent power performance.<sup>[47]</sup> The first supercapacitors worked in an aqueous medium but were characterized by a low cell voltage, which restricted their use to mostly memory backup applications.<sup>[48]</sup> This evidence the main shortcoming of aqueous electrolytes, i.e., the narrow stability window of water. Once this limit is exceeded, water splitting occurs, leading to oxygen evolution reactions (OER) and hydrogen evolution reactions (HER) at the positive and negative electrode of the capacitor, respectively. Both OER and HER (and the potential at which they occur) are highly pH-dependent. Given the large  $\text{H}^+/\text{OH}^-$  concentration, water splitting is mainly promoted in highly acidic (e.g.,  $\text{HCl}$ ,  $\text{H}_2\text{SO}_4$ ) and alkaline (e.g.,  $\text{KOH}$ ,  $\text{NaOH}$ ) solutions.<sup>[30,47]</sup> In such cases, the overall cell voltage must be maintained within the thermodynamic limit of 1.23 V (practically even  $<1 \text{ V}$ ). On the other hand, larger overpotentials are commonly observed for both OER and

HER in a neutral medium (e.g.,  $\text{Li}_2\text{SO}_4$ ,  $\text{LiNO}_3$ ,  $\text{Na}_2\text{SO}_4$ ,  $\text{K}_2\text{SO}_4$ ), allowing for cell voltages beyond 1.5 V depending on the salt type and concentration, and the testing conditions.<sup>[38,49]</sup>

Ratajczak et al. comprehensively studied the fading mechanisms of symmetric AC supercapacitors using a neutral 1  $\text{Li}_2\text{SO}_4$  electrolyte.<sup>[38]</sup> As shown in **Figure 5A,B**, a substantial pressure increase was recorded when the cell voltage exceeded 1.4 V. Upon normal GC/GD cycling up to 1.8 V, this resulted only in a minor gas evolution each cycle since the electrodes spend a relatively short time at potentials where OER and HER occur. However, upon floating tests at 1.8 V, the pressure increased linearly with time reaching 95 mbar after 1 h. This highlights the importance of testing conditions when assessing the stability of the electrolyte. The authors noticed a substantial capacitance fading and resistance increase when progressively increasing the float voltage from 1.5 to 1.7 V (**Figure 5C**). While the primary fading mechanism could be attributed to the electrolyte decomposition leading to increased resistance (**Figure 5D**), the decreased surface area of the electrodes was also identified as a possible cause for the reduced capacitance (**Table 1**). This was evident at the positive electrode, where CO and  $\text{CO}_2$  evolving surface group types were identified.<sup>[50]</sup> Such findings strongly hint at the oxidation of the AC, eventually leading to pore blocking.

Despite gas evolution caused by electrolyte decomposition being generically detrimental to the cycle life of supercapacitors, if properly controlled, it can also be exploited to unlock additional Faradaic charge storage.  $\text{H}_2$  generated at the negative electrode due to water decomposition can be reversibly elec-



torsoberbed/desorbed in porous carbons, at least over an extended potential window width beyond 1.23 V.<sup>[7]</sup> Hydrogen appears to be stabilized by weak chemical bonds with the carbon substrate, which, on the one hand, reduces self-discharge.<sup>[51]</sup> On the other hand, the overpotential for the oxidation of H<sub>2</sub> appears relatively large, suggesting either trapping or sluggish diffusion kinetics in the pores.<sup>[7]</sup>

One of the strategies adopted to suppress water splitting is to increase the OER/HER overpotential by blocking the adsorption of intermediate species and/or inhibiting charge transfer at the electrode/electrolyte interphase, for example, using redox additives dissolved in the aqueous electrolyte.<sup>[3,30,47,52]</sup> To be effective, such redox couples should be close to the OER/HER potential, be highly reversible, and be used in pairs, one for OER and one for HER.<sup>[30,47]</sup> Several redox additives have been proposed so far, such as ferrocyanides (e.g., [Fe(CN)<sub>6</sub>]<sup>3+</sup>/[Fe(CN)<sub>6</sub>]<sup>4+</sup>),<sup>[53]</sup> quinones (e.g., 2,6-dihydroxyanthraquinone)<sup>[54]</sup> and halides (e.g., Br<sup>-</sup>/Br<sup>3-</sup>),<sup>[55]</sup> to name few. Besides suppressing water splitting, the redox-active electrolyte introduces additional capacity, which increases the energy of aqueous supercapacitors. On the other hand, the Faradaic reactions can produce parasitic products that are detrimental to the cycle and calendar life of the system.

For example, Platek et al. comprehensively studied the fading mechanisms of supercapacitors using an iodide-based redox electrolyte (specifically, 1 M KI).<sup>[31]</sup> Since the redox process (2I<sup>-</sup> ⇌ I<sub>2</sub> + 2e<sup>-</sup>) occurs at the positive electrode, this component is mainly affected by side reactions such as the formation of polyiodides at high potentials (I<sub>3</sub><sup>-</sup>, I<sub>5</sub><sup>-</sup>, and I<sub>7</sub><sup>-</sup>). Besides the changes in surface functionalities, confirmed previously by operando studies,<sup>[56]</sup> postmortem analysis evidenced the precipitation of solid products on the electrode surface. Considering the solubility of potentially formed compounds, KIO<sub>3</sub> is most likely the main component of the solid deposit. These solid deposits block access to microporosity, leading to decreased surface area and, in turn, specific capacitance degradation. This fading mechanism primarily affects the positive electrode, where the surface area was more than halved after prolonged floating tests (Figure 5E). Pore blocking was also observed at the negative electrode, suggesting the movement of iodides within the system.<sup>[31]</sup> This was confirmed using a hybrid electrolyte system (K<sub>2</sub>SO<sub>4</sub>/KI) using a cation-selective membrane (Figure 5F).

Despite the numerous strategies adopted to suppress water splitting, including pH regulation,<sup>[57]</sup> mass balancing of the electrodes,<sup>[58]</sup> and addition of redox additives to block active sites, it has been demonstrated to be very challenging to achieve cell voltages >2 V with conventional dilute aqueous electrolytes.<sup>[59]</sup> To overcome this barrier, highly concentrated electrolytes such as hydrate melts and water-in-salt (WiSE) electrolytes have been explored.<sup>[47,60]</sup> First reported by Suo et al. in 2015, WiSEs are solutions of highly soluble salts, where the salt outnumber the solvent (water) in terms of both weight and volume.<sup>[61]</sup> A typical example of WiSE is using 21 mol kg<sup>-1</sup> LiTFSI. Here, Li<sup>+</sup> ions are coordinated to the few water molecules available and the abundant TFSI<sup>-</sup> anions. Interestingly, the decomposition of TFSI<sup>-</sup> taking place close to the HER potential leads to forming a LiF-containing solid-electrolyte interphase (SEI) at the negative electrode.<sup>[61,62]</sup> The hydroxides generated during the hydrogen evolution reaction can chemically react with TFSI and catalyze the formation

of such SEI.<sup>[63]</sup> Additionally, a water-exclusion zone is generated at the positive electrode due to the adsorption of hydrophobic TFSI<sup>-</sup> anions.<sup>[64]</sup> These two phenomena substantially suppress water splitting, leading to ESW as high as 3 V. Although initially employed mainly for aqueous battery applications,<sup>[65]</sup> WiSEs were soon investigated for electrical double-layer and hybrid capacitors.<sup>[49,66]</sup> Tian et al. have reviewed the most recent developments of WiSE in supercapacitors.<sup>[59]</sup> However, since the development of WiSE for supercapacitors is still in its infancy, comprehensive studies on aging/failure mechanisms are not available yet. Furthermore, as the most expensive part of the electrolyte is the conductive salt, this approach also must be carefully evaluated from a techno-economical perspective.<sup>[67]</sup>

The most critical aspect concerning the cycle life of capacitors employing these novel electrolytes is related to the high salt concentration. While this leads to increased electrolyte viscosity, WiSE still possesses sufficiently fast ionic transport for application in high-power devices. However, it substantially increases the risk of salt precipitation under demanding conditions such as, for example, operation at extremely low and/or high temperatures (Figure 5G).<sup>[68]</sup> Since most WiSE systems are nearly saturated (or even supersaturated) solutions, salt precipitation may occur upon prolonged cycling and/or floating up to/at high voltages due to water decomposition. Besides causing a drop in ionic conductivity of the electrolyte, with a resulting ESR increase, the precipitate would also clog the electrode porosity leading to a capacitance drop. It is also unclear whether precipitation may occur simply over time, for example, during storage. This would undoubtedly affect the calendar life of capacitors with WiSE. However, these aspects have rarely been explored and deserve major attention.

### 3.2. Organic Electrolytes

Investigating the aging processes in EDLCs, Ruch et al. showed that the aging of a single electrode dominates the aging rate of symmetric EDLCs and that the limiting electrode strongly depends on the chosen solvent.<sup>[42,69]</sup> In the case of acetonitrile-based EDLCs, the positive electrode experiences a more significant capacitance loss and an increase of internal resistance, whereas in propylene carbonate-based supercapacitors, the negative electrode ages faster (Figure 6).<sup>[42,69]</sup>

The different behavior of the respective positive or negative electrodes during aging results in an uneven electrode potential shift. Instead of performing within the intended electrode potential limits, the respective electrode that experiences faster degradation shows a more significant potential change during charging and discharging, leading to even faster aging. This is due to charge-consuming Faradaic decomposition processes on the less stable electrode, which lead to an incomplete discharge of the more stable electrode. Thus, the more stable electrode accumulates charges when the cell is continuously cycled, leading to the previously mentioned potential shift. After prolonged aging, in acetonitrile-based EDLCs the positive electrode experiences a more significant potential change, whereas, in the case of PC-based EDLCs, the negative does. Thus, a strong dependency of aging on both the electrode polarity and the chosen solvent is evident.<sup>[69]</sup>

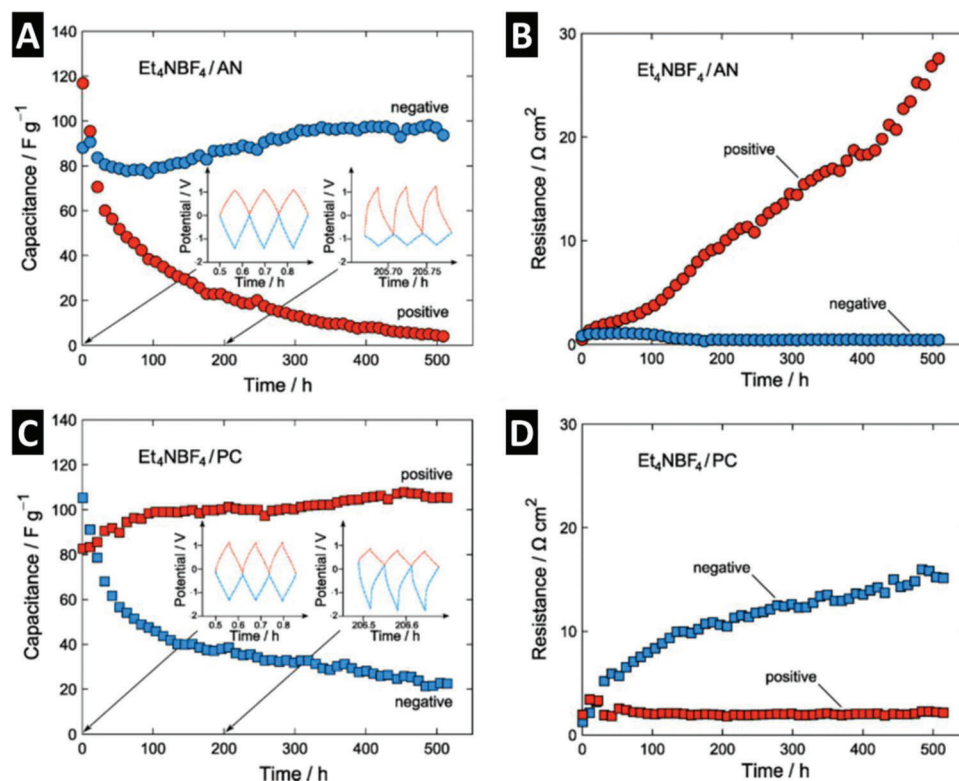


**Figure 6.** Capacitance and resistance behavior of acetonitrile (here AN) and propylene carbonate (PC) based EDLCs while floating at 3.5 V. A,C) The capacitance fading of the single electrode specific capacitances of symmetric EDLC cells with AN and PC based 1 M TEABF<sub>4</sub> electrolytes. The inserted graphs show galvanostatic charge–discharge curves twice during the floating period (at 0 h and 200 h). B,D) The resistance evolution of the respective electrodes. Reproduced with permission.<sup>[69]</sup> Copyright 2010, Elsevier.

### 3.2.1. Failure Mechanisms in Acetonitrile-Based Supercapacitors

Acetonitrile-based supercapacitors are the most thoroughly investigated devices concerning performance and cell aging. Various studies have been published focusing on gas evolution, electrode degradation, and electrolyte decomposition.

Pioneering work by Kurzweil and Chwistek displays detailed investigations of the liquid and gas phase of aged EDLCs using various spectroscopic techniques and gas chromatography-mass spectrometry (GC-MS).<sup>[70]</sup> Investigating the aging of symmetric supercapacitors containing a 1 M solution of TEABF<sub>4</sub> in acetonitrile at constant cell voltages (floating) at 4 V and 6 V, they identified several decomposition products and postulated degradation mechanisms generating the former. Acetonitrile, water vapor, carbon dioxide, ethene, and fragments of metaboric acid and alkyl boranes were detected within the gas phase. In the liquid phase of the aged electrolyte acetamide, acetic acid, several heterolytic compounds (e.g., pyrazines), triethylamine, and fluoroacetic acid were identified. The formation of the latter product was observed only during floating at cell voltages as high as 6 V.<sup>[70]</sup> This finding is consistent with the Simons' process (electrochemical fluorination), which requires cell voltages of 5–8 V on nickel electrodes.<sup>[70,71]</sup>

The recent development of an operando GC-MS technique for investigating aging processes in electrochemical energy storage devices enabled the detection of arising decomposition products as a function of the applied potential. Implementing a custom-

made three-electrode cell allowing the liquid electrolyte extraction during an electrochemical measurement, Kreth et al. investigated the behavior of EDLCs containing an electrolyte consisting of 1 M TEABF<sub>4</sub> in acetonitrile (Figure 7).<sup>[72]</sup> By identifying potentials at which the respective positive and negative electrolyte-electrode interphase begin to form soluble decomposition products, they confirmed that the primary cause for the aging of acetonitrile-based symmetric EDLCs is the degradation of the positive electrode. With an open circuit voltage (OCV) of 0.3 V vs Ag<sup>+</sup>/Ag and the first degradation processes of the positive and negative electrode, respectively occurring at +1.75 V and –1.50 V vs Ag<sup>+</sup>/Ag, the positive electrode was the first one that reached its potential stability limit. Observed degradation reactions involving acetonitrile have been reported to be caused mainly by interactions between the acetonitrile solvent and the containing oxygen functions on the surface of the activated carbon, the binder (sodium carboxymethyl cellulose, NaCMC), and/or trace water molecules (Figure 8). Some decomposition products were generated regardless of the electrode's polarity. Hydrolysis reaction leading to the formation of acetamide and its derivate N-ethylacetamide and cyclotrimerization of acetonitrile forming 2,4,6-trimethyl-1,3,5-triazine were observed to occur at both electrodes. Decomposition of the salt has been reported only to occur at the negative electrode at potentials lower than –1.75 V vs. Ag<sup>+</sup>/Ag, forming triethylamine and ethene (Figure 9A). This reaction is well known as the Hofmann elimination, where quaternary amines form tertiary amines and alkenes, while a strong base

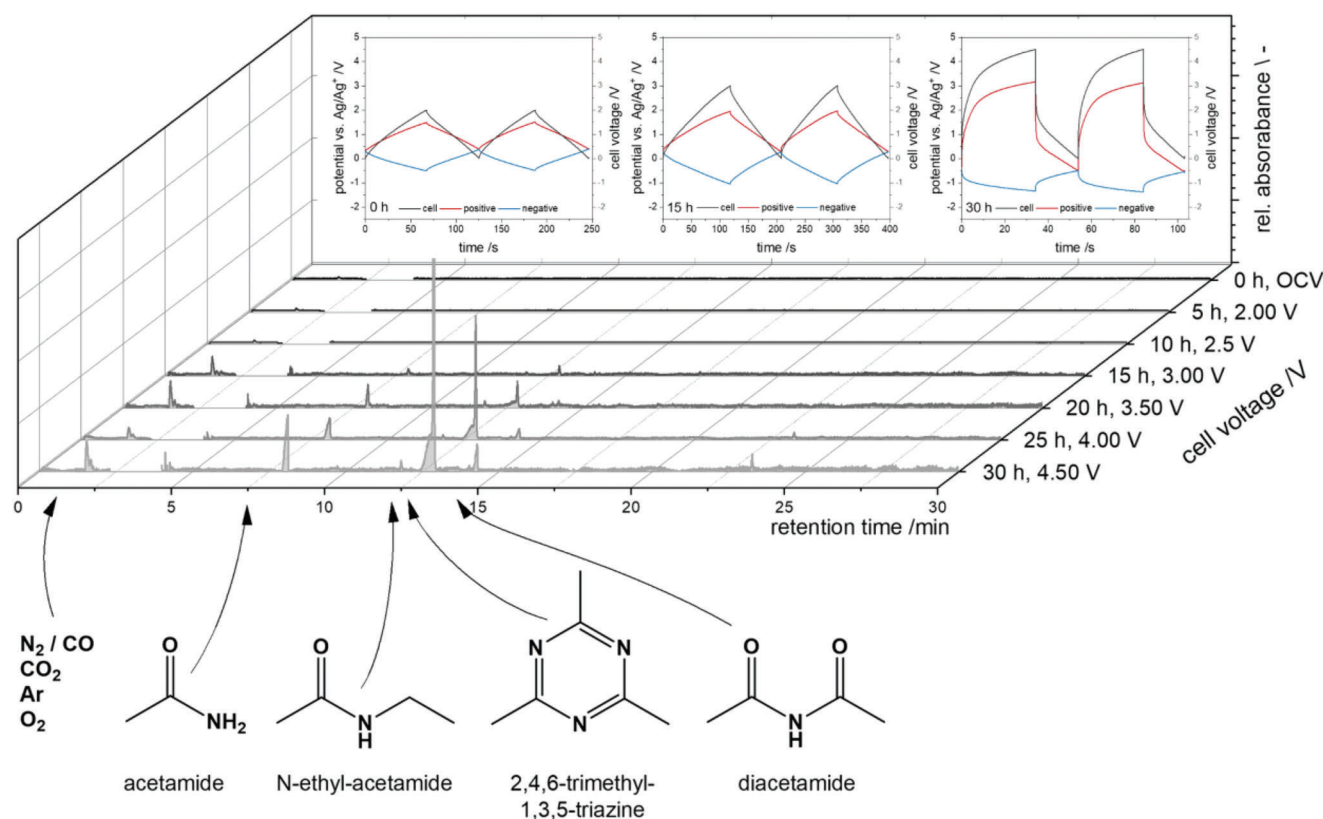


**Figure 7.** Total ion chromatograms (TICs) of the operando GC-MS measurements obtained during aging tests of a symmetric EDLC consisting of activated carbon electrodes and 1 M TEABF<sub>4</sub> in acetonitrile. Additional voltage profiles of the positive (red) and negative (blue) electrodes, and of the cell voltage (grey), are shown above. Four degradation products were identified: acetamide ( $t_R$  8 min), N-ethyl-acetamide ( $t_R$  12 min), 2,4,6-trimethyl-1,3,5-triazine ( $t_R$  12.5 min), and diacetamide ( $t_R$  14 min). The observed decomposition products are the same as in the aging test of the positive electrode, indicating that the decomposition of the positive electrode-electrolyte interphase primarily causes the aging of this device. Reproduced with permission.<sup>[72]</sup> Copyright 2023, Elsevier.

(here BF<sub>4</sub><sup>-</sup> or OH<sup>-</sup>) eliminates a proton. Further, no fluorinated decomposition products were detected within the liquid phase of the aged electrolyte. It has been proposed that potentially formed fluor-containing compounds remain at the electrode surface, precipitate from solution, or in the case of gases (HF,  $m/z$  20), outgas and/or do not dissolve within the limit of detection of the device.<sup>[72]</sup>

Investigating pressure variation by dilatometry and thus gas evolution within EDLCs containing a 1 M solution of TEABF<sub>4</sub> in either acetonitrile, PC, or  $\gamma$ -butyrolactone (GBL), Kötzer et al. showed that the extent of cell pressure increase is strongly dependent on the stability of the chosen solvent.<sup>[46]</sup> A noteworthy release of gas was observed in GBL at 2.5 V, in PC at 3.0 V, and in acetonitrile at 3.25 V. Although the onset of gas evolution in acetonitrile occurred at higher potentials compared to PC, the authors remarked that PC exhibited considerably lower Faradaic currents than acetonitrile (and GBL). Thus, attributing the higher leakage currents in acetonitrile to the formation of soluble electrolyte decomposition products instead of gas evolution reactions.<sup>[46]</sup>

With a focus on the interaction between organic electrolytes and supercapacitor electrodes, carbon materials, and surface functionalities, Azaïs et al., Zhu et al., Bittner et al., Liu et al., and Huang et al. published several studies concerning possi-

ble failure mechanisms.<sup>[29,73,74]</sup> For example, utilizing gas sorption, XPS, and NMR data, Azaïs et al. showed that occurring capacitance losses and resistance increases are related to the electrolyte decomposition at the electrode-electrolyte interphase, creating surface defects and decreasing porosity (Figure 9B). Here, the amount and kind of generated decomposition products vary with the respective carbon material and electrode polarity. While fresh electrodes showed traces of sodium and oxygen, which were attributed to the binder sodium carboxymethylcellulose, the aged positive electrode contained an increased amount of nitrogen (especially on the surface) and no sodium. On the other hand, the aged negative electrode contained more fluorine and boron and showed the same amount of sodium as the pristine electrode. One has to note that this behavior contradicts the direction of ion transport during polarization and cannot be fully explained. Further, they showed that acidic surface functionalities and water traces inside the electrolyte cause and increase supercapacitor aging. The authors concluded that poor surface functionality, enough narrow micropores, and the absence of water are the most critical requirements for the good long-term stability of supercapacitors.<sup>[74]</sup> With regard to the latter, a water content of less than 20 ppm has been determined to be necessary to achieve long-term stability of nonaqueous supercapacitors.<sup>[74]</sup>

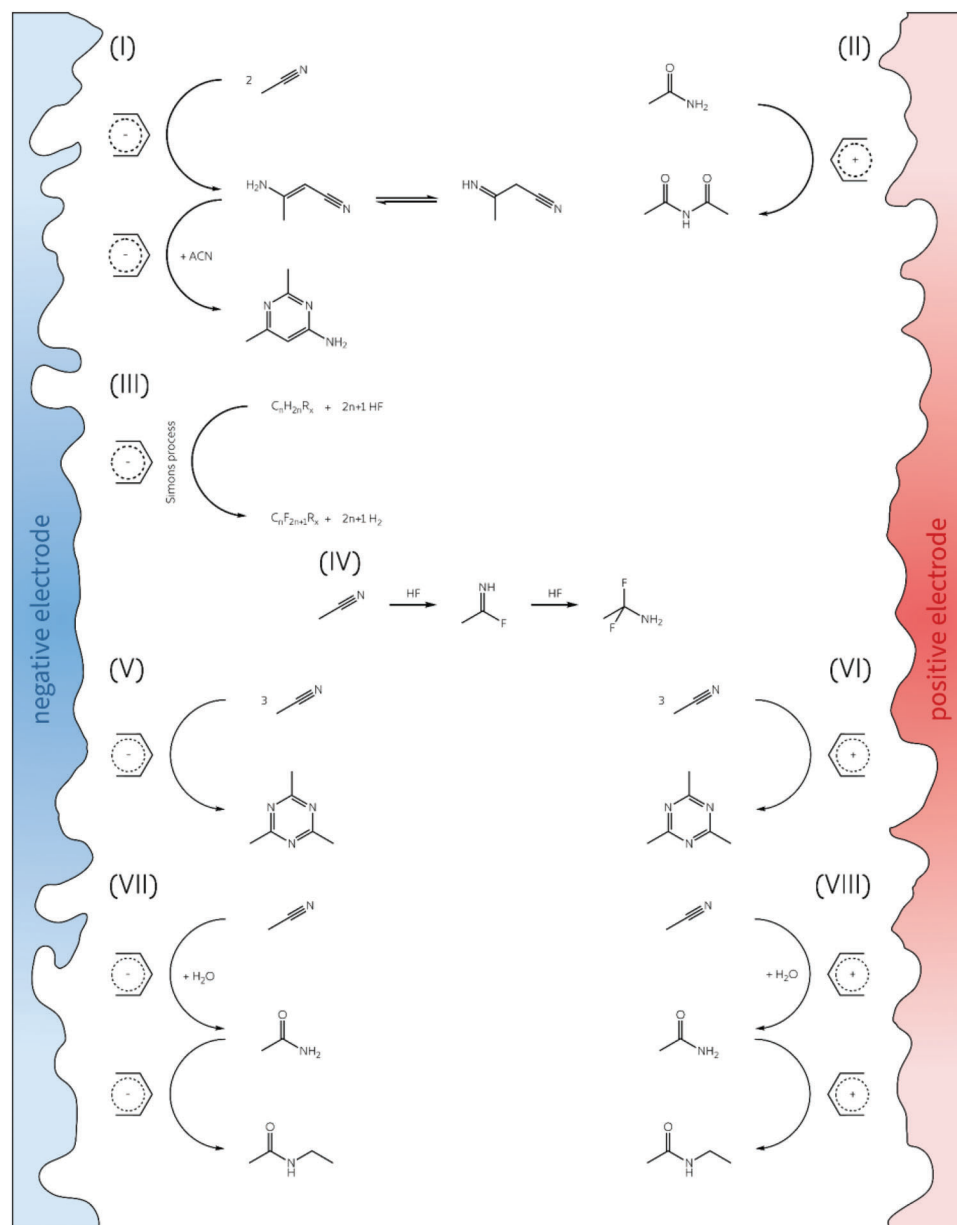


**Figure 8.** Proposed degradation mechanisms of the electrode-electrolyte-interphase in acetonitrile-based EDLCs. Primary failure mechanisms that can be attributed to the negative electrode are the dimerization and subsequent (cyclo)trimerization (reaction I) and the reductive electrofluorination (known as Simons process) at cell voltages above 5 V (reaction III). Degradation reactions reported to occur at the positive electrode is the formation of diacetamide (reaction II). The formation of diacetamide has been reported to occur at the positive electrode. Several reactions have been reported to occur during aging of both electrodes: The hydrolysis (reactions VII and VIII) and (cyclo-)polymerization (reactions V and VI) of acetonitrile. Further, in-situ formed HF (for example, due to the hydrolysis of the  $\text{BF}_4^-$  anion) can cause a hydrofluorination reaction of acetonitrile (reaction IV).<sup>[70,72]</sup>

Zhu et al. and Bittner et al. examined aged supercapacitors containing the same electrolyte through post-mortem analysis techniques such as infrared, Raman, XPS, and nitrogen porosimetry.<sup>[73,75]</sup> They identified polymerization products from acetonitrile (pyridine, amines, and polyacetonitrile), and traces of nitrogen, fluorine, and oxygen on both the negative and positive electrodes. As previously reported, the degradation processes affected the positively polarized electrode more than the negative electrode. The carbon material of the positive electrode was oxidized and incorporated nitrogen, fluorine, and oxygen, resulting

in the formation of various surface functionalities (particularly carboxyl species). In contrast, the carbon material of the negative electrode was partially reduced and formed CH groups. Additionally, the study suggests the formation of reactive  $\text{BF}_4^-$  radicals, which could cause the formation of HF, fluorination reactions, and oligo-/polymerization of acetonitrile.<sup>[73,75]</sup>

Liu et al. investigated aging mechanisms occurring within acetonitrile-based supercapacitors containing electrodes based on two different carbon materials by electrochemical impedance spectroscopy, Raman and FTIR spectroscopy, Boehm's titration,

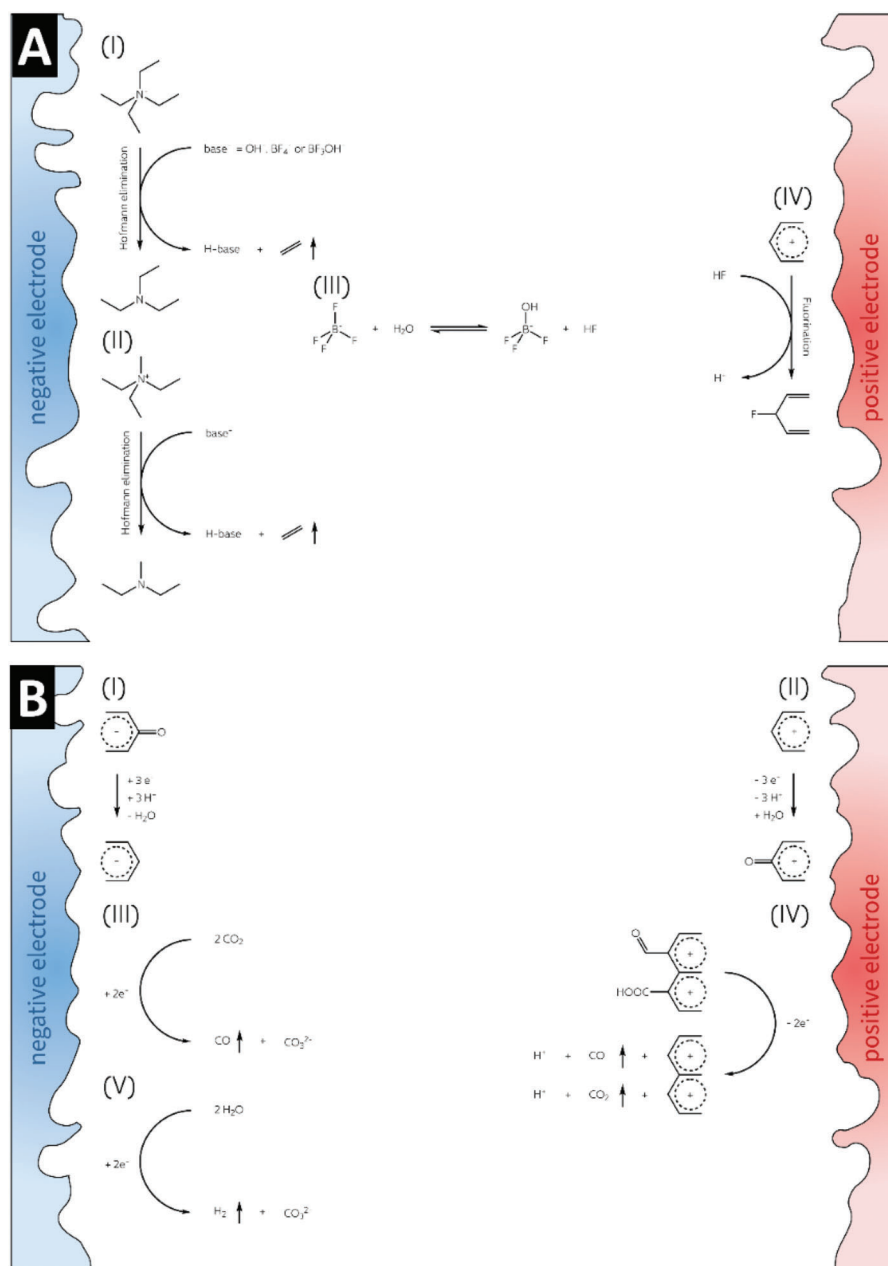


**Figure 9.** A) Proposed degradation mechanisms of the salts TEABF<sub>4</sub> and TEMABF<sub>4</sub>, contained in most EDLCs. Following the Hofmann elimination reaction, at the negative electrode, the respective cation forms triethylamine or diethylmethylamine and ethene (reaction I and II). On the positive electrode, in situ formed HF (hydrolysis of the BF<sub>4</sub><sup>-</sup> anion (reaction III)) can cause fluorination reaction of the carbon surface (reaction IV).<sup>[26,70,72,77]</sup> B) Proposed degradation mechanisms of the carbon material in EDLCs. While the carbon material of the negative electrode gets reduced (reaction I), the positive electrode experiences oxidation (reaction II) (the reduction and oxidation of a carbonyl group is shown as an example). Further, CO<sub>2</sub> and H<sub>2</sub>O are reduced, at the negative electrode, forming CO, H<sub>2</sub>, and CO<sub>3</sub><sup>2-</sup> (reactions III and V). While releasing CO, CO<sub>2</sub>, and H<sup>+</sup>, oxygen-containing surface functions are oxidized at the positive electrode (reaction IV) (the oxidation of a carbonyl and carboxy group are shown as an example).<sup>[29,73–75,77,80]</sup>

and temperature-programmed desorption coupled mass spectrometry. They were able to distinguish between two failure mechanisms based on the carbon surface functionalities, with the content of surface functional groups on the positive electrode being the key factor. In both mechanisms, the hydrolysis of BF<sub>4</sub><sup>-</sup> to fluorine-containing acids occurs at the positive electrode in the presence of water traces, leading to the formation of defects in

the carbon network. These acids can then diffuse to the negative electrode. For carbons containing a small amount of acidic surface functionalities (mechanism A), the defects can react further, resulting in the formation of surface functionalities such as carboxylic, anhydride, lactone, ether, phenol, and carbonyl groups.

Additionally, the formation of soluble polymerization products of acetonitrile leads to the yellowish tint of the electrolyte

**Table 2.** Determined cell voltages ( $E_{\text{cell}}$ ) and electrode potential potentials ( $E_+$  and  $E_-$ ) limits of PC-based EDLCs at which gas evolution and cell degradation has been observed by Hahn et al.<sup>[76]</sup> and Ishimoto et al.<sup>[77]</sup>

$E_{\text{cell}}$ [V]	$E_+$ vs Li <sup>+</sup> /Li [V]	$E_-$ vs Li <sup>+</sup> /Li [V]	Evolving gases and observed changes	Refs.
>0.7	–	<2.6	Propylene	[76]
>2.6	–	<1.5	Strongly increased amount of propylene	[76]
>2.7	>4.3 V	–	Carbon dioxide	[76]
>3.4	–	<1.1 V	Hydrogen	[76]
3.0–3.7	4.9–5.2	1.9–1.5	CO, CO <sub>2</sub> , H <sub>2</sub> O, H <sub>2</sub> , OH <sup>-</sup> , N,N-diethylmethylamine, propylene glycol	[77]
3.7–4.0	>5.2	<1.5	Formation of resistive PC-based passivation layer on both electrodes	[77]

and is another consequence of cell aging. This aging is characterized by a decrease in capacitance and a gradual rise in the equivalent series resistance (ESR). In the presence of a significant number of acidic surface functionalities (mechanism B), a protective layer with ion-conductive and electronically-resistive properties is believed to develop on the electrode's surface. In this case, cell aging expresses itself through increased ESR while the capacitance remains constant. The authors propose the formation of an insoluble polymer film from the polymerization products of acetonitrile via hydrogen bonds with acidic surface functionalities.<sup>[29]</sup>

To summarize, primary failure mechanisms in acetonitrile-based EDLCs (Table 1) attributed to electrolyte decomposition have been identified as hydrolysis, (cyclo-)polymerization, Hofmann elimination, and fluorination reactions.

### 3.2.2. Failure Mechanisms in Propylene Carbonate-Based Supercapacitors

Degradation processes at the negative electrode–electrolyte interface are the primary cause of aging in propylene carbonate-based supercapacitors, with significant gas evolution occurring at cell voltages above 3.0 V.<sup>[46,69]</sup> The latter has been comprehensively investigated by Hahn et al. utilizing dilatometry and differential electrochemical online mass spectrometry (DEMS). During voltage scans up to 3 V cell voltage, reversible and irreversible cell pressure changes were observed. When cycled within a cell voltage range of 2.5 V, a drop in pressure during charging and a reversible increase during discharging were detected. These pressure changes were attributed to concentration-dependent volume fluctuations of the electrolyte. Significant irreversible gas evolution was observed when applying cell voltages above 2.5 V. Here, hydrogen (H<sub>2</sub>,  $m/z = 2$ ), propylene ( $m/z = 41$ ), and carbon dioxide (CO<sub>2</sub>,  $m/z = 44$ ) were detected as the dominant gaseous decomposition products, respectively forming at different cell voltages  $E_{\text{cell}}$  and electrode potentials  $E_+$  and  $E_-$  (Table 2).<sup>[76]</sup>

The formation of propene and hydrogen has been assigned to reducing the solvent at the negative electrode. Hahn et al. proposed an electrochemical reduction of propylene carbonate to propene and carbonate anions. While the hydrogen formation was attributed to a general reduction product of organic compounds, the evolution of CO<sub>2</sub> was ascribed to the solvent oxidation at the positive electrode.<sup>[76]</sup>

Ishimoto et al. identified three different cell voltage ranges (Table 2) for the aging of supercapacitors containing a 1 M solution of TEMABF<sub>4</sub> in PC by SEM, EIS, and ion-chromatography-coupled mass spectroscopy measurements.<sup>[77]</sup> Here, region 1 ( $E_{\text{cell}} < 3.0$  V) was described as the voltage/potential range where no degradation at either electrode is observed. In region 2 ( $E_{\text{cell}} 3.0\text{--}3.7$  V), several decomposition reactions of the electrolyte–electrode interphase start to arise: While the positive electrode is oxidized, releasing CO and CO<sub>2</sub> as volatile decomposition products, water is released from the surface functional groups of the activated carbon. Subsequently, at potentials below 1.9 V versus Li<sup>+</sup>/Li, water molecules, either dissolved within the electrolyte or adsorbed on the electrode surface, are reduced, generating H<sub>2</sub> and hydroxide (OH<sup>-</sup>). These hydroxides can further react with the TEMA<sup>+</sup> cation forming ethene, N,N-diethylmethylamine, and water (alkaline-induced Hofmann elimination). Further, the hydroxide hydrolyzes propylene carbonate generating propylene glycol (PG) and CO<sub>2</sub>. Region 3 ( $E_{\text{cell}} 3.7\text{--}4.0$  V) was defined as the voltage range in which propylene carbonate gets electrochemically oxidized at the positive electrode (while generating CO<sub>2</sub>) and reduced at the negative electrode (while simultaneously forming propylene and carbonate anions). Here, oxidation and reduction lead to the formation of a resistive PC-based passivation layer.<sup>[77]</sup>

Through operando calorimetric measurements, the changes in heat flow resulting from charge redistribution effects during cycling can be precisely monitored. Munteshari et al. investigated PC-based EDLCs and observed endothermic heat generation when operated above 3 V cell voltage, which they attributed to the reductive decomposition of the solvent.<sup>[78]</sup>

Hess et al. designed a cell for use in thermogravimetric/differential thermal analysis, which allowed them to investigate the changes in heat flow, mass loss, internal resistance increase, and capacitance loss during cycling and floating of propylene carbonate-based supercapacitors.<sup>[79]</sup> They found a significantly greater increase in the cumulative heat and faster mass loss when the supercapacitors were floated at 3.5 V cell voltage, compared to 2.5 V. This was attributed to irreversible exothermic degradation reactions of the electrode–electrolyte interphase leading to the formation of volatile decomposition products. Coinciding with previous results shown by calorimetry, dilatometry, and DEMS, this technique enables the complementary monitoring of heat and mass variation during electrochemical and/or thermal aging for the first time.<sup>[79]</sup>

Concluding, the primary failure mechanism causing an early failure of PC-based EDLCs is the reductive decomposition of propylene carbonate, forming propylene and carbonates. This process further explains the more significant capacitance loss and resistance increase of the negative electrode compared to the respective positive.

### 3.2.3. Nonconventional Organic Electrolytes

Data regarding supercapacitors' aging and possible failure mechanisms containing nonconventional organic electrolytes are scarce. Nonetheless, some information on failure mechanisms in electrochemical capacitors containing ethyl isopropyl sulfone-based (EiPS) electrolytes can be provided (Table 1).

Chiba et al. analyzed evolved gases by gas chromatography using an H-type cell in which the positive and negative electrodes are placed in separate sections.<sup>[80]</sup> Ethane and hydrogen were determined to be the primary volatile decomposition products, originating from the decomposition of EiPS and present water traces occurring at cell voltages higher than 3.5 V. Minor amounts of propane are evolving at voltages higher than 4 V. The amount of detected CO and CO<sub>2</sub> is reported to increase slightly with increasing voltage and has been attributed to the decomposition of the carbon surface functions. Investigations by ion chromatography show that no soluble (charged or strongly polar) decomposition products of EiPS are formed by removing alkyl groups (removal of ethyl or isopropyl group). Coinciding with morphological changes determined by SEM and EDX measurements, the authors propose that the formed alkylsulfonyl radicals further undergo reactions forming a passivation layer primarily at the positive electrode surface. Measurements of the H<sub>2</sub>O content by Karl-Fischer titration showed an increase of water at both electrodes but a more significant increase in the positive compartment. Showing a neutral pH environment before aging, after floating at 4.0 V, the positive compartment shows acidic, and the negative shows alkalic pH values. The increase of OH<sup>-</sup> and H<sub>2</sub> at the negative electrode has been assigned to the decomposition of surface functions or trace water contained in the electrolyte. Since oxygen evolution has not been observed at the positive electrode (which would indicate oxidative decomposition of water), the increase in acidity has been assigned to the hydrolysis of the BF<sub>4</sub><sup>-</sup> anion, which is generating HF. Concluding, it has been shown that EiPS does not decompose by reaction with water or hydroxide but that the primary decomposition of EiPS is the removal of alkyl groups and the evolution of ethane and propane.<sup>[80]</sup>

Köps et al. investigated using EiPS in EDLCs at high voltages and temperatures.<sup>[81]</sup> By investigating the aged electrolyte by GC-MS and the aged electrodes by XRD and XPS, the authors propose several degradation mechanisms that coincide well with the previously mentioned works. GC-MS analysis of the aged electrolyte revealed that no soluble decomposition products originating from the solvent were formed. Floating at 3.0 V cell voltage showed that the formation of triethylamine occurred at temperatures higher than 80 °C. The latter has been attributed to the decomposition of the conducting salt cation (tetraethylammonium), known as the Hofmann elimination (previously described). BF<sub>4</sub><sup>-</sup> or its hydrolysis products F<sup>-</sup> and BF<sub>3</sub>(OH)<sup>-</sup> could

act as the respective base in the presented case. The authors proposed that aging processes occurring in EiPS-based EDLCs primarily lead to the formation of volatile or solid decomposition products. Subsequently, those can either outgas, precipitate from the solution, or deposit on the electrode surface. This has been validated by XPS analysis of the electrodes. Detecting non-soluble (i.e., fluorine and sulfur-containing) decomposition products on both electrodes, the formation of passivation layers at temperatures higher than +60 °C has been proposed. While resulting in pore blocking and thus capacitance-reducing effects, this layer drastically increased the electrochemical long-term stability.<sup>[81]</sup>

In summary, primary failure mechanisms of EiPS-based EDLCs are the evolution of volatile decomposition products (ethane, propane) and the deposition of insoluble decomposition products on the positive and negative electrodes.

### 3.3. Ionic Liquids Electrolytes

Ionic liquid (IL) electrolytes are a class of liquid salts consisting entirely of ions, typically organic cations and inorganic or organic anions.<sup>[2]</sup> They are also referred to as room-temperature ILs because they are characterized by having a melting point below 100 °C and are often liquid at or near room temperature.<sup>[82]</sup> Unlike traditional electrolyte solutions, ILs combine non-flammability, high chemical, thermal, and electrochemical stability, and negligible volatility.<sup>[2]</sup> In addition, they offer the benefit of having unique structures and properties and being composed solely of ions (cations and anions).<sup>[83]</sup> However, several drawbacks with most ILs, such as low ionic conductivity, high viscosity, high melting point, and limited availability, limit their big-scale use as supercapacitors electrolytes.<sup>[2,84]</sup> Furthermore, the high cost of ILs is a significant issue from an industrial perspective, as they are typically more expensive than traditional electrolytes due to their complex synthesis and purification processes.<sup>[85]</sup> Additionally, while IL-based supercapacitors have higher energy density than conventional capacitors, they still have relatively low power compared to other energy storage technologies, leading to significant voltage drop and energy loss in many practical applications.<sup>[86]</sup>

Low conductivity and high viscosity of IL-based electrolytes significantly impact (increase) the ESR values of supercapacitors, limiting their lifespan, mainly when targeting room-to-low temperature applications.<sup>[87]</sup> Nevertheless, the physical and chemical properties of ILs are tunable owing to the almost unlimited possible combinations of anions and cations.<sup>[88]</sup> In this regard, the composition of IL electrolytes can be turned to meet specific requirements of supercapacitors' performance, including reducing their degradation.

One of the most critical parameters limiting the cycle life of supercapacitors when applying ILs as electrolytes relates to their high viscosity.<sup>[88]</sup> The viscosity of ILs is much higher than that of water, decreasing with increasing temperature. Usually, higher viscosity values are reported for ILs with a small-size anion because of stronger electrostatic interactions and hydrogen bonds.<sup>[89]</sup> It has been observed that the viscosity decreases as follows: chloride Cl<sup>-</sup> > hexafluorophosphate PF<sub>6</sub><sup>-</sup> > methanesulfonate CH<sub>3</sub>SO<sub>3</sub><sup>-</sup> ≈ CH<sub>3</sub>CO<sub>2</sub><sup>-</sup> > trifluoromethanesulfonate CF<sub>3</sub>SO<sub>3</sub><sup>-</sup> > trifluoroacetate

$\text{CF}_3\text{CO}_2^-$  > bis(trifluoromethylsulfonyl)imide TFSI<sup>-</sup> for anions (with the same common cation) and piperidinium > pyrrolidinium > imidazolium for cations (with the same common anion).<sup>[90]</sup> Among the most currently implemented ILs as electrolytes for supercapacitors, imidazolium-based cations IMIm<sup>+</sup>, coupled with fluorinated (TFSI<sup>-</sup>, FSI<sup>-</sup>, BF<sub>4</sub><sup>-</sup>, PF<sub>6</sub><sup>-</sup>) anions, exhibit the highest ionic conductivity and the lowest viscosity.<sup>[91]</sup> In contrast, ILs with pyrrolidinium, Pyr<sup>+</sup> and piperidinium, Pip<sup>+</sup> type cations are known for their high electrochemical stability window.<sup>[88]</sup> However, the cations of some ILs applied in supercapacitors have a similar structure to that of surfactants. Consequently, such cations tend to accumulate in ILs like surfactants, affecting the ion mobility and the ionic conductivity of the electrolyte and limiting the cycle life of the cells. Moreover, there is a trade-off regarding conductivity/viscosity/stability window and the degradation mechanism of IL-based supercapacitors. To understand the aging or failure mechanisms of IL-based supercapacitors (Table 1), the electrochemical decomposition of ILs has been investigated using in situ infrared and electrochemical spectroscopy methods<sup>[92]</sup> and in situ XPS.<sup>[93]</sup>

The failure mechanisms of IL-based supercapacitors as solvent-free electrolytes differ from that in the conventional media, where solvent molecules distribute the charged ions.<sup>[1,83]</sup> At high charging/discharging rates, the life span of IL-based supercapacitors is lower than that of both aqueous and organic electrolyte-based ones due to the low conductivity of ILs. Many other factors limiting the long-term stability of IL electrolytes include the effects of electrode morphology and pore size and dynamics of ILs ions.

Since ILs consist entirely of ions, they have been found to be suitable electrolytes for assessing the correlation between the effective ion size, determined by the dimensions required for pore entry, and the pores' size, both factors influencing the lifespan of supercapacitors. An earlier study showed that when using porous carbon electrodes for supercapacitors, the specific capacitance decreases with increasing the length of alkyl substituent on the phosphonium cation of IL from 0.8 nm to 2 nm, demonstrating the requirement of pore-to-ion size compatibility for high cycling stability.<sup>[94]</sup> Another research showed that, when using various microporous carbons with controlled pore size and the EMImTFSI electrolyte, good cycling stability is obtained when the pore sizes match those of the ions.<sup>[95]</sup> It was also demonstrated that the specific capacitance of supercapacitors decreases when the pores are i) smaller than IL ions, hence sterically hindered from their entering, and ii) bigger than ions because they still could accommodate only one ion, while the double-layer thickness increases.<sup>[95]</sup> Thus, both research supports the assumption that elongated ions enter pores with the orientation enabling them to align their largest dimension to the pore walls.<sup>[94,95]</sup> This implies that a greater number of ions can be accommodated in pore confinement.<sup>[7]</sup>

Many authors have reported the room temperature performance of supercapacitors with various types of IL electrolytes.<sup>[96]</sup> Supercapacitors with a pyrrolidinium-based IL electrolyte were claimed to operate at a high cell voltage of 3.7 V (though this value did not account for the high ohmic drop);<sup>[97]</sup> however, the long-term performance of the cell was limited by the relatively high viscosity and low ionic conductivity of the IL (78 mPa s and 3.0 mS cm<sup>-1</sup> at +25 °C<sup>[98]</sup>). Supercapacitors with

imidazolium-based ionic liquids typically operate with a smaller cell potential of  $\leq 3.5$  V but perform better even at higher rates due to their more favorable physical properties (e.g., EMImBF<sub>4</sub> with  $\eta = 37$  mPa s<sup>[99]</sup> and  $\sigma = 14$  mS cm<sup>-1</sup> at +25 °C<sup>[100]</sup>).

Micropores may limit the practical application of IL electrolytes.<sup>[101]</sup> A symmetric cell based on common activated carbon and using the BMImBF<sub>4</sub> as the electrolyte demonstrated a good capacitive signature from +20 to 0 °C. Yet, the specific capacitance of the device was reduced by 72% between +20 °C and -20 °C.<sup>[101]</sup> Since activated carbons are dominantly microporous, the IL ions' movement within the pores is hindered, and the diffusion resistance increases with cycle number or by lowering temperature.<sup>[101]</sup> This issue can (partially) be addressed by reducing the overall diffusion path length via employing smaller-sized particles (like in activated carbon black).<sup>[102]</sup>

The beneficial effect of micropores on the EDL capacitance is well established since ions are essentially accumulated herein.<sup>[103]</sup> Nonetheless, mesopores play an essential role in ion transport,<sup>[104]</sup> and their presence leads to enhanced capacitance retention under harsh currents.<sup>[105]</sup> Therefore, electrode materials with well-fitted micropores are highly desirable for enhancing the cycle life of supercapacitors. The presence of mesopores is mandatory for the transportation of large and often anisometric IL ions, especially when targeting low-temperature applications.<sup>[101,87]</sup> To improve the cycling performance of IL-based supercapacitors, optimization of the selection of IL composition and cell design has been carried out through both experimental and theoretical understanding to provide fundamental insights into the electrochemical behavior at the IL/electrode interface.<sup>[106]</sup>

Notwithstanding, due to their relatively high melting points, single ILs are unsuitable for harsher environments found in space, aeronautics, automotive and military applications.<sup>[107]</sup> Therefore, the use of IL mixtures (binary<sup>[108,91]</sup> and ternary<sup>[87]</sup> mixtures) or the mixture of ILs with organic solvents<sup>[109]</sup> have been suggested as convenient strategies for designing suitable ILs electrolytes operating in a broader temperature range (typically from -50 °C to +80 °C). However, the performance of supercapacitors based on IL mixtures compared ILs mixed with solvents has not yet been evaluated regarding the effects of aging and performance fading. The degradation of IL electrolytes mixed with a solvent for supercapacitors can be caused by various factors such as electrochemical oxidation and reduction, chemical instability of the electrolyte, and solvent evaporation.<sup>[110,42]</sup> The presence of impurities, high operating temperatures, and exposure to light can also contribute to the degradation of the electrolyte. To mitigate these issues, it is important to use high-quality ILs and solvents and to store the electrolyte in a controlled environment to minimize exposure to external factors. Nevertheless, one may anticipate better cycling stability for supercapacitors based on electrolytes made of IL mixtures compared to those based on ILs mixed with organic solvents, as ILs' higher thermal and chemical stability helps to reduce the risk of thermal and oxidation degradation.

Overall, the long-term performance of supercapacitors based on IL electrolytes is a complex issue that requires further research and development to realize their potential and fully overcome the current limitations.



### 3.4. Quasi-Solid and Solid-State Electrolytes

Solid-state ionic conductors are less popular than their liquid counterparts as electrolytes for supercapacitors, mainly due to the moderate ionic conductivity and poor pore accessibility leading to low capacitance values.<sup>[111]</sup> Despite the reduced electrochemical performance, solid-state electrolytes are appealing to improve safety by reducing the risk of leakage, flammability, and corrosion.<sup>[112]</sup> Additionally, as most of them can bear mechanical stresses, they may enable the construction of flexible or structural capacitors for specific applications (e.g., wearable devices, aerospace, etc.).<sup>[113]</sup> While countless research papers and reviews have been published on the topic, little effort has been made to understand their fading mechanisms.

Most solid electrolytes developed for supercapacitors have been polymer based.<sup>[2]</sup> For ionic conductivity reasons, gel polymer electrolytes (GPE) are commonly preferred to solid polymer electrolytes (SPE). While in SPE, the charge is transported by the polymeric chain, in GPE, the polymer does not typically take part in the conduction mechanism but rather acts as a host scaffold that is swollen by a liquid electrolyte mixture of solvent (aqueous, organic, or ionic liquid) and salt.<sup>[2]</sup> Although GPE can, in certain conditions, maintain the properties of a solid (e.g., leakage-free, act as a separator), they are technically quasi-solid state electrolytes because of the solvent content.<sup>[112]</sup> Aqueous GPEs (hydrogels) show the same limited electrochemical stability window as the correspondent aqueous solution. The polymer and the aqueous electrolyte interaction may also cause additional fading mechanisms. The most studied GPE are hydrogels based on polyvinyl alcohol (PVA), which possess good hydrophilicity and chemical resistance.<sup>[114]</sup> PVA is compatible with alkaline (KOH) and acidic (H<sub>2</sub>SO<sub>4</sub>) electrolytes. In the case of PVA-H<sub>2</sub>SO<sub>4</sub> GPE, however, more rapid decomposition of the polymer can be observed at the high acid concentrations needed to achieve maximum capacitance. For this reason, acid-resistant GPEs based on lignocellulose (LC) have been recently developed.<sup>[115]</sup> Although hemicellulose (one of the components of LC) would still dissolve in the electrolyte upon prolonged cycling, this introduced additional pseudocapacitance due to the abundant oxygen-containing functional groups.<sup>[115]</sup>

Despite being chemically stable in a neutral environment, PVA hydrogels comprising Na<sub>2</sub>SO<sub>4</sub> salt suffered from poor mechanical strength due to a weakening of the OH bond network. To overcome this issue, PVA-PEO blends have been recently proposed.<sup>[116]</sup> As the temperature increases, PVA-based GPEs also typically suffer from increased fluidity,<sup>[2]</sup> which may lead to a short circuit if no additional spacer/membrane is physically used to separate the electrode. In general, all hydrogels are affected by dehydration issues. For example, PVA-KOH gels showed KOH crystallization upon exposure to ambient conditions, leading to massive capacitance loss.<sup>[117]</sup> Replacing KOH with TEOH (tetraethylammonium hydroxide) could substantially improve the water retention capability of the gel.<sup>[117]</sup> To increase water retention at higher temperatures, further strategies have been proposed, including cross-linking<sup>[118]</sup> and adding fillers.<sup>[2,119]</sup> Of course, being constituted mainly by water, hydrogels can hardly be employed at sub-zero temperatures without additives capable of disrupting the hydrogen bond network, thus reducing the freezing point.<sup>[120]</sup> Typically, co-solvents such

as dimethyl sulfoxide and ethylene glycol should be used for this purpose.<sup>[121]</sup>

Compared to SPE and GPE, all-solid-state inorganic conductors have received much less attention concerning their implementation in supercapacitors, with most works focusing on thin-film micro-capacitors.<sup>[122]</sup> Nevertheless, some examples of bulk-type capacitors employing sulfide (Li<sub>2</sub>S-P<sub>2</sub>S<sub>5</sub>) and oxide (0.4LiClO<sub>4</sub>-0.6Al<sub>2</sub>O<sub>3</sub>, Li<sub>1.4</sub>Al<sub>0.4</sub>Ti<sub>1.6</sub>(PO<sub>4</sub>)<sub>3</sub>) electrolytes have been reported.<sup>[123]</sup> In all cases, the operation was restricted to high temperatures (>100 °C), and the cell voltage was limited to values lower than state-of-the-art organic electrolytes (typically between 0.5 and 2 V). This suggests that, besides the limited ionic conductivity at room temperature, such solid-state electrolytes do not possess sufficient electrochemical stability. It is worth noting that Hakari et al. recently reported a high-temperature ceramic electrolyte constituted by 33Li<sub>3</sub>BO<sub>3</sub>·33Li<sub>2</sub>SO<sub>4</sub>·33Li<sub>2</sub>CO<sub>3</sub> that could sustain cell voltages up to 3 V without massive degradation.<sup>[124]</sup> At cutoff voltages comprised between 3.5 and 5 V, oxidation of the lithium oxyacid salts would then occur.<sup>[125]</sup>

So-called ionogels have also been investigated as solid-state like electrolytes in micro-supercapacitors and supercapacitors.<sup>[126]</sup> The confinement of known liquid electrolytes presents an alternative solution to pure ionic liquids using a polymer or silica confining matrix. The main drawback of such systems is their low-temperature operation, limiting their use to temperatures above 20 °C. Over 100 000 cycles have been demonstrated with virtually no fade in capacitance using silicon nanowires as electrodes, and EMIMTFSI entrapped in a silica matrix as quasi solid-state electrolyte.<sup>[127]</sup> The cycling ability is also quite fair (10 000 cycles) when used together with carbon-based electrodes, although the cycling ability seems to be improved when operated at higher temperatures (100 °C).<sup>[128]</sup> Similar solutions were proposed with pseudocapacitive electrodes in micro-supercapacitors, but a fade in capacitance occurs over 50,000 cycles without a reasonable explanation of its origin.<sup>[129]</sup>

## 4. Failure Mechanisms of Electrode Materials

### 4.1. Degradation of Carbons

Supercapacitor degradation is a complex effect of multiple reactions involving cell casing, current collector, binder, electrode material, and electrolytes.<sup>[130]</sup> The degradation of carbon materials within the electrode plays a significant role during this aging process and can involve interactions with the electrolyte and electrode foil.<sup>[11]</sup> Carbon materials supercapacitors interact with the electrolyte materials and can age by losing part of their microporosity to electrolyte decomposition products,<sup>[131]</sup> reducing surface area and thus reducing capacitance.<sup>[132]</sup> This aging process relates to the carbon particles' internal pore structure. They can additionally age by forming nonconductive electrolyte byproducts on the outside of carbon particles, resulting in loss of conductivity and an increase in ESR for the whole electrode structure.<sup>[7]</sup>

Carbon materials for supercapacitors can contain oxygenated or nitrogenated surface groups and impurities stemming from their sources or synthesis processes, such as metals and their oxides, halides, or sulfides.<sup>[133]</sup> While the maximum operating voltage is usually chosen based on the stability of the

carbon–electrolyte interface, supercapacitors still age when kept below their maximum operating voltage.<sup>[134]</sup> This behavior is attributed to the increased reactivity of the impurity-containing sites.

The commonly used porous carbon materials in supercapacitors application include activated carbons,<sup>[135]</sup> carbide-derived carbons,<sup>[136]</sup> carbon nanotubes,<sup>[137]</sup> onion-like carbons,<sup>[137,138]</sup> graphene,<sup>[139]</sup> carbon black materials,<sup>[140]</sup> and templated carbons.<sup>[141]</sup> However, the pore size of the carbon electrodes can impact the accessibility of electrolyte ions to the surface of the electrode, which affects the supercapacitor's capacitance and charge/discharge rate.<sup>[142]</sup> A mismatch between the carbon electrode's pore size and the electrolyte ions' size can lead to reduced performance and cell degradation over time.<sup>[1]</sup> For example, suppose the pore sizes of the carbon electrode are too small, the electrolyte ions may not be able to access the entire electrode surface, leading to decreased capacitance and increased resistance.<sup>[143]</sup> This can cause the supercapacitor to degrade (Table 3), reducing its overall performance.<sup>[83]</sup>

Conversely, when the pore sizes of the carbon electrode are too large, the electrolyte ions may diffuse too quickly through the electrode, leading to a decrease in capacitance and energy density.<sup>[144]</sup> This can also lead to the degradation of the supercapacitor, as the rapid diffusion of electrolyte ions can cause damage to the electrode surface.<sup>[145]</sup> Therefore, matching the carbon electrode's pore size to the electrolyte ions' size is critical in designing and operating high-performance supercapacitors with optimal energy density, power density, and cycle life.

Studies on the performance degradation of different carbon-based supercapacitors have revealed that their failure mechanisms depend highly on the type of carbon material used.<sup>[1,146]</sup> For example, in activated carbon-based supercapacitors, the loss of active material and electrolyte decomposition are the major factors contributing to performance degradation.<sup>[145,147]</sup> In contrast, carbon nanotube-based supercapacitors suffer from issues such as bundling and alignment of the tubes, resulting in the loss of conductivity and increased resistance.<sup>[148]</sup> Similarly, for carbide-derived carbon-based supercapacitors, the degradation mechanisms are related to the structural stability of the carbon material, and the surface chemistry of the carbon material plays a crucial role in the degradation process.<sup>[143,149]</sup> Onion-like carbon-based supercapacitors, on the other hand, suffer from structural deformation and surface oxidation.<sup>[138,150]</sup> Graphene-based supercapacitors exhibit high specific capacitance<sup>[108]</sup> and good cycle stability but are prone to structural defects and aggregation,<sup>[139,151]</sup> leading to decreased performance over long-time cycling. Carbon black-based supercapacitors are susceptible to particle aggregation and low electrical conductivity due to impurities in the material.<sup>[152]</sup> In templated carbon-based supercapacitors, the performance degradation is related to the stability of the template material,<sup>[153]</sup> and the carbon material's pore size distribution and surface chemistry play a crucial role in the degradation process.<sup>[144]</sup>

While carbon-based supercapacitors show great potential for energy storage applications, their performance degradation mechanisms depend highly on the type of carbon material used (Table 3). Therefore, understanding these mechanisms can aid in developing more reliable and high-performance carbon-based supercapacitors.

## 4.2. Degradation of Pseudocapacitive Metal Oxides and Metal Nitrides

In the field of electrochemical capacitors, the term “pseudocapacitance” is used to designate electrode materials, such as RuO<sub>2</sub>, that have the electrochemical signature of a capacitive electrode (such as observed with activated carbon), i.e., exhibiting a linear dependence of the charge stored with the width of the potential window, but where charge storage originates from different reaction mechanisms.<sup>[154]</sup> Indeed, the emergence of pseudocapacitance on electrode surfaces stems from rapid and reversible Faradaic reactions that involve the transfer of charge across the double layer. However, unlike in battery-type electrodes, pseudocapacitance arises in a manner where the degree of reaction,  $Q$ , is a continuous function of potential,  $V$ , leading to the development of a derivative,  $dQ/dV$ , possessing capacitance-like properties. This definition can be found in Conway's book “Electrochemical Supercapacitors: Scientific Fundamentals and Technological Applications”.<sup>[154a]</sup> Moreover, it has been explained in detail in a perspective paper on this topic.<sup>[154]</sup> Subsequently, only the materials fulfilling this definition will be examined in this paragraph. Nevertheless, only a few compounds exhibit such peculiar electrochemical signatures, including some transition metal oxides (RuO<sub>2</sub>,<sup>[155]</sup> MnO<sub>2</sub>,<sup>[156,17]</sup> Fe<sub>3</sub>O<sub>4</sub>,<sup>[157]</sup> V<sub>2</sub>O<sub>5</sub>,<sup>[158]</sup> transition metal nitrides (VN,<sup>[159]</sup> Mo<sub>x</sub>N,<sup>[160]</sup> and multicationic oxides which have been depicted in a recent review.<sup>[161]</sup>

The typical double-layer capacitance is a result of the potential-dependent accumulation of charges that are stored electrostatically (i.e., non-Faradaically) at the interfaces of the capacitor electrodes.<sup>[154]</sup> The common point between all these materials is their electrochemical signature, such as their cyclic voltammogram having a quasi-rectangular shape and a corresponding charge and discharge diagram closely similar to that of a capacitor. It must be emphasized that such peculiar properties are highlighted in aqueous electrolytes. Indeed only a few reports focus on the operation of pseudocapacitive materials in ionic liquids.<sup>[129,162]</sup>

Concomitantly to their operation as electrodes in aqueous electrolytes, pseudocapacitive materials usually show poor capacitance retention upon cycling (Table 3). Most related papers are reported on hundreds or thousands of cycles, unlike carbon-based electrodes from electrical double-Layer capacitors exhibiting over 100 000 or 1 000 000 cycles with minor capacitance fade. The exception to this assumption can be found in a few publications: Trasatti and Buzzanca<sup>[155]</sup> recognized the pseudocapacitive behavior of this RuO<sub>2</sub> film material formed on Ti with TiO<sub>2</sub>, or with Ta<sub>2</sub>O<sub>5</sub>, the cycle life in capacitor charge and discharge between 0.05 V and 1.2 V, or even to 1.40 V (RHE) under some conditions is remarkable, allowing cycling over 10<sup>5</sup> times with little degradation.<sup>[163]</sup> Recently, VN thin films were cycled in KOH electrolyte with impressive capacitance retention upon 150 000 cycles (Figure 10A).<sup>[164]</sup>

Although many studies have been published on RuO<sub>2</sub> electrodes with a large performance in capacitance, energy, and power densities in H<sub>2</sub>SO<sub>4</sub> electrolytes, the lack of reports on extended cycle life is quite puzzling. The same applies to MnO<sub>2</sub> electrodes operated in mild aqueous electrolytes (pH ≈ 7) or VN electrodes cycled in 1 M KOH (Table 3). This can be explained as redox reactions occurring at the electrode surface when cycled in

**Table 3.** Lifespan of supercapacitors based on carbon materials, metal oxides, and metal nitrides.

Capacitive or pseudocapacitive electrode material	Electrolyte	Cycling rate	Cycle number (or duration)	Capacitance retention [%]	Refs.	
Carbon	Activated carbon	1 M Na <sub>2</sub> SO <sub>4</sub>	0.3 A g <sup>-1</sup>	5000	100	[261]
		1 M Li <sub>2</sub> SO <sub>4</sub>	0.2 A g <sup>-1</sup>	10 000	99	[262]
		1 M Na <sub>2</sub> SO <sub>4</sub>	1 A g <sup>-1</sup>	20 000	97	[263]
		BMImBF <sub>4</sub>	1.5 A g <sup>-1</sup>	10 000	80	[264]
		0.5 M K <sub>2</sub> SO <sub>4</sub>	0.1 A g <sup>-1</sup>	1000	96	[265]
		1 M CsF	1 A g <sup>-1</sup>	10 000	80	[266]
		Pyr <sub>1,4</sub> B(CN) <sub>4</sub>	2 A g <sup>-1</sup>	50 000	99.8	[267]
		6 M KOH	1 A g <sup>-1</sup>	10 000	92.6	[268]
	Carbide-derived carbon	1 M H <sub>2</sub> SO <sub>4</sub>	2 A g <sup>-1</sup>	10 000	96	[269]
		1 M TEABF <sub>4</sub> /ACN	0.5 A g <sup>-1</sup>	10 000	85	[95]
	Carbon nanotubes	0.5 M Na <sub>2</sub> SO <sub>4</sub>	0.5 A g <sup>-1</sup>	1000	80	[270]
		0.8 M H <sub>3</sub> PW <sub>12</sub> O <sub>40</sub>	1 A g <sup>-1</sup>	12 000	90	[271]
		TBAP/TH	0.25 A g <sup>-1</sup>	10 000	92	[272]
		LiCl/PVA	0.1 A g <sup>-1</sup>	1000	97.7	[273]
	Onion-like carbon	2 M KNO <sub>3</sub>	25 A g <sup>-1</sup>	4000	71	[274]
		1 M Li <sub>2</sub> SO <sub>4</sub>	1 A g <sup>-1</sup>	10 000	62	[275]
		1 M TEABF <sub>4</sub> /ACN	0.5 A g <sup>-1</sup>	100 h	92	[137]
	Graphene	1 M EMImBF <sub>4</sub> /ACN	0.5 A g <sup>-1</sup>	50 000	98	[276]
		0.5 M H <sub>2</sub> SO <sub>4</sub>	0.5 A g <sup>-1</sup>	5000	94.9	[277]
	Carbon black	1.5 M TEABF <sub>4</sub> /ACN	0.75 A g <sup>-1</sup>	7000	80	[140]
		1 M BeSO <sub>4</sub>	0.2 A g <sup>-1</sup>	10 000	94	[278]
6 M KOH		5 A g <sup>-1</sup>	5000	94	[279]	
Templated carbon	1 M Li <sub>2</sub> SO <sub>4</sub>	1 A g <sup>-1</sup>	120 h	80	[141]	
	EMImFSI/EMImBF <sub>4</sub>	0.2 A g <sup>-1</sup>	10 000	80	[87]	
	6 M KOH	0.1 A g <sup>-1</sup>	4000	95.4	[280]	
	1 M Li <sub>2</sub> SO <sub>4</sub>	1 A g <sup>-1</sup>	100 000	80	[281]	
	6 M KOH	1 A g <sup>-1</sup>	75 000	80	[281]	
Metal oxides	MnO <sub>2</sub>	2 M Na <sub>2</sub> SO <sub>4</sub>	0.5 A g <sup>-1</sup>	3000	100	[282]
		1 M Na <sub>2</sub> SO <sub>4</sub>	0.5 A g <sup>-1</sup>	5000	92.4	[283]
	RuO <sub>2</sub>	H <sub>2</sub> SO <sub>4</sub>	1 A g <sup>-1</sup>	10 000	95	[282]
	Fe <sub>2</sub> O <sub>3</sub>	1 M KOH	1 A g <sup>-1</sup>	1000	84	[284]
	V <sub>2</sub> O <sub>5</sub>	1 M Na <sub>2</sub> SO <sub>4</sub>	0.5 A g <sup>-1</sup>	5000	89.7	[285]
	Fe <sub>2</sub> O <sub>3</sub>	1 M Na <sub>2</sub> SO <sub>4</sub>	1 A g <sup>-1</sup>	1000	99	[286]
	CuO	1 M Na <sub>2</sub> SO <sub>4</sub>	2 A g <sup>-1</sup>	1000	90	[287]
	TiO <sub>2</sub>	1 M Na <sub>2</sub> SO <sub>4</sub>	2 A g <sup>-1</sup>	1000	100	[288]
	TiO <sub>2</sub>	1 M KOH	1 A g <sup>-1</sup>	10 000	94	[288]
	ZnO	1 M Na <sub>2</sub> SO <sub>4</sub>	1 A g <sup>-1</sup>	5000	92	[289]
	SnO <sub>2</sub>	1 M Na <sub>2</sub> SO <sub>4</sub>	1 A g <sup>-1</sup>	5000	95	[283]
	Metal nitrides	VN	1 M KOH	100 mV s <sup>-1</sup>	150 000	98
1 M KOH			5 A g <sup>-1</sup>	10 000	100	[290]
1 M H <sub>2</sub> SO <sub>4</sub>			2 A g <sup>-1</sup>	5000	96	[291]
PVA/H <sub>3</sub> PO <sub>4</sub>			0.5 A g <sup>-1</sup>	10 000	84.7	[292]
1 M LiCl			4 A g <sup>-1</sup>	20 000	99	[293]
CrN	0.5 M H <sub>2</sub> SO <sub>4</sub>	1 A g <sup>-1</sup>	20 000	94	[294]	

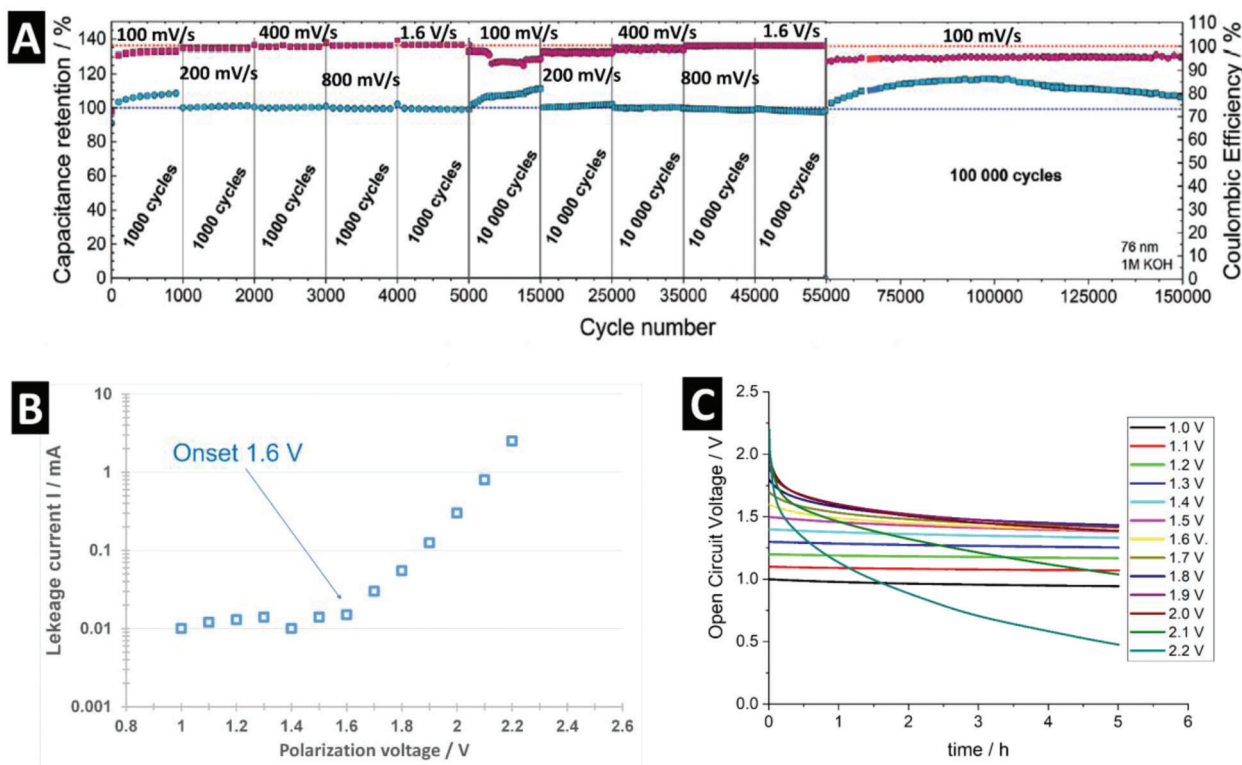


**Figure 10.** A) Evaluation of the cycling stability and rate capability of 76 nm-thick sputtered VN film in 1 M KOH. capacitance retention and Coulombic efficiency of VN film evaluated during 150,000 cycles at different scan rates (Reproduced with permission.<sup>[164]</sup> Copyright 2023, Wiley VCH). Activated carbon (-)//5 M LiNO<sub>3</sub>//MnO<sub>2</sub> (+) asymmetric supercapacitor; B) residual current recorded at different polarization voltages; C) self-discharge of the cell previously polarized at different cell voltages (A. Morel, D. Bélanger and T. Brousse, unpublished results).

aqueous electrolytes, gas evolution reactions that can damage the mechanical integrity of the electrode or the cell when operated in a sealed vial, and corrosion of the current collectors used for such electrodes. The two last causes are extrinsic to the electrode material, while the first one is intrinsic to the investigated compound. They are not systematically investigated in studies dealing with pseudocapacitive materials. Moreover, they are scarcely evidenced when only a few hundred or thousands of charge-discharge cycles are shown. This is even more critical when fast charge/discharge rates are reported since all these reactions are kinetically hindered when the operating potential window is exceeded for a very short period.

The type of electrolyte used can significantly affect the electrochemical behavior and degradation of MnO<sub>2</sub> in pseudocapacitive applications. In aqueous electrolytes, MnO<sub>2</sub> undergoes a redox reaction with H<sup>+</sup> or OH<sup>-</sup> ions, resulting in the formation of MnOOH or Mn(OH)<sub>2</sub>, which act as active sites for pseudocapacitance. Prolonged cycling in aqueous electrolytes can lead to the dissolution of MnO<sub>2</sub> particles, resulting in the loss of active sites and a decrease in capacitance.<sup>[165]</sup> In contrast, in nonaqueous electrolytes, MnO<sub>2</sub> undergoes a surface adsorption reaction with the electrolyte species, resulting in the formation of a surface-bound layer that acts as an active site for pseudocapacitance.<sup>[13,166]</sup> The non-aqueous electrolyte systems typically used with MnO<sub>2</sub> include organic solvents such as acetonitrile, propylene carbonate, and ethylene carbonate. The cycling stability of MnO<sub>2</sub> in non-aqueous electrolytes can be im-

proved by controlling the nature of the surface-bound layer and preventing its degradation.

#### 4.2.1. Redox Reactions Occurring at the Surface of the Electrode Material

Redox reactions occurring at the surface of pseudocapacitive materials have been documented in the early literature related to RuO<sub>2</sub>. Indeed, Trasatti et al. evidenced that small capacitance degradation upon cycling arises due to RuO<sub>4</sub><sup>2-</sup> formation at the high potential ends of the anodic potential excursions.<sup>[155]</sup> Irreversible Faradaic reactions have also been depicted in RuO<sub>2</sub> thin films. They seem to be located at grain boundaries, and their advanced characterization has not been carried out.<sup>[167]</sup>

The capacity reduction of MnO<sub>2</sub>-based electrodes in neutral aqueous electrolytes has been explored in various studies.<sup>[168]</sup> Most of these studies aim at evidencing side reactions occurring when incursions out of the operating potential window of the electrode occur. One of the most commonly reported causes for such redox reactions is the reduction of Mn<sup>4+</sup> to Mn<sup>3+</sup> below 0 V vs. Ag/AgCl, which further leads to the dismutation of Mn<sup>3+</sup> as Mn<sup>4+</sup> and Mn<sup>2+</sup> soluble species. Upon subsequent oxidation, Mn<sup>2+</sup> is deposited as MnO<sub>2</sub> on the top surface or pristine MnO<sub>2</sub> particles. This aligns with a reported change in the microstructure of MnO<sub>2</sub> grains upon repeated cycling.<sup>[169]</sup> The initial dense oxide coating has evolved into a petal-like

morphology after cycling, typical of dissolution/deposition processes.<sup>[170]</sup> Such behavior can be predicted from the reading of Pourbaix diagrams. To mitigate the fading problem in MnO<sub>2</sub>-catalyzed electrodes, the accumulated electrons in the oxide electrode are transferred to dissolved oxygen molecules through the oxygen reduction reaction (ORR) to prevent the formation of Mn(II) species. This strategy is effective as the lower potential limit is close to the onset potential of the ORR. Increasing the dissolved oxygen content in the electrolyte or using the Ti(IV)/Ti(III) redox pair as a charge-transfer mediator to enhance the electrocatalytic activity of MnO<sub>2</sub> for ORR are two solutions that have induced significant improvement of capacitance retention upon cycling and 10 000 cycles have been demonstrated instead of 3000 for the pristine electrode design.<sup>[171]</sup>

The degradation mechanism of MnO<sub>2</sub> electrodes mainly relies upon the type of MnO<sub>2</sub> polymorph used as electrode material. Increasing the operating temperature of the cryptomelane electrode resulted in a higher degree of structural distortion caused by the Jahn–Teller distortion of MnO<sub>6</sub> octahedra. This structural distortion had an adverse effect on the redox reactions that involved the reversible intercalation of K<sup>+</sup> into the MnO<sub>2</sub> lattice. It led to a significant increase in the charge-transfer resistance at the solid-electrolyte interface, thus accelerating capacity fading.<sup>[172]</sup> Cycling increased the electrical resistivity of the layered birnessite electrode, which can be assigned to the large cyclic volume variations in the birnessite structure.<sup>[173]</sup> Such volume variations induce debonding of the binder from the particulate components of the electrode and a loss of active material. Such behavior is drastically emphasized when increasing the operating temperature from +25 °C to +50 °C.

The same effect of cation reduction in transition metal oxides while cycling the electrodes can be depicted from the literature on Fe<sub>3</sub>O<sub>4</sub> pseudocapacitive electrodes. The reduction current increase below –0.6 V versus Ag/AgCl in neutral aqueous electrolytes is related to the irreversible reduction of Fe<sup>3+</sup> to Fe<sup>2+</sup>. Although such a reduction current tail is systematically observed in the studies related to magnetite, the influence of this reduction reaction has not been systematically investigated.<sup>[174]</sup> Multicationic compounds involving Fe active cation and spectator cations, such as W in FeWO<sub>4</sub>, have demonstrated an improved cycle life. However, after 10 000 cycles, only a slight amorphization of the surface of the particles was evidenced by electron diffraction and high-resolution electron microscopy.<sup>[175]</sup>

Transition metal nitrides are also affected by redox reactions occurring at their surfaces. VN was initially proposed as a pseudocapacitive electrode in an aqueous KOH electrolyte using quite a wide potential window, namely –1.2 to 0 V versus Hg/HgO. The related electrodes exhibited a drastic capacitance fade upon only a few hundred cycles.<sup>[176]</sup> This potential window must be narrowed from –1.0 to –0.4 V versus Hg/HgO to avoid excessive surface oxidation of vanadium species at the electrode surface.<sup>[177]</sup> The charge storage mechanism was also evidenced.<sup>[178]</sup> This led to materials engineering with the deposition of thin film electrodes by magnetron sputtering in a nitrogen-rich reactive atmosphere, thus drastically decreasing the amount of vanadium oxide species at the surface. After that, 150 000 cycles were demonstrated with virtually no fade in capacitance (Figure 10A).<sup>[164]</sup>

All these examples should promote the in-depth electrochemical investigation of pseudocapacitive electrodes, especially re-

garding the useful and safe electrochemical window that can be used to avoid redox reactions at the surface of the particles of the active material. To reach this goal, a slow cycling rate (<5 mV s<sup>–1</sup>) must be used to unveil these Faradaic reactions and try to find alternative solutions to cancel or avoid them.

Not only redox reactions involving the active material are responsible for capacity fade, but a too-wide potential window is also the source of problems since gas evolution reactions are likely to occur.

#### 4.2.2. Gas Evolution Reactions

When using aqueous electrolytes, gas evolution reactions concomitant to water electrolysis are commonly seen in pseudocapacitive electrodes.<sup>[169]</sup> As for Faradaic reactions that can occur at the electrode surface, kinetic is a major parameter that can help to evidence or to hide the presence of OER and/or HER. Many studies on pseudocapacitive electrodes in a given potential window have reported a large irreversible capacity upon oxidation or reduction at a slow scan rate related to HER or OER, but without a detailed discussion.

The volume of generated hydrogen and oxygen gases have been evaluated from linear sweep voltammetry plots in a (–) asymmetric activated carbon//0.65 M K<sub>2</sub>SO<sub>4</sub>//MnO<sub>2</sub> (+) cell.<sup>[179]</sup> When operated up to a 2.2 V cell voltage, the volumes of O<sub>2</sub> and H<sub>2</sub> gases evolved per cycle are 2.62 nL cm<sup>–2</sup> (cm<sup>2</sup> of electrode loaded at 5 mg cm<sup>–2</sup>) and 1.71 μL cm<sup>–2</sup>, respectively. For cells with significantly higher areas and operated over many charge/discharge cycles, such an amount of gases is not negligible. This will lead to a pressure build-up in the cell and a potential hazard due to the combination of hydrogen and oxygen in a confined volume.<sup>[168]</sup> When the upper cell voltage is limited to 1.5 V, these quantities decrease to reasonable numbers, thus allowing a longer cycle life with 20% energy fade after 10 000 cycles instead of 4000 when the cell was operated at 2.2 V. A systematic study of the optimum operating cell voltage was conducted for such asymmetric design (Figure 10B,C). The onset of residual current due to gas evolution reaction occurs above 1.6 V (Figure 10B). The self-discharge measurements also suggest that the safe operating cell voltage for the asymmetric design is close to 1.6 V (Figure 10C). The same findings were reported by other groups.<sup>[180]</sup>

Irreversible reactions are not the only concern with gas evolution reactions: the bubbles generated at the electrode surface can lead to mechanical degradation of the electrode with the particles of active materials falling apart, disconnected from the binder and conductive additive by the action of nanoscopic bubbles.<sup>[181]</sup> This is a common feature that can be experimentally evidenced. A MnO<sub>2</sub> electrode cycled within a too-wide potential window leads to a brownish deposit at the bottom of the electrochemical cell due to mechanical disaggregation induced by OER.<sup>[168]</sup>

The gas formation can also occur when chloride-based electrolytes such as aqueous KCl or NaCl are used.<sup>[169]</sup> The oxidation reaction leads to the formation of chlorine gas which builds up pressure inside sealed cells and generates the opening of coin cells, as observed by Mosqueda et al.<sup>[182]</sup> The same behavior is observed and amplified with aqueous bromide-based electrolytes. Gas evolution is generally not commonly studied whenever

pseudocapacitive electrodes are used with aqueous electrolytes. The main reason may be that the experiments are often conducted in open beaker-type cells with no visible effect on the cycling ability of the electrode material. As previously stated, for intrinsic Faradaic reactions, a slow cycling rate must be used to unveil these gas evolution reactions and help to tune the safe electrochemical window. Gas evolution reactions can also impact the current collector, which becomes a potential source of trouble mainly due to its use in aqueous electrolytes.

#### 4.3. Degradation of 2D Materials

Since early work on the exfoliation of graphene in 2004,<sup>[183]</sup> 2D materials have been attracting significant attention thanks to the qualitative changes in their physical and chemical properties due to the quantum size effect related to their nanosized thickness.<sup>[184]</sup> The 2D structure of graphene consists of sp<sup>2</sup>-hybridized carbon atoms in planar monolayers, characterized by a high conductivity (owing to enhanced electron mobility), very good mechanical strength, chemical stability, and a high accessible surface, with theoretical specific surface area value above 2500 m<sup>2</sup> g<sup>-1</sup>.<sup>[185]</sup> However, the restacking of graphene sheets by  $\pi$ - $\pi$  interactions is a primary limiting factor that minimizes its intrinsic surface area and application as electrode materials for supercapacitors.<sup>[186]</sup> Stoller et al. explored the direct exploitation of graphite into graphene oxide with chemical modifications for supercapacitors applications.<sup>[187]</sup> Although the authors did not report on the lifespan of the obtained devices, the resistive character of the cells observed from the cyclic voltammograms and Nyquist plots is a sign of the poor cycling stability of such capacitors. The degradation of graphene-based supercapacitors is mainly due to the preparation method of graphene,<sup>[188]</sup> which is based on the chemical exfoliation of graphite with strong oxidants, giving graphite oxide.<sup>[185,186]</sup> Next, graphite oxide is reduced to obtain graphene, which tends to restack and contains a relatively high amount of residual oxygen.<sup>[189]</sup> Consequently, the lifespan of supercapacitors using graphene electrodes in various electrolytes is limited by more or less oxygen amount and the number of stacked layers.<sup>[184]</sup>

Another important family of 2D materials in supercapacitor applications is transition metal dichalcogenides (TMDs).<sup>[190]</sup> TMDs are compounds of the type MX<sub>2</sub>, where M is a transition metal atom (Mo, W, etc.), and X is a chalcogen atom (S, Se, or Te).<sup>[191]</sup> TMDs exhibit versatile chemistry and have remarkable properties like large surface area, high electrical conductivity with variable oxidation states, and tunable electronic properties from metallic to insulating depending on their composition, crystal symmetry, and the number of layer.<sup>[190,192]</sup> Among the currently implemented TMDs as supercapacitors electrodes, molybdenum disulfide (MoS<sub>2</sub>) is mainly used due to its unique property like its small size and high conductivity.<sup>[191,193]</sup> MoS<sub>2</sub> can be used as pure or to enhance the conductivity of composite electrodes.<sup>[192]</sup> Some authors reported pure MoS<sub>2</sub> and its composites as electrodes for supercapacitors.<sup>[194]</sup> Compared to MoS<sub>2</sub> electrodes, the composites demonstrated higher specific capacitance and better capacity retention after 5000 GC/GD cycles.<sup>[194]</sup> The improved cycle stability of the composite material was attributed to the smooth mass diffusion and rapid electron transfer within the electrode.<sup>[194]</sup>

**Table 4.** Lifespan of various supercapacitors based on various 2D materials, including reduced graphite oxide (rGO), transition metal dichalcogenides (TMDs), layered metal oxides (LMOs), and transition metal carbides/nitrides (MXenes) and MXene-based composite electrodes.

Electrode	Cycling rate	Cycle number	Capacitance retention (%)	Reference
rGO	50 mV s <sup>-1</sup>	600	100.0	[186]
rGO/CoMn <sub>2</sub> O <sub>4</sub>	5 A g <sup>-1</sup>	3,000	90.2	[186]
rGO/MnO <sub>2</sub> -CNTs	4 A g <sup>-1</sup>	1,200	88.5	[189]
MoS <sub>2</sub>	1 A g <sup>-1</sup>	5,000	83.5	[194]
MoO <sub>4</sub> @MoS <sub>2</sub>	1 A g <sup>-1</sup>	5,000	88.4	[194]
MoS <sub>2</sub> @rGO	8 A g <sup>-1</sup>	4,000	92.0	[196]
MoS <sub>2</sub> /NiS	1 A g <sup>-1</sup>	5,000	81.5	[196]
MoS <sub>2</sub> @N-rGO	1 A g <sup>-1</sup>	50,000	94.5	[196]
Ni <sub>3</sub> S <sub>2</sub> @rGO@NiAl	1 A g <sup>-1</sup>	10,000	87.7	[196]
MoSe <sub>2</sub> @VACNTF	15 A g <sup>-1</sup>	5,000	84.1	[196]
MoSe <sub>2</sub> @Ni	1 A g <sup>-1</sup>	1,500	100.0	[196]
rGO/MXene	100 A g <sup>-1</sup>	40,000	90.0	[215]
rGO/Ti <sub>3</sub> C <sub>2</sub> T <sub>x</sub>	1 A g <sup>-1</sup>	10,000	100.0	[215]
CNTs/D-Ti <sub>3</sub> C <sub>2</sub>	5 mV s <sup>-1</sup>	10,000	100.0	[215]
MXene/CNTs	5 mV s <sup>-1</sup>	10,000	86.3	[215]
MXene/Ni-Fe	0.2 mA cm <sup>-2</sup>	10,000	90.0	[215]
MXene/V <sub>2</sub> O <sub>5</sub>	1 mA cm <sup>-2</sup>	6,000	93.0	[215]
MXene@cotton/PPy	1 A g <sup>-1</sup>	10,000	87.0	[215]
MXene/PPy/PVA	1 A g <sup>-1</sup>	1,000	83.0	[215]
MXene/PSS/PEDOT	5 mV s <sup>-1</sup>	10,000	95.0	[215]
MXene/PEDOT	1 A g <sup>-1</sup>	10,000	96.5	[215]
MXene/MnO <sub>2</sub>	10 mV s <sup>-1</sup>	10,000	85.0	[215]
MXene/MnO <sub>2</sub> /CC	5 A g <sup>-1</sup>	10,000	83.0	[215]
MXene/MnO <sub>2</sub>	1 A g <sup>-1</sup>	1,000	96.0	[215]
MXene@HHK-CC	0.5 mA cm <sup>-2</sup>	1,000	94.2	[215]
MXene/carbon cloth	1 mA cm <sup>-2</sup>	8,000	97.0	[215]

This claim was later linked to low charge transfer resistance for the hierarchical core-shell nanostructure.<sup>[195]</sup> **Table 4** summarizes the cycling stability performance of various supercapacitors based on TMDs and other 2D materials.<sup>[186,194,196]</sup>

Beyond graphene and TMDs, various 2D materials have also attracted considerable attention as supercapacitors' electrode materials due to their unique physical and chemical properties. These materials include layered metal oxides (LMOs),<sup>[197]</sup> layered oxides and hydroxides,<sup>[198]</sup> transition metal nitrides (TMNs),<sup>[199]</sup> transition metal selenides (TMSSs),<sup>[200]</sup> transition metal carbides/nitrides (MXenes),<sup>[201]</sup> and layered metal-organic frameworks (MOFs). Among them, 2D MXenes are a rapidly growing and very large family of 2D layered metal carbides, carbonitrides, and nitrides, typically obtained by MAX phase etching.<sup>[202]</sup> The general formula of MXene is M<sub>n+1</sub>X<sub>n</sub>T<sub>x</sub>, where n+1 (n = 1–3) represents the layers of early transition metals (M = Sc, Ti, Zr, V, Nb, Cr, or Mo) interwoven with n layers of carbon or nitrogen (X), and T<sub>x</sub> is introduced by liquid-phase etching.<sup>[203]</sup> Accordingly, MXenes have wealthy surface functional groups (e.g., -OH, -F, -O), which provide a considerably large number of active sites with great potential for efficient loading of active materials and surface modification.<sup>[201]</sup> Hence, MXenes have high

electrical conductivity, hydrophilicity, and ion intercalation.<sup>[204]</sup> Furthermore, their high mechanical strength and volumetric specific capacity are beneficial for preparing binder-free electrode materials, increasing the interest in using MXenes in supercapacitor applications.

Among the large MXene group,  $\text{Ti}_3\text{C}_2\text{T}_x$  has been extensively studied for supercapacitors and capacitive deionization.<sup>[205]</sup> However, numerous MXenes, including  $\text{Ti}_3\text{C}_2\text{T}_x$ , are synthesized by a chemical etching method,<sup>[203]</sup> usually using nonenvironmentally friendly fluorine-containing solutions,<sup>[206]</sup> which often leads to obtaining materials with many defects.<sup>[207]</sup> Additionally, MXene sheets tend to close packing, restricting electrolyte ion transport and diffusion, thus affecting the energy storage performance of MXenes-based supercapacitors and limiting their lifespan. Besides, MXenes easily oxidize, especially at high positive potentials, reducing supercapacitors' cycle life and efficiency. To address these issues and develop MXenes-based supercapacitors with excellent performance and long cycle life, composite electrodes combining MXenes with carbon nanomaterials, metal oxides, or conductive polymers have been proposed and extensively studied.<sup>[208]</sup> Composite materials offer the advantage of weakening the MXene heavy stacking phenomenon and improving the oxidation resistance, thus boosting supercapacitors' energy density and cycle life.<sup>[209]</sup>

Zhang et al. reported a symmetric supercapacitor based on composite MXene@carbon electrodes with excellent capacitance retention.<sup>[208]</sup> The authors prepared the composite material by introducing layered porous carbon into  $\text{Ti}_3\text{C}_2\text{T}_x$  films. The former acted as the pillar to create a rapid passageway for good contact between  $\text{Ti}_3\text{C}_2\text{T}_x$  and ions. As a result, the supercapacitor with 60% layered porous carbon in the  $\text{Ti}_3\text{C}_2\text{T}_x$ @HPC composite with 6 M KOH aqueous electrolyte retained 86% of its initial capacitance after 10 000 charge/discharge cycles at a current density as high as  $10 \text{ mA cm}^{-2}$ . Sun and co-workers also reported a symmetrical supercapacitor based on composite hierarchical porous  $\text{Ti}_3\text{C}_2\text{T}_x$ /biomass-derived carbon fibers (MXene/CF) with excellent electrochemical and cycling stability.<sup>[210]</sup> After 5000 galvanostatic charge/discharge cycles, the device retained 99.8% and 63.9% of its initial capacitance at high rates of  $10 \text{ A g}^{-1}$  and  $100 \text{ A g}^{-1}$ , respectively. Zhang et al.<sup>[208]</sup> reported very high cycling stabilities of composite MXene electrodes obtained via surface coating of MXene, which simultaneously improved the conductivity and ion penetration within the electrodes. Liu et al. demonstrated that a supercapacitor with electrodes made of  $\text{Ti}_3\text{C}_2\text{T}_x$  combined with nanoscale polymer poly(3,4-ethylene dioxythiophene) (PEDOT) additive exhibits improved capacitive performance and good cycling stability (96.5% capacitance retention at  $10 \text{ A g}^{-1}$  after 10 000 cycles of charge/discharge process) then the device made of pristine  $\text{Ti}_3\text{C}_2\text{T}_x$ .<sup>[211]</sup> The long cycle life of the  $\text{Ti}_3\text{C}_2\text{T}_x$ @PEDOT symmetric cell compared to the capacitor made with the original  $\text{Ti}_3\text{C}_2\text{T}_x$  material was linked to the synergetic effect between PEDOT and the unique accordion-like structure of  $\text{Ti}_3\text{C}_2\text{T}_x$  with sufficient interlayer space for doping with sulfur-containing substances, facilitating charge transfer processes. Many other symmetric supercapacitors have been reported with various lifespans in different  $\text{Ti}_3\text{C}_2\text{T}_x$  composites with  $\text{MnO}_2$ ,<sup>[208]</sup>  $\text{Co}_3\text{O}_4$ ,<sup>[212]</sup>  $\text{TiO}_2$ ,<sup>[208]</sup>  $\text{CuS}$ ,<sup>[208]</sup> or  $\text{Cu}_{0.5}\text{Co}_{0.5}\text{Se}_2$ ,<sup>[208]</sup> among others.

Despite the improved electrochemical stability of MXene-based composite electrodes in symmetric supercapacitors, their

voltage window is only about 0.6 V due to the oxidation of the positive electrode. Therefore, pseudocapacitive materials are suggested in asymmetric cell configurations to increase the operating voltage of MXene-based supercapacitors. A 1.6 V asymmetric capacitor based on a negative  $\text{Ti}_3\text{C}_2\text{T}_x$ /multiwalled carbon nanotube electrode and a positive polypyrrole (PPy) coated multiwalled carbon nanotube electrode was reported with 94% capacitance retention after only 1000 cycles in 1 M  $\text{Na}_2\text{SO}_4$  electrolyte.<sup>[213]</sup> Jiang et al. demonstrated an asymmetric pseudocapacitor design by combining positive  $\text{RuO}_2$  with negative  $\text{Ti}_3\text{C}_2\text{T}_x$  electrodes.<sup>[214]</sup> The  $\text{RuO}_2/\text{Ti}_3\text{C}_2\text{T}_x$  cell operated at 1.5 V in an acidic 1 M  $\text{H}_2\text{SO}_4$  electrolyte and retained 86% of its initial capacitance after 20 000 charge/discharge cycles at a high specific current of  $20 \text{ A g}^{-1}$ .<sup>[214]</sup>

Implementing MXenes as electrodes for flexible supercapacitors has been broadly studied in recent years.<sup>[201,215]</sup> In flexible supercapacitors, MXenes play a multifunctional role in the electrodes. They can be used not only as active material but also as a binder, flexible backbone, and conductive additive.<sup>[201]</sup> The combination of  $\text{Ti}_3\text{C}_2\text{T}_x$  MXene and rGO for preparing composite electrodes for flexible supercapacitors was reported with excellent cycling stability of 90% capacitance retention after 40 000 cycles at a high current of  $100 \text{ A g}^{-1}$  (Figure 11A).<sup>[215]</sup> The lifespan of the main performance of MXene-based flexible supercapacitors at different rates is summarized in Table 4.<sup>[215]</sup>

The main factor limiting the long-time stability of supercapacitors based on MXene electrodes is the oxidation of MXene with large surface functional groups during long-time cycling. This hypothesis was proven by post-analysis on MXene electrodes, where the SEM images revealed many  $\text{TiO}_2$  particles on the MXene nanosheet.<sup>[210]</sup> The same authors implemented inductively coupled plasma mass spectrometry to test titanium content in the electrolyte after the long-term cycling of MXene-based supercapacitors. The results revealed a significantly higher titanium content in the electrolyte after cycling a cell made with pristine MXene electrodes compared to the supercapacitors made of composite MXene@carbon electrodes.

## 5. Beyond Electrolyte and Electrode Degradations

### 5.1. Degradation of Interfaces/Interphases

The contact area between the electrode and the electrolyte is of great importance as the place where the energy storage of supercapacitors takes place. While the 2D surface between the phases is described as an interface, this concept can be expanded to a 3D model with a small volume. This so-called interphase includes more than the first atomic layer of the electrode surface and extends into the electrolyte.

While, within this interphase, the double-layer is formed in the case of EDLCs, for pseudocapacitive materials, the charge-storing redox reactions occur.<sup>[11]</sup> Considering this, the nature and intactness of electrode/electrolyte interphases play a crucial role in the electrochemical performance of supercapacitors and their ability to store charges and energy. At the same time, the interphase is the primary reaction site for reduction and/or oxidation decomposition reactions due to the availability of the necessary energy from charges and reactive chemical species from the electrolyte.<sup>[72]</sup> Thus, the decomposition products within the

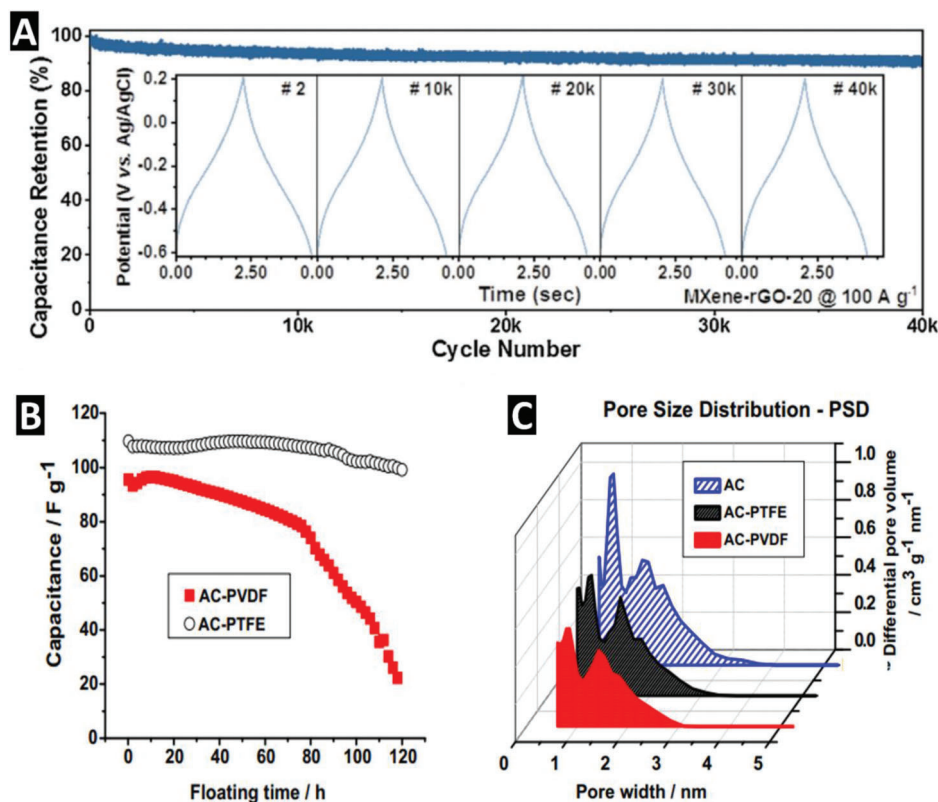


**Figure 11.** A) Cycling stability of MXene/rGO-based flexible supercapacitor at  $100 \text{ A g}^{-1}$  in  $3 \text{ M H}_2\text{SO}_4$  electrolyte. The inset represents the GC/GC obtained after 2, 10 000, 20 000, 30 000, and 40 000 cycles. Reproduced with permission.<sup>[215]</sup> Copyright 2020, Elsevier. B) Capacitance of AC/AC supercapacitors with PTFE and PVDF binders plotted versus floating time at  $1.6 \text{ V}$  and room temperature in  $1 \text{ M NaNO}_3$  electrolyte. C) QSDFT pore size distribution of activated carbon (AC) powder, AC-PTFE, and AC-PVDF electrodes. Reproduced with permission.<sup>[223]</sup> Copyright 2014, Elsevier.

electrolyte and on the electrode surface originate from the electrode/electrolyte interphase. When supercapacitors age, not only do the electrode materials and electrolyte components decompose, but also the interphase between these altered systems degrades. This has various effects, such as deteriorated electron conductivity, reduced surface area, or accessibility.<sup>[12]</sup> The degraded interphase has a detrimental effect on the performance of the aged supercapacitors, which can be observed in decreasing capacitance and energy and increasing resistances.

Different decomposition products have different impacts on the degradation of the electrode/electrolyte interphase. By forming gaseous decomposition products, which are trapped on the electrode surface, the electrode and electrolyte are separated and unable to form an interphase in these areas.<sup>[50,74]</sup> Thus, the energy storage mechanisms are inhibited at these specific locations. Additionally, the deposition of insoluble decomposition compounds on the electrode surface strongly influences the electrode/electrolyte interphase. The decomposition products' surface area reduction and passivation effects complicate the efficient contact between the active electrode material and electrolyte.<sup>[80]</sup> While this type of separation of reaction site and electrolyte compounds is greatly beneficial in LIBs and enables their proper function by forming an SEI, forming a passive layer leads to a significant loss in energy storage capacity for surface-based energy storage processes.<sup>[216]</sup> This connection can be highlighted when considering electrolytes based on EIPS,

which tend to form a passive layer on the electrode surface at higher temperatures.<sup>[81]</sup> With the degradation of the original microstructure in the first hours of operation, the capacitance of the EDLC decreases significantly. However, it results in less decomposition in the further operation of the device. This being said, the materials of the supercapacitor and their forming decomposition products directly impact the integrity of the respective electrode/electrolyte interphase. Upon their degradation, the device's electrochemical performance is significantly affected due to the strong connection between the interphase and the surface-based energy storage mechanisms in supercapacitors.

## 5.2. Effect of Pores Blocking and Functional Groups

The active materials for preparing supercapacitors electrodes are in a powder state and, in some cases, have relatively low electronic conductivity. Therefore, a few percent of a conductive additive, such as carbon black, is generally added to improve the electrode conductivity. Moreover, a polymer binder is often implemented to ensure the mechanical strength of all the electrode components, the particles' cohesion, and the electrode's adhesion to the current collector.<sup>[217]</sup> However, several limitations have risen due to the use of polymer binders in supercapacitors electrode fabrication: i) polymer binders block part of the pores of the porous electrodes, reducing the available



surface area, which affects the capacitance and lifespan of the cells.<sup>[217,218]</sup> ii) Polymer binders are electrical insulators, increasing the electrical resistance of the electrodes, which reduces the power density of supercapacitors.<sup>[219]</sup> iii) Binders and conductive additives typically occupy 5–25% of the electrode mass with no capacitance benefit, which is unfavorable to the energy density of supercapacitors.<sup>[220]</sup> (iv) Mainly used binders contain fluorine, generating highly toxic fluorinated compounds upon disposal by incineration, which are not ecofriendly. v) Electrodes prepared with polymer binders have insufficient strength for fabricating flexible supercapacitors applicable in wearables and flexible electronics, limiting their commercial application.<sup>[217,218,221]</sup>

Among the binders used for supercapacitors electrode preparation, polyvinylidene fluoride (PVDF) and polytetrafluoroethylene (PTFE) are mainly considered owing to their high electrochemical stability and binding capability.<sup>[222]</sup> However, the capacitance and life span of carbon/carbon supercapacitors with electrodes prepared using PTFE binder were higher than that of PVDF-based electrodes (Figure 11B).<sup>[223]</sup> The better cycle life and higher capacitance of PTFE-based electrodes are due to the difference in porosity of the two types of electrodes (Figure 11C). Compared to the pristine carbon powder, the PVDF-based electrodes lost 22% of their total pore volume against only 9% loss observed for the electrode made with PTFE binder.<sup>[223]</sup> Moreover, the specific surface area of the PVDF-based electrodes was 522 m<sup>2</sup> g<sup>-1</sup> lower than the initial carbon powder against 231 m<sup>2</sup> g<sup>-1</sup> drops for the PTFE ones. Hence, although it cannot be extrapolated that PTFE is a better binder than PVDF for all types of supercapacitors electrode preparation, researchers should consider the gas analysis data of the electrodes instead of the original powder.

PVDF was also found to be the best binder for pseudocapacitive materials (including transition metal sulfides and MXene) because PVDF can form separate domains within the composite electrode, leaving the surface of metal oxides free while enhancing the ionic transport through the electrode material and increasing the charging/discharging reactions.<sup>[224]</sup> However, the electrochemical performance of the cell is hindered by factors such as inadequate cyclic stability, low electrical conductivity, poor mechanical stability, and low specific surface area.<sup>[224,225]</sup> Therefore, different polymer binders were proposed to improve the electrochemical performance of metal oxides-based supercapacitors, of which PVDF and its copolymers were found more suitable for fabricating electrodes.<sup>[225,226]</sup> It was shown that incorporating the PVDF/graphene composite binder can bridge the gap between the MnO<sub>2</sub> spheres and create a network structure, thereby enhancing the conductivity of the pseudocapacitive electrode.<sup>[224,227]</sup>

Some authors proposed to replace the insulating fluorinated polymer binders with reduced graphene oxide (rGO)<sup>[228]</sup> or environmentally benign and economically viable water-soluble polymers like polyacrylic acid (PAA),<sup>[229]</sup> PVA,<sup>[230]</sup> polyvinylpyrrolidone (PVP),<sup>[220]</sup> cellulose-derivatives as sodium-carboxymethyl cellulose (CMC),<sup>[231]</sup> bacterial cellulose (BC),<sup>[232]</sup> or mixtures of polyvinylpyrrolidone/polyvinyl butyral (PVP/PVB).<sup>[229]</sup> However, the mechanical strength of these electrodes is inadequate for their consideration in flexible supercapacitors. In addition, electrodes prepared with such binders have relatively low electronic conductivity and poor stability. To address these challenges, efforts have been made to propose binder-free MXene

electrodes for supercapacitors.<sup>[233]</sup> Various strategies for preparing binder-free electrodes and composite electrodes based on metal-organic frameworks (MOFs) have been developed and recently reviewed.<sup>[234]</sup> Electrospinning has emerged as an advanced tool for fabricating binder-free, scalable, and suitable supercapacitor electrodes.<sup>[235]</sup> Free-standing carbon nanofiber electrodes and composite electrodes prepared with the electrospinning technique are highly conducting, flexible, and hold enormous potential for use in wearable electronic devices. A recent critical review on electrospinning-derived electrodes and their applications in supercapacitors can be found in ref.[236] Nevertheless, the lifespan of most supercapacitors based on binder-free electrodes is limited to less than 10 000 galvanostatic charge/discharge cycles.

Apart from binders, the life span of supercapacitors electrodes deteriorates due to the presence of surface functional groups in the electrodes. In carbon/carbon supercapacitors, the functional groups generally detected on the surface of carbon materials contain oxygen, hydrogen, nitrogen, and/or other heteroatoms.<sup>[133]</sup> Those groups include carboxyl, phenol, hydroxyl, lactone, amine, amide, pyridine, lactam, pyrrole, carbonyl, ether, pyrone, and sulfonic acid.<sup>[237]</sup> In addition, the wettability of the supercapacitors electrode can be affected by the surface groups, which impact the electrochemical performance of the cell through Faradaic contributions (considerable capacitance enhancement).<sup>[238]</sup> Yet, surface functional groups should be controlled before using electrode material for supercapacitors.

### 5.3. Corrosion, Anodic Dissolution, and Passivation of Current Collectors

#### 5.3.1. Current Collectors for Supercapacitors

The current collector material requirements are incredibly complex to provide stable support for the active material coating and a low-resistive distribution of charges while ideally being inert in the cell environment and low-priced. While current collectors do not play an active role in the charge storage mechanisms of supercapacitors, the choice of material for the specific application can significantly affect the overall performance of the energy storage device. Therefore, various materials, from widely used metals to polymers, ceramics, or carbons, have been investigated for their use as current collectors in supercapacitors.<sup>[239]</sup> For supercapacitors based on organic electrolytes, such as those commercially available, aluminum is the most commonly used current collector material due to its high availability at low costs, low electric resistivity, and good stability against most materials used in supercapacitors.

The aging mechanisms of supercapacitors' current collectors can be divided into corrosion and anodic dissolution. While corrosion is the spontaneous reaction of the current collector with the surrounding compounds and relies on their reactivity and forming reaction products, anodic dissolution requires a current to oxidize the current collector.<sup>[240]</sup> Due to the widespread use of aluminum as a current collector, the specific aging of aluminum in energy storage devices has already been investigated in detail, especially for batteries and supercapacitors. Naturally, aluminum is considered corrosion-resistant due to an oxide layer that forms on the aluminum surface when in contact with air. Although this

oxidation by air is a corrosive process of the aluminum surface, it prevents the material from further corrosion after forming a stable, protective layer. Since aluminum oxides are additionally insoluble in water and organic solvents, the properties of the protective passivation layer can be exploited to promote the integrity of the current collector in the cell environment. However, the solubility of the oxide layer in strong acids and bases and its ability to form complexes can lead to the destruction of the protective layer.<sup>[241]</sup> In addition to the formation of aluminum oxides, the aluminum current collector can be further protected by a passivation layer of aluminum fluoride containing  $\text{AlF}_3$ .<sup>[242]</sup> To form a layer of aluminum fluoride on top of the existing oxide layer, the current collectors need to be fluorinated by a species such as HF, which can be realized by the addition of HF as an additive to the electrolyte or by in situ HF formation through the decomposition of the conductive salt or the solvent.<sup>[243]</sup> Like the oxidation of aluminum, this fluorination process is also considered a corrosion process. The aluminum current collector's corrosion resistance can also be enhanced by the design of artificial protective layers. These can be realized by magnetron sputter deposition of ceramics such as chromium nitrides and significantly improve the oxidative stability of aluminum. However, these coatings can influence electrolyte degradation and overall cell performance.<sup>[244]</sup>

Despite the passivation possibilities aluminum offers, this current collector material is not unsusceptible to aging. Especially at voltages  $>3.0$  V, anodic dissolution of the current collector can occur, while the damage's extent is directly related to the strength of the current.<sup>[245]</sup> Anodic dissolution of aluminum current collectors results in pitting holes in the surface and, thus, less favorable charge transport. Extensive research over the last few years revealed the strong influence of the electrolyte on the aging behavior of aluminum current collectors. Thus, the electrolyte (solvent) and the salt ions (anion and cations) play a vital role in the degradation processes. Since the solubility of forming aluminum complexes strongly drives the anodic dissolution, the dielectric constant of the solvent, as well as the concentration of dissolved compounds, impacts the level of anodic dissolution.<sup>[246]</sup> With the temperature affecting the solubility of salts in solvents, a higher temperature promotes the anodic aluminum dissolution due to the improved solubility even further.<sup>[247]</sup> Furthermore, the anodic oxidation of aluminum comprises other Faradaic reactions, such as the oxidation of electrolytic compounds.<sup>[248]</sup> Thus, the electrolyte's stability in the respective cell environment and the nature of formed degradation products, especially under oxidative conditions, influence aluminum degradation and its water content.<sup>[249]</sup>

In addition to the solvent, both the anion and the electrolyte salt's cation influence the aluminum's degradation. Naturally, the cations have a minor impact on the anodic dissolution of aluminum compared to the influence of the respective anions of the electrolyte. Due to the different grades of coordination of solvent molecules by the cations, the electrolytic solution's overall saturation relies on the cation's utilized type.<sup>[250]</sup> Thus, the amount of dissolvable aluminum and the possible grade of aluminum dissolution is influenced. On the other hand, the anions have a more significant influence on the anodic dissolution with their possibility to form dissolvable aluminum complexes. However, the extent of anodic dissolution depends strongly on the anion used since different anions show different tendencies to form sol-

uble aluminum complexes. The most prominent examples showing high anodic dissolution are the bis(fluorosulfonyl) imide and bis(trifluoromethanesulfonyl)imide anions.<sup>[251]</sup> By forming the soluble  $\text{Al}(\text{TFSI})_3$  and  $\text{Al}(\text{FSI})_3$  complex,  $\text{TFSI}^-$  and  $\text{FSI}^-$  are known for strong current collector aging in multiple solvents limiting the overall performance and longevity of the supercapacitor.<sup>[252]</sup> Another example for increasing anodic dissolution of aluminum is the  $\text{Cl}^-$  ion. When present in the system, chloride forms transitory compounds like  $\text{Al}(\text{OH})_2\text{Cl}$ ,  $\text{Al}(\text{OH})\text{Cl}_2$ , and  $\text{AlCl}_3$  with the aluminum oxide layer. When dissolving as  $\text{AlCl}_4^-$  above a certain pitting potential, the  $\text{Cl}^-$  ions cause pitting in the aluminum surface similar to  $\text{TFSI}^-$  and  $\text{FSI}^-$ .<sup>[253]</sup> Conversely, anions like  $\text{BF}_4^-$  or  $\text{PF}_6^-$  can even inhibit the current collector degradation by in-situ formation of HF and following passivation of the aluminum surface by fluorination (Figure 12A,B).<sup>[254]</sup>

To tune the stability of the current collector in a specific cell environment, additives can be used to stabilize the aluminum and reduce its degradation. Recently, the use of (difluoromethanesulfonyl)(trifluoromethanesulfonyl)imide anion was proposed, which forms an unstable  $\text{Al}(\text{DFTFSI})_3$  complex that decomposes to stable passivation species such as  $\text{AlF}_3$ .<sup>[255]</sup> In addition to additives that further passivate the current collector surface, the solubility of soluble aluminum complexes can be tuned. By the addition of other salts or ionic liquids such as  $\text{Al}(\text{TFSI})_3$ , (fluorosulfonyl)(trifluoromethanesulfonyl)imide or  $\text{Pyr}_{14}\text{TFSI}$ , the load of dissolved compounds can be increased while maintaining the electrochemical properties and performance of the supercapacitor.<sup>[256]</sup> Thus, the dissolution of soluble aluminum complexes is limited to a certain extent.

### 5.3.2. Current Collectors for Pseudocapacitors

The corrosion of current collectors is rarely reported in the literature. Using aqueous electrolytes together with pseudocapacitive electrodes drastically limits the number of potential candidates. Moreover, the choice of the current collector strongly depends on the nature of the studies. Fundamental studies aiming at an in-depth investigation of the pseudocapacitive electrode can advantageously use "model type" current collectors such as glassy carbon, platinum, or gold.<sup>[58]</sup> However, such materials are not convenient for building cells. As for gas evolution reactions, the corrosion of current collectors is not often reported in the literature. Brousse et al. provide an insightful description of the mechanism that can lead to the de-passivation of stainless steel current collectors.<sup>[257]</sup> It involves the role of trapped air during the fabrication of electrodes and the concomitant formation of a "concentration cell".<sup>[258]</sup>

Consequently, the oxidation of metal occurs in restricted regions, causing the dissolution of metallic ions such as iron, chromium, and nickel. This effect is more pronounced in stainless steel due to the lack of oxygen, which prevents the formation of a protective layer on the metal surface in confined areas. When highly concentrated sulfate solutions undergo hydrolysis, the pH level drops significantly, further accelerating the corrosion process. Anodization of the current collector can also occur whenever high oxidative potentials are used, which merges with the previous remarks on gas evolution reactions.

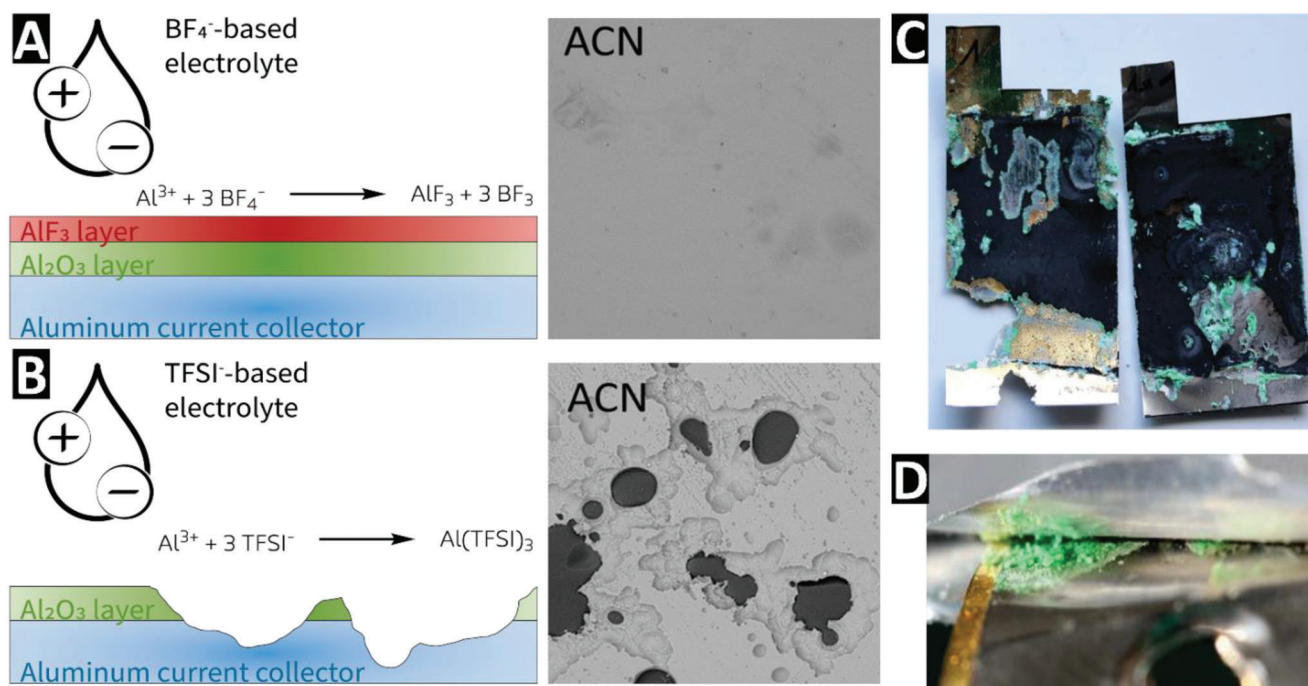


**Figure 12.** Schematic illustration of the degradation of the aluminum current collector with protective layers and post-mortem scanning electron micrographs of the aluminum in A)  $\text{BF}_4^-$ - and B)  $\text{TFSI}^-$ -based electrolytes. The scanning electron micrographs. (Reproduced with permission.<sup>[245]</sup> Copyright 2017, Wiley-VCH). Nickel current collectors coated with  $\text{MnO}_2$  electrodes C) after 1 year of storage at room temperature inside a pouch cell, D) leakage at the sealing of the pouch cell, and subsequent oxidation of the welded tab (pictures courtesy of David Brown, IMN).

Apart from less common solutions ranging from the use of carbon fabrics to that of MXene, which can indeed be potential solutions as current collectors for microdevices or stretchable devices,<sup>[259]</sup> the choice is drastically limited for real-life cells. It consists mainly of stainless steel and nickel, which can be obtained as 10–25  $\mu\text{m}$  thick foils processable in pilot lines. These materials have been carefully investigated through different studies using different aqueous electrolytes.<sup>[260]</sup>

The drastic effect of corrosion can be illustrated by Figure 12C, where a  $\text{MnO}_2$ -based cell has been stored for one year at OCV at room temperature. The nickel-based current collector has been severely corroded without a clear explanation of how this happened. A similar observation can be made on a welded tab of a nickel current collector (Figure 12D), where corrosion led to electrolyte leakage after a few thousand cycles of operation.

Many potential issues can cause the failure of pseudocapacitive electrodes implemented in supercapacitors. Most of them remained unclear due to the few hundred cycles shown in literature data that do not enable evidence of the failure of the electrodes or the related devices. However, the main reasons for such failure are the too-wide potential window for pseudocapacitive electrodes, which generate parasitic Faradaic reactions. These reactions are irreversible oxidation or reduction of a cation in the electrode composition or gas evolution reaction due to water electrolysis. Both reactions lead to the electrode's chemical, structural, microstructural, and/or mechanical degradation. To prevent such reactions, a careful investigation of the safe electrochemical window in which the pseudocapacitive material can be operated must be conducted. Moreover, the adequate selection of current collec-

tor and electrode material must be explored before choosing the right combination. Unfortunately, unlike the operating potential window that can be easily determined, the choice of a safe current collector appears as a challenge for cells implementing pseudocapacitive electrodes.

## 6. Conclusion and Outlook

Supercapacitors have emerged as a promising energy storage technology for a wide range of applications, but their performance degradation and aging mechanisms remain a challenge for researchers and engineers. In this review paper, we have explored the various factors contributing to supercapacitors' performance fading and failure, with particular attention to the industrial point of view.

Monitoring the degradation of supercapacitors is crucial for understanding their performance decay. Parameters such as capacitance and equivalent series resistance are commonly used to assess degradation. However, it is important to conduct these measurements under controlled thermal conditions to account for the sensitivity of supercapacitors to temperature variations. While galvanostatic charge/discharge cycling tests have traditionally been used, they can be time-consuming. Alternative methods such as the floating test, performed in potentiostatic mode, have shown promise in providing a more accurate assessment of supercapacitor lifespan in a shorter time.

Understanding the degradation mechanisms of supercapacitors is essential for developing strategies to mitigate performance decay. The degradation processes are complex and depend on various factors such as material composition, charge storage

mechanisms, operating conditions, and impurities. Redox-based systems, which rely on redox reactions for charge storage, are particularly prone to degradation due to the irreversibility of these reactions. Universal aging processes for all types of supercapacitors are challenging to define, but by studying specific systems in detail, tailored solutions can be developed to address their aging mechanisms. In-situ/operando techniques and post-mortem methods play a crucial role in unraveling the degradation mechanisms of supercapacitors. These advanced characterization techniques provide valuable insights into the structural and morphological changes occurring during the operation of supercapacitors. They include electrochemical dilatometry, X-ray diffraction, atomic force microscopy, spectroscopy techniques (such as XPS and nuclear magnetic resonance), and more. Further advancements in these techniques will continue to enhance our understanding of degradation processes and aid in the development of improved supercapacitor designs.

Looking ahead, reducing the performance degradation of supercapacitors remains a significant challenge. Future research efforts should focus on developing new electrode materials with enhanced stability and improved charge storage properties. Advances in electrolyte formulations, including the use of novel electrolytes such as ionic liquids and solid-state electrolytes, can also contribute to better supercapacitor performance and longevity. Additionally, the development of effective methods for in-situ monitoring of supercapacitor degradation will enable real-time assessment of their health and facilitate proactive maintenance.

In conclusion, understanding the degradation and aging mechanisms of supercapacitors is crucial for improving their performance and extending their lifespan. This review has provided insights into the factors influencing supercapacitor degradation, monitoring techniques, and future directions for mitigating performance decay. By addressing these challenges, supercapacitors can continue to play a vital role in high-power applications and contribute to the advancement of electrochemical energy storage systems. The findings and recommendations presented here will be of interest to researchers, engineers, and others working in the energy storage and supercapacitor technology field.

## Acknowledgements

The authors acknowledge funding of the joint Polish-German project SUPILMIX (PR-1173/27) by the German Research Foundation (DFG, Deutsche Forschungsgemeinschaft) and the Polish National Science Centre (NCN, National Science Centre). Further funding from the DFG and the French National Research Agency (ANR) within the German-French project NECES (BA4956/16) and from the German Federal Ministry for Economic Affairs and Climate Action (BMWK, Bundesministerium für Wirtschaft und Klimaschutz) within the project "SUPREME" (03EI6060B) is gratefully acknowledged. A.V. acknowledges the financial support from the Bundesministerium für Wirtschaft und Klimaschutz (BMWK) within the project "SUPREME" (03EI6060C). E.P. acknowledges the financial support from the Alexander von Humboldt Foundation.

Open access funding enabled and organized by Projekt DEAL.

## Conflict of Interest

The authors declare no conflict of interest.

## Keywords

aging, degradation, failure mechanism, pseudocapacitors, supercapacitors

Received: April 3, 2023

Revised: May 20, 2023

Published online:

- [1] M. Salanne, B. Rotenberg, K. Naoi, K. Kaneko, P. L. Taberna, C. P. Grey, B. Dunn, P. Simon, *Nat. Energy* **2016**, *1*, 16070.
- [2] C. Zhong, Y. Deng, W. Hu, J. Qiao, L. Zhang, J. Zhang, *Chem. Soc. Rev.* **2015**, *44*, 7484.
- [3] a) P. Simon, Y. Gogotsi, *Nat. Mater.* **2020**, *19*, 1151; b) K. Fic, A. Platek, J. Piwek, E. Frackowiak, *Mater. Today* **2018**, *21*, 437.
- [4] a) H. Au, M. Crespo-Ribadeneyra, M.-M. Titirici, *One Earth* **2022**, *5*, 207; b) A. Noori, M. F. El-Kady, M. S. Rahmanifar, R. B. Kaner, M. F. Mousavi, *Chem. Soc. Rev.* **2019**, *48*, 1272.
- [5] A. Muzaffar, M. B. Ahamed, K. Deshmukh, J. Thirumalai, *Renewable Sustainable Energy Rev.* **2019**, *101*, 123.
- [6] a) G. Wang, L. Zhang, J. Zhang, *Chem. Soc. Rev.* **2012**, *41*, 797; b) S. Fleischmann, Y. Zhang, X. Wang, P. T. Cummings, J. Wu, P. Simon, Y. Gogotsi, V. Presser, V. Augustyn, *Nat. Energy* **2022**, *7*, 222.
- [7] F. Béguin, V. Presser, A. Balducci, E. Frackowiak, *Adv. Mater.* **2014**, *26*, 2219.
- [8] a) E. Frackowiak, in *Supercapacitors: Materials, Systems, and Applications* (Eds: F. Béguin, E. Frackowiak), Wiley-VCH, Weinheim **2013**, pp. 207–233; b) T. Brousse, D. Bélanger, D. Guay, in *Supercapacitors: Materials, Systems, and Applications* (Eds: F. Béguin, E. Frackowiak), Wiley-VCH, Weinheim **2013**, pp. 257–283; c) K. Naoi, P. Simon, *Electrochem. Soc. Interface* **2008**, *17*, 34; d) B. E. Conway, in *Electrochemical Supercapacitors: Scientific Fundamentals and Technological Application* (Ed: B. E. Conway), Springer, Boston **1999**, pp. 221–257.
- [9] A. Burke, M. Miller, *Electrochim. Acta* **2010**, *55*, 7538.
- [10] S. Zhang, N. Pan, *Adv. Energy Mater.* **2015**, *5*, 1401401.
- [11] P. Kurzweil, J. Schottenbauer, C. Schell, *J. Energy Storage* **2021**, *35*, 102311.
- [12] a) M. Vangari, T. Pryor, L. Jiang, *J. Energy Eng.* **2013**, *2*, 72; b) S. Pourhosseini, A. Bothe, A. Balducci, F. Béguin, P. Ratajczak, *Energy Storage Mater.* **2021**, *38*, 17; c) A. Oz, D. Gelman, E. Goren, N. Shomrat, S. Baltianski, Y. Tsur, *J. Power Sources* **2017**, *355*, 74.
- [13] P. Simon, Y. Gogotsi, B. Dunn, *Science* **2014**, *343*, 1210.
- [14] a) P. Simon, P.-L. Taberna, F. Béguin, in *Supercapacitors: Materials, Systems, and Applications* (Eds: F. Béguin, E. Frackowiak), Wiley-VCH, Weinheim **2013**, pp. 131–163; b) Z. Lin, E. Goikolea, A. Balducci, K. Naoi, P.-L. Taberna, M. Salanne, G. Yushin, P. Simon, *Mater. Today* **2018**, *21*, 419; c) Y. Wang, L. Zhang, H. Hou, W. Xu, G. Duan, S. He, K. Liu, S. Jiang, *J. Mater. Sci.* **2021**, *56*, 173.
- [15] A. F. Burke, J. Zhao, *J. Energy Storage* **2021**, *35*, 102310.
- [16] E. Frackowiak, Q. Abbas, F. Béguin, *J. Energy Chem.* **2013**, *22*, 226.
- [17] H. Y. Lee, J. B. Goodenough, *J. Solid State Chem.* **1999**, *144*, 220.
- [18] a) Z. Wu, Y. Zhu, X. Ji, C. E. Banks, in *Nanomaterials in Advanced Batteries and Supercapacitors* (Eds: K. I. Ozoemena, S. Chen), Springer International Publishing, Cham, Switzerland **2016**, pp. 317–344; b) S. Ardizzone, G. Fregonara, S. Trasatti, *Electrochim. Acta* **1990**, *35*, 263.
- [19] a) K. Naoi, Y. Nagano, in *Supercapacitors: Materials, Systems, and Applications* (Eds: F. Béguin, E. Frackowiak), Wiley-VCH, Weinheim **2013**, pp. 239–255; b) V. Khomenko, E. Raymundo-Piñero, F. Béguin, *J. Power Sources* **2008**, *177*, 643; c) A. Yoshino, T. Tsubata, M. Shimoyamada, H. Satake, Y. Okano, S. Mori, S. Yata, *J. Electrochem.*

- Soc. **2004**, 151, A2180; d) B. Babu, P. Simon, A. Balducci, *Adv. Energy Mater.* **2020**, 10, 2001128.
- [20] M. Arnaiz, J. Ajuria, *Batteries Supercaps* **2021**, 4, 733.
- [21] a) I. Hasa, S. Mariyappan, D. Saurel, P. Adelhelm, A. Y. Kopsosov, C. Masquelier, L. Croguennec, M. Casas-Cabanas, *J. Power Sources* **2021**, 482, 228872; b) K. Kubota, M. Dahbi, T. Hosaka, S. Kumakura, S. Komaba, *Chem. Rec.* **2018**, 18, 459; c) A. Eftekhari, D.-W. Kim, *J. Power Sources* **2018**, 395, 336.
- [22] a) A. Borenstein, R. Attias, O. Hanna, S. Luski, R. B. Kaner, D. Aurbach, *ChemElectroChem* **2017**, 4, 2660; b) D. Torregrossa, M. Paolone, *J. Energy Storage* **2016**, 5, 85; c) P. Kreczanik, P. Venet, A. Hijazi, G. Clerc, *IEEE Trans. Ind. Electron.* **2013**, 61, 4895.
- [23] a) A. Bothe, A. Balducci, *Electrochim. Acta* **2021**, 374, 137919; b) R. Kötz, P. W. Ruch, D. Cericola, *J. Power Sources* **2010**, 195, 923.
- [24] a) A. Balducci, *J. Power Sources* **2016**, 326, 534; b) H. V. T. Nguyen, J. Kim, K.-K. Lee, *J. Mater. Chem. A* **2021**, 9, 20725.
- [25] L. H. Hess, N. Fulik, J. Röhner, E. Zhang, S. Kaskel, E. Brunner, A. Balducci, *Energy Storage Mater.* **2021**, 37, 501.
- [26] L. Köps, F. Kreth, A. Bothe, A. Balducci, *Energy Storage Mater.* **2022**, 44, 66.
- [27] a) S. W. Donne, *Supercapacitors: Materials, Systems, and Applications*, Wiley, New York **2013**; b) P. Sinha, K. K. Kar, in *Handbook of Nanocomposite Supercapacitor Materials III* (Ed: K. K. Kar), Springer International Publishing, Cham, Switzerland **2021**, pp. 39–79; c) P. Nigam, P. Sinha, K. K. Kar, in *Handbook of Nanocomposite Supercapacitor Materials III* (Ed: K. K. Kar), Springer International Publishing, Cham, Switzerland **2021**, pp. 1–38; d) T. Pandolfo, V. Ruiz, S. Sivakkumar, J. Nerkar, in *Supercapacitors: Materials, Systems, and Applications* (Eds: F. Béguin, E. Frackowiak), Wiley-VCH, Weinheim **2013**, pp. 69–109.
- [28] a) K. S. Teoh, M. Melchiorre, F. A. Kreth, A. Bothe, L. Köps, F. Ruffo, A. Balducci, *ChemSusChem* **2023**, 16, 202201845; b) C. Schütter, A. Bothe, A. Balducci, *Electrochim. Acta* **2020**, 331, 135421.
- [29] a) Y. Liu, B. Réty, C. M. Ghimbeu, B. Soucaze-Guillous, P.-L. Taberna, P. Simon, *J. Power Sources* **2019**, 434, 226734; b) A. Yoshida, I. Tanahashi, A. Nishino, *Carbon* **1990**, 28, 611; c) Y. Liu, B. Soucaze-Guillous, P.-L. Taberna, P. Simon, *J. Power Sources* **2017**, 366, 123.
- [30] Q. Wu, T. He, Y. Zhang, J. Zhang, Z. Wang, Y. Liu, L. Zhao, Y. Wu, F. Ran, *J. Mater. Chem. A* **2021**, 9, 24094.
- [31] a) J. Zhao, A. F. Burke, *J. Energy Chem.* **2021**, 59, 276; b) A. Platek, J. Piwek, K. Fic, E. Frackowiak, *Electrochim. Acta* **2019**, 311, 211.
- [32] P. Kreczanik, C. Martin, P. Venet, G. Clerc, G. Rojat, Y. Zitouni, presented at 13th EPE – ECCE Europe, Barcelona, Spain 08–10 September, **2009**.
- [33] J. Zhao, Y. Gao, A. F. Burke, *J. Power Sources* **2017**, 363, 327.
- [34] D. B. Murray, J. G. Hayes, *IEEE Trans. Power Appar. Syst.* **2014**, 30, 2505.
- [35] a) A. Bothe, A. Balducci, *J. Power Sources* **2022**, 548, 232090; b) J. Schiffer, D. Linzen, D. U. Sauer, *J. Power Sources* **2006**, 160, 765.
- [36] D. Weingarth, A. Foelske-Schmitz, R. Kötz, *J. Power Sources* **2013**, 225, 84.
- [37] N. Rizoug, B. Patrick, L. M. Philippe, *IEEE Trans. Energy Convers.* **2012**, 27, 220.
- [38] P. Ratajczak, K. Jurewicz, P. Skowron, Q. Abbas, F. Béguin, *Electrochim. Acta* **2014**, 130, 344.
- [39] a) I. Escher, M. Hahn, G. A. Ferrero, P. Adelhelm, *Energy Technol.* **2022**, 10, 2101120; b) N. Jäckel, S. Patrick Emge, B. Krüner, B. Roling, V. Presser, *J. Phys. Chem. C* **2017**, 121, 19120; c) N. Jackel, B. Krüner, K. L. Van Aken, M. Alhabeib, B. Anasori, F. Kaasik, Y. Gogotsi, V. Presser, *ACS Appl. Mater. Interfaces* **2016**, 8, 32089; d) L. Hu, D. Guo, G. Feng, H. Li, T. Zhai, *J. Phys. Chem. C* **2016**, 120, 24675; e) C. Prehal, D. Weingarth, E. Perre, R. T. Lechner, H. Amenitsch, O. Paris, V. Presser, *Energy Environ. Sci.* **2015**, 8, 1725.
- [40] A. Patra, K. Namsheer, J. R. Jose, S. Sahoo, B. Chakraborty, C. S. Rout, *J. Mater. Chem. A* **2021**, 9, 25852.
- [41] P. Przygocki, P. Ratajczak, F. Béguin, *Angew. Chem.* **2019**, 58, 17969.
- [42] P. W. Ruch, D. Cericola, A. Foelske-Schmitz, R. Kötz, A. Wokaun, *Electrochim. Acta* **2010**, 55, 4412.
- [43] H. Gualous, R. Gallay, M. Al Sakka, A. Oukaour, B. Tala-Ighil, B. Boudart, *Microelectron. Reliab.* **2012**, 52, 2477.
- [44] R. Barrero, X. Tackoen, J. Van Mierlo, presented at 13th IPEMC, New York, USA 01–03 September, **2008**.
- [45] J. Aubry, P. Bydlowski, B. Multon, H. B. Ahmed, B. Borgarino, presented at ICCE 2010, Bilbao, Spain 06–08 October, **2010**.
- [46] R. Kötz, M. Hahn, P. Ruch, R. Gallay, *Electrochem. Commun.* **2008**, 10, 359.
- [47] X. Wu, H. Yang, M. Yu, J. Liu, S. Li, *Mater. Today Energy* **2021**, 21, 100739.
- [48] a) M. Lu, *Supercapacitors: Materials, Systems, and Applications*, John Wiley & Sons, New York **2013**; b) H. I. Becker, U2800616A, **1957**; c) J. R. Miller, *Battery + Energy Storage Technology*, Autumn, **2007**, pp. 61–78.
- [49] a) P. Lannelongue, R. Bouchal, E. Mourad, C. Bodin, M. Olarte, S. le Volt, F. Favier, O. Fontaine, *J. Electrochem. Soc.* **2018**, 165, A657; b) S. Thareja, A. Kumar, *ACS Sustainable Chem. Eng.* **2021**, 9, 2338; c) K. Fic, G. Lota, M. Meller, E. Frackowiak, *Energy Environ. Sci.* **2012**, 5, 5842.
- [50] M. He, K. Fic, E. Fra, P. Novák, E. J. Berg, *Energy Environ. Sci.* **2016**, 9, 623.
- [51] a) F. Béguin, M. Friebe, K. Jurewicz, C. Vix-Guterl, J. Dentzer, E. Frackowiak, *Carbon* **2006**, 44, 2392; b) F. Béguin, K. Kierzek, M. Friebe, A. Jankowska, J. Machnikowski, K. Jurewicz, E. Frackowiak, *Electrochim. Acta* **2006**, 51, 2161.
- [52] a) Y. Zhao, Y. Ding, Y. Li, L. Peng, H. R. Byon, J. B. Goodenough, G. Yu, *Chem. Soc. Rev.* **2015**, 44, 7968; b) Y. Li, R. Cao, J. Song, L. Liang, T. Zhai, H. Xia, *Mater. Res. Bull.* **2021**, 139, 111249.
- [53] J. Y. Hwang, M. Li, M. F. El-Kady, R. B. Kaner, *Adv. Funct. Mater.* **2017**, 27, 1605745.
- [54] M. Tian, J. Wu, R. Li, Y. Chen, D. Long, *Chem. Eng. J.* **2019**, 363, 183.
- [55] S.-E. Chun, B. Evanko, X. Wang, D. Vonlanthen, X. Ji, G. D. Stucky, S. W. Boettcher, *Nat. Commun.* **2015**, 6, 7818.
- [56] a) P. Przygocki, Q. Abbas, F. Béguin, *Electrochim. Acta* **2018**, 269, 640; b) K. Fic, M. Meller, E. Frackowiak, *J. Electrochem. Soc.* **2015**, 162, A5140; c) P. Przygocki, Q. Abbas, P. Babuchowska, F. Béguin, *Carbon* **2017**, 125, 391.
- [57] M. Bichat, E. Raymundo-Piñero, F. Béguin, *Carbon* **2010**, 48, 4351.
- [58] V. Khomenko, E. Raymundo-Piñero, F. Béguin, *J. Power Sources* **2006**, 153, 183.
- [59] X. Tian, Q. Zhu, B. Xu, *ChemSusChem* **2021**, 14, 2501.
- [60] E. Pameté, F. Béguin, *Electrochim. Acta* **2021**, 389, 138687.
- [61] L. Suo, O. Borodin, T. Gao, M. Olguin, J. Ho, X. Fan, C. Luo, C. Wang, K. Xu, *Science* **2015**, 350, 938.
- [62] L. Suo, D. Oh, Y. Lin, Z. Zhuo, O. Borodin, T. Gao, F. Wang, A. Kushima, Z. Wang, H. C. Kim, Y. Qi, W. Yang, F. Pan, J. Li, K. Xu, C. Wang, *J. Am. Chem. Soc.* **2017**, 139, 18670.
- [63] N. Dubouis, P. Lemaire, B. Mirvaux, E. Salager, M. Deschamps, A. Grimaud, *Energy Environ. Sci.* **2018**, 11, 3491.
- [64] a) M. McEldrew, Z. A. Goodwin, A. A. Kornyshev, M. Z. Bazant, *J. Phys. Chem. Lett.* **2018**, 9, 5840; b) J. Vatamanu, O. Borodin, *J. Phys. Chem. Lett.* **2017**, 8, 4362.
- [65] L. Suo, O. Borodin, Y. Wang, X. Rong, W. Sun, X. Fan, S. Xu, M. A. Schroeder, A. V. Cresce, F. Wang, *Adv. Energy Mater.* **2017**, 7, 1701189.
- [66] a) A. Gambou-Bosca, D. Bélanger, *J. Power Sources* **2016**, 326, 595; b) G. Hasegawa, K. Kanamori, T. Kiyomura, H. Kurata, T. Abe, K. Nakanishi, *Chem. Mater.* **2016**, 28, 3944.

- [67] C. Schütter, S. Pohlmann, A. Balducci, *Adv. Energy Mater.* **2019**, *9*, 1900334.
- [68] S.-W. Xu, M.-C. Zhang, G.-Q. Zhang, J.-H. Liu, X.-Z. Liu, X. Zhang, D.-D. Zhao, C.-L. Xu, Y.-Q. Zhao, *J. Power Sources* **2019**, *441*, 227220.
- [69] P. W. Ruch, D. Cericola, A. Foelske, R. Kötz, A. Wokaun, *Electrochim. Acta* **2010**, *55*, 2352.
- [70] P. Kurzweil, M. Chwistek, *J. Power Sources* **2008**, *176*, 555.
- [71] a) G. Moore, J. Hansen, T. Barrett, J. Waddell, K. Jewell, T. Kestner, R. Payfer, *J. Fluor. Chem.* **1986**, *32*, 41; b) E. A. Kauck, J. H. Simons, *US2567011* **1952**.
- [72] F. A. Kreth, L. H. Hess, A. Balducci, *Energy Storage Mater.* **2023**, *56*, 192.
- [73] a) A. Shashurin, M. Keidar, *Carbon* **2008**, *46*, 1826; b) A. Bittner, M. Zhu, Y. Yang, H. Waibel, M. Konuma, U. Starke, C. Weber, *J. Power Sources* **2012**, *203*, 262; c) Y. Huang, M. Weng, Q. Gong, K. Du, D. Wang, S. Zhang, C. Wu, M. Zhao, D. Zhuang, H. Zhu, *ACS Appl. Mater. Interfaces* **2021**, *13*, 39379.
- [74] P. Azaïs, L. Duclaux, P. Florian, D. Massiot, M.-A. Lillo-Rodenas, A. Linares-Solano, J.-P. Peres, C. Jehoulet, F. Béguin, *J. Power Sources* **2007**, *171*, 1046.
- [75] M. Zhu, C. Weber, Y. Yang, M. Konuma, U. Starke, K. Kern, A. Bittner, *Carbon* **2008**, *46*, 1829.
- [76] a) M. Hahn, A. Würsig, R. Gally, P. Novák, R. Kötz, *Electrochem. Commun.* **2005**, *7*, 925; b) M. Hahn, R. Kötz, R. Gally, A. Siggel, *Electrochim. Acta* **2006**, *52*, 1709.
- [77] S. Ishimoto, Y. Asakawa, M. Shinya, K. Naoi, *J. Electrochem. Soc.* **2009**, *156*, A563.
- [78] O. Munteshari, A. Borenstein, R. H. DeBlock, J. Lau, G. Whang, Y. Zhou, A. Likitchawankun, R. B. Kaner, B. Dunn, L. Pilon, *ChemSusChem* **2020**, *13*, 1013.
- [79] L. H. Hess, A. Bothe, A. Balducci, *Energy Technol.* **2021**, *9*, 2100329.
- [80] K. Chiba, T. Ueda, Y. Yamaguchi, Y. Oki, F. Shimodate, K. Naoi, *J. Electrochem. Soc.* **2011**, *158*, A872.
- [81] L. Köps, F. A. Kreth, D. Leistenschneider, K. Schütjajew, R. Gläßner, M. Oschatz, A. Balducci, *Adv. Energy Mater.* **2023**, *13*, 2203821.
- [82] L. Xia, L. Yu, D. Hu, G. Z. Chen, *Mater. Chem. Front.* **2017**, *1*, 584.
- [83] X. Wang, M. Salari, D.-e. Jiang, J. Chapman Varela, B. Anasori, D. J. Wesolowski, S. Dai, M. W. Grinstaff, Y. Gogotsi, *Nat. Rev. Mater.* **2020**, *5*, 787.
- [84] A. Brandt, S. Pohlmann, A. Varzi, A. Balducci, S. Passerini, *MRS Bull.* **2013**, *38*, 554.
- [85] B. Gorska, L. Timperman, M. Anouti, J. Pernak, F. Béguin, *RSC Adv.* **2016**, *6*, 55144.
- [86] M. Armand, F. Endres, D. R. MacFarlane, H. Ohno, B. Scrosati, *Nat. Mater.* **2009**, *8*, 621.
- [87] a) E. Pamaté, B. Gorska, V. Pavlenko, F. Béguin, *Electrochim. Acta* **2020**, *350*, 136416; b) E. Pamaté, B. Gorska, F. Béguin, *ChemSusChem* **2021**, *14*, 1196.
- [88] A. Eftekhari, *Energy Storage Mater.* **2017**, *9*, 47.
- [89] D. R. MacFarlane, N. Tachikawa, M. Forsyth, J. M. Pringle, P. C. Howlett, G. D. Elliott, J. H. Davis, M. Watanabe, P. Simon, C. A. Angell, *Energy Environ. Sci.* **2014**, *7*, 232.
- [90] a) S. A. S. Amiril, E. A. Rahim, S. Syahrullail, *J. Cleaner Prod.* **2017**, *168*, 1571; b) C. A. Angell, Y. Ansari, Z. Zhao, *Faraday Discuss.* **2012**, *154*, 9.
- [91] E. Pamaté, B. Gorska, F. Béguin, *J. Mol. Liq.* **2020**, *298*, 111959.
- [92] T. Romann, O. Oll, P. Pikma, H. Tammé, E. Lust, *Electrochim. Acta* **2014**, *125*, 183.
- [93] J. Kruusma, A. Tõnisoo, R. Pärna, E. Nõmmiste, E. Lust, *J. Electrochem. Soc.* **2014**, *161*, A1266.
- [94] C. O. Ania, J. Pernak, F. Stefaniak, E. Raymundo-Piñero, F. Béguin, *Carbon* **2006**, *44*, 3126.
- [95] C. Largeot, C. Portet, J. Chmiola, P.-L. Taberna, Y. Gogotsi, P. Simon, *J. Am. Chem. Soc.* **2008**, *130*, 2730.
- [96] a) V. L. Martins, R. M. Torresi, A. J. R. Rennie, *Electrochim. Acta* **2018**, *270*, 453; b) A. Laheäär, A. Arenillas, F. Béguin, *J. Power Sources* **2018**, *396*, 220; c) C. Arbizzani, S. Beninati, M. Lazzari, F. Soavi, M. Mastragostino, *J. Power Sources* **2007**, *174*, 648; d) C. Wolff, S. Jeong, E. Paillard, A. Balducci, S. Passerini, *J. Power Sources* **2015**, *293*, 65; e) H. Kurig, M. Vestli, A. Jänes, E. Lust, *Electrochem. Solid-State Lett.* **2011**, *14*, A120.
- [97] M. Lazzari, F. Soavi, M. Mastragostino, *J. Power Sources* **2008**, *178*, 490.
- [98] A. J. R. Rennie, V. L. Martins, R. M. Torresi, P. J. Hall, *J. Phys. Chem. C* **2015**, *119*, 23865.
- [99] F. B. Sillars, S. I. Fletcher, M. Mirzaeiian, P. J. Hall, *Phys. Chem. Chem. Phys.* **2012**, *14*, 6094.
- [100] T. Nishida, Y. Tashiro, M. Yamamoto, *J. Fluorine Chem.* **2003**, *120*, 135.
- [101] Y. Kado, K. Imoto, Y. Soneda, N. Yoshizawa, *J. Power Sources* **2014**, *271*, 377.
- [102] a) K. Breitsprecher, M. Janssen, P. Srimuk, B. L. Mehdi, V. Presser, C. Holm, S. Kondrat, *Nat. Commun.* **2020**, *11*, 6085; b) S. Kondrat, P. Wu, R. Qiao, A. A. Kornyshev, *Nat. Mater.* **2014**, *13*, 387.
- [103] a) C. Vix-Guterl, E. Frackowiak, K. Jurewicz, M. Friebe, J. Parmentier, F. Béguin, *Carbon* **2005**, *43*, 1293; b) L. Zhang, X. Yang, F. Zhang, G. Long, T. Zhang, K. Leng, Y. Zhang, Y. Huang, Y. Ma, M. Zhang, *J. Am. Chem. Soc.* **2013**, *135*, 5921.
- [104] a) P. J. Hall, M. Mirzaeiian, S. I. Fletcher, F. B. Sillars, A. J. Rennie, G. O. Shitta-Bey, G. Wilson, A. Cruden, R. Carter, *Energy Environ. Sci.* **2010**, *3*, 1238; b) M. E. Suss, T. F. Baumann, M. A. Worsley, K. A. Rose, T. F. Jaramillo, M. Stadermann, J. G. Santiago, *J. Power Sources* **2013**, *241*, 266.
- [105] M. Enterria, A. Castro-Muniz, F. Suarez-Garcia, A. Martinez-Alonso, J. Tascon, T. Kyotani, *J. Mater. Chem. A* **2014**, *2*, 12023.
- [106] a) C. Merlet, B. Rotenberg, P. A. Madden, P.-L. Taberna, P. Simon, Y. Gogotsi, M. Salanne, *Nat. Mater.* **2012**, *11*, 306; b) M. V. Fedorov, A. A. Kornyshev, *Chem. Rev.* **2014**, *114*, 2978.
- [107] J. R. Miller, A. Burke, *Electrochem. Soc. Interface* **2008**, *17*, 53.
- [108] a) W.-Y. Tsai, R. Lin, S. Murali, L. Li Zhang, J. K. McDonough, R. S. Ruoff, P.-L. Taberna, Y. Gogotsi, P. Simon, *Nano Energy* **2013**, *2*, 403; b) Y. Zhou, M. Ghaffari, M. Lin, H. Xu, H. Xie, C. M. Koo, Q. M. Zhang, *RSC Adv.* **2015**, *5*, 71699.
- [109] a) R. Palm, H. Kurig, K. Tõnurist, A. Jänes, E. Lust, *Electrochim. Acta* **2012**, *85*, 139; b) L. Dagoussset, G. Pognon, G. T. M. Nguyen, F. Vidal, S. Jus, P.-H. Aubert, *J. Power Sources* **2017**, *359*, 242; c) J. Li, Y. A. Zhou, J. R. Tian, L. L. Peng, J. Deng, N. Wang, W. Z. Qian, W. Chu, *J. Mater. Chem. A* **2020**, *8*, 10386.
- [110] X. Wang, A. Y. Mehandzhyski, B. Arstad, K. L. Van Aken, T. S. Mathis, A. Gallegos, Z. Tian, D. Ren, E. Sheridan, B. A. Grimes, D. E. Jiang, J. Wu, Y. Gogotsi, D. Chen, *J. Am. Chem. Soc.* **2017**, *139*, 18681.
- [111] K. Nasrin, S. Gokulnath, M. Karnan, K. Subramani, M. Sathish, *Energy Fuels* **2021**, *35*, 6465.
- [112] M. M. Amaral, R. Venâncio, A. C. Peterlevitz, H. Zanin, *J. Energy Chem.* **2022**, *67*, 697.
- [113] a) Y. Xu, W. Lu, G. Xu, T.-W. Chou, *Compos. Sci. Technol.* **2021**, *204*, 108636; b) D. P. Dubal, N. R. Chodankar, D.-H. Kim, P. Gomez-Romero, *Chem. Soc. Rev.* **2018**, *47*, 2065; c) X. Lu, M. Yu, G. Wang, Y. Tong, Y. Li, *Energy Environ. Sci.* **2014**, *7*, 2160.
- [114] S. Alipoori, S. Mazinani, S. H. Aboutaleb, F. Sharif, *J. Energy Storage* **2020**, *27*, 101072.
- [115] F. Qiu, Y. Huang, C. Luo, X. Li, M. Wang, H. Cao, *Energy Technol.* **2020**, *8*, 2000009.
- [116] H. T. T. Thanh, P. A. Le, M. D. Thi, T. Le Quang, T. N. Trinh, *Bull. Mater. Sci.* **2018**, *41*, 145.
- [117] H. Gao, J. Li, K. Lian, *RSC Adv.* **2014**, *4*, 21332.
- [118] H. Fei, C. Yang, H. Bao, G. Wang, *J. Power Sources* **2014**, *266*, 488.

- [119] H. Gao, K. Lian, *J. Electrochem. Soc.* **2013**, *160*, A505.
- [120] J. Wei, G. Wei, Y. Shang, J. Zhou, C. Wu, Q. Wang, *Adv. Mater.* **2019**, *31*, 1900248.
- [121] V. Kumaravel, J. Bartlett, S. C. Pillai, *Adv. Energy Mater.* **2021**, *11*, 2002869.
- [122] J. Wang, F. Li, F. Zhu, O. G. Schmidt, *Small Methods* **2019**, *3*, 1800367.
- [123] a) A. Ulihin, Y. G. Mateyshina, N. Uvarov, *Solid State Ionics* **2013**, *251*, 62; b) B. E. Francisco, C. M. Jones, S.-H. Lee, C. R. Stoldt, *Appl. Phys. Lett.* **2012**, *100*, 103902; c) G. Liao, T. Mahrholz, S. Geier, P. Wierach, M. Wiedemann, *J. Solid State Electrochem.* **2018**, *22*, 1055.
- [124] T. Hakari, S. Yoshimi, K. Nagao, A. Sakuda, M. Tatsumisago, A. Hayashi, *J. Power Sources* **2022**, *543*, 231821.
- [125] T. Hakari, Y. Fujita, M. Deguchi, Y. Kawasaki, M. Otoyama, Y. Yoneda, A. Sakuda, M. Tatsumisago, A. Hayashi, *Adv. Funct. Mater.* **2022**, *32*, 2106174.
- [126] J. Le Bideau, L. Viau, A. Vioux, *Chem. Soc. Rev.* **2011**, *40*, 907.
- [127] M. Brachet, D. Gaboriau, P. Gentile, S. Fantini, G. Bidan, S. Sadki, T. Brousse, J. Le Bideau, *J. Mater. Chem. A* **2016**, *4*, 11835.
- [128] a) M. Brachet, T. Brousse, J. Le Bideau, *ECS Electrochem. Lett.* **2014**, *3*, A112; b) B. Asbani, C. Douard, T. Brousse, J. Le Bideau, *Energy Storage Mater.* **2019**, *21*, 439.
- [129] T. Guillemin, C. Douard, K. Robert, B. Asbani, C. Lethien, T. Brousse, J. Le Bideau, *Energy Storage Mater.* **2022**, *50*, 606.
- [130] L. Zhang, X. Hu, Z. Wang, F. Sun, D. G. Dorrell, *Renewable Sustainable Energy Rev.* **2018**, *81*, 1868.
- [131] A. G. Pandolfo, A. F. Hollenkamp, *J. Power Sources* **2006**, *157*, 11.
- [132] P. Simon, Y. Gogotsi, *Nat. Mater.* **2008**, *7*, 845.
- [133] J. Jagiello, A. Chojnacka, S. E. M. Pourhosseini, Z. Wang, F. Beguin, *Carbon* **2021**, *178*, 113.
- [134] P. Simon, Y. Gogotsi, *Acc. Chem. Res.* **2011**, *46*, 1094.
- [135] a) B. R. Puri, in *Chemistry and Physics of Carbon* (Eds: P. L. Walker Jr), Vol. 6, **1970**, p. 191; b) N. L. Wu, S. Y. Wang, *J. Power Sources* **2002**, *10*, 233; c) C. Portet, P. L. Taberna, P. Simon, E. Flahaut, C. Laberty-Robert, *Electrochim. Acta* **2005**, *50*, 4174.
- [136] a) V. Presser, M. Heon, Y. Gogotsi, *Adv. Funct. Mater.* **2011**, *21*, 810; b) L. Wei, M. Sevilla, A. B. Fuentres, R. Mokaya, G. Yushin, *Adv. Funct. Mater.* **2012**, *22*, 827; c) G. Yushin, A. Nikitin, Y. Gogotsi, in *Carbon Nanomaterials* (Eds: Y. Gogotsi), CRC Taylor & Francis, Boca Raton FL **2006**, p. 211; d) S. Osswald, J. Chmiola, Y. Gogotsi, *Carbon* **2012**, *50*, 4880; e) M. Rose, Y. Korenblit, E. Kockrick, L. Borchardt, M. Oschatz, S. Kaskel, G. Yushin, *Small* **2011**, *7*, 1108.
- [137] a) A. Kumar, K. Sharma, A. R. Dixit, *Carbon Lett.* **2020**, *31*, 149; b) S.-M. Bak, K.-H. Kim, C.-W. Lee, K.-B. Kim, *J. Mater. Chem.* **2011**, *21*, 1984; c) M. Zeiger, N. Jäckel, D. Weingarh, V. Presser, *Carbon* **2015**, *94*, 507.
- [138] a) A. Shaikh, B. K. Singh, D. Mohapatra, S. Parida, *Electrocatalysis* **2019**, *10*, 222; b) M. Zeiger, N. Jäckel, V. N. Mochalin, V. Presser, *J. Mater. Chem. A* **2016**, *4*, 3172.
- [139] a) S. I. Wong, H. Lin, J. Sunarso, B. T. Wong, B. Jia, *Appl. Mater. Today* **2020**, *18*, 100522; b) Q. Shao, J. Tang, Y. Lin, J. Li, F. Qin, K. Zhang, J. Yuan, L.-C. Qin, *Electrochim. Acta* **2015**, *176*, 1441; c) Y. Chen, Y. Jiang, Z. Liu, L. Yang, Q. Du, K. Zhuo, *Electrochim. Acta* **2021**, *366*, 137414; d) E. A. Arkhipova, A. S. Ivanov, K. I. Maslakov, S. V. Savilov, *J. Energy Storage* **2020**, *30*, 101464; e) A. G. Olabi, M. A. Abdelkareem, T. Wilberforce, E. T. Sayed, *Renewable Sustainable Energy Rev.* **2021**, *135*, 110026.
- [140] a) P. J. F. Harris, *Crit. Rev. Solid State Mater. Sci.* **2005**, *30*, 235; b) Y. Wang, A. Du Pasquier, D. Li, P. Atanassova, S. Sawrey, M. Oljaca, *Carbon* **2018**, *133*, 1; c) S. J. Harris, A. M. Weiner, *Ann. Rev. Phys. Chem.* **1985**, *36*, 31.
- [141] a) N. Fechler, T. P. Fellingner, M. Antonietti, *Adv. Mater.* **2013**, *25*, 75; b) X. Liu, M. Antonietti, *Carbon* **2014**, *69*, 460; c) E. Masika, R. Mokaya, *RSC Adv.* **2013**, *3*, 17677; d) D. Qiu, T. Cao, J. Zhang, S.-W. Zhang, D. Zheng, H. Wu, W. Lv, F. Kang, Q.-H. Yang, *J. Energy Chem.* **2019**, *31*, 101; e) A. Platek, C. Nita, C. M. Ghimbeu, E. Frąckowiak, K. Fic, *Electrochim. Acta* **2020**, *338*, 135788; f) Y. Xia, Z. Yang, R. Mokaya, *Nanoscale* **2010**, *2*, 639; g) S. Han, K. Sohn, T. Hyeon, *Chem. Mater.* **2000**, *12*, 3337; h) T. Morishita, T. Tsumura, M. Toyoda, J. Przepiórski, A. W. Morawski, H. Konno, M. Inagaki, *Carbon* **2010**, *48*, 2690.
- [142] R. Yan, M. Antonietti, M. Oschatz, *Adv. Energy Mater.* **2018**, *8*, 1800026.
- [143] J. Chmiola, G. Yushin, R. Dash, Y. Gogotsi, *J. Power Sources* **2006**, *158*, 765.
- [144] Y. M. Liu, C. Merlet, B. Smit, *ACS Cent. Sci.* **2019**, *5*, 1813.
- [145] O. Barbieri, M. Hahn, A. Herzog, R. Kötz, *Carbon* **2005**, *43*, 1303.
- [146] P. Ratajczak, M. E. Suss, F. Kaasik, F. Béguin, *Energy Storage Mater.* **2019**, *16*, 126.
- [147] M. Deschamps, E. Gilbert, P. Azais, E. Raymundo-Pinero, M. R. Ammar, P. Simon, D. Massiot, F. Beguin, *Nat. Mater.* **2013**, *12*, 351.
- [148] R. Lin, P.-L. Taberna, S. Fantini, V. Presser, C. R. Pérez, F. Malbosc, N. L. Rупesinghe, K. B. K. Teo, Y. Gogotsi, P. Simon, *J. Phys. Chem. Lett.* **2011**, *2*, 2396.
- [149] W. Y. Tsai, P. L. Taberna, P. Simon, *J. Am. Chem. Soc.* **2014**, *136*, 8722.
- [150] F. W. Richey, B. Dyatkin, Y. Gogotsi, Y. A. Elabd, *J. Am. Chem. Soc.* **2013**, *135*, 12818.
- [151] Y. Huang, J. Liang, Y. Chen, *Small* **2012**, *8*, 1805.
- [152] W. Zhu, D. E. Miser, W. Geoffrey Chan, M. R. Hajaligol, *Carbon* **2004**, *42*, 1841.
- [153] V. Pavlenko, S. Khosravi H, S. Żółtowska, A. B. Haruna, M. Zahid, Z. Mansurov, Z. Supiyeva, A. Galal, K. I. Ozoemena, Q. Abbas, T. Jesionowski, *Mater. Sci. Eng. Rep.* **2022**, *149*, 100682.
- [154] a) B. E. Conway, *Electrochemical Supercapacitors: Scientific Fundamentals and Technological Applications*, Springer Science & Business Media, Berlin **2013**; b) T. Brousse, D. Bélanger, J. W. Long, *J. Electrochem. Soc.* **2015**, *162*, A5185.
- [155] a) S. Trasatti, G. Buzzanca, *J. Electroanal. Chem.* **1971**, *29*, A1; b) S. Hadz, H. Angerstein-Kozłowska, M. Vukovič, B. Conway, *J. Electrochem. Soc.* **1978**, *125*, 1471; c) J. Zheng, P. Cygan, T. Jow, *J. Electrochem. Soc.* **1995**, *142*, 2699.
- [156] a) M. Toupin, T. Brousse, D. Bélanger, *Chem. Mater.* **2002**, *14*, 3946; b) Y. Jeong, A. Manthiram, *J. Electrochem. Soc.* **2002**, *149*, A1419.
- [157] S. Wang, N. Wu, *J. Appl. Electrochem.* **2003**, *33*, 345.
- [158] H. Y. Lee, J. Goodenough, *J. Solid State Chem.* **1999**, *148*, 81.
- [159] D. Choi, P. N. Kumta, *Electrochem. Solid-State Lett.* **2005**, *8*, A418.
- [160] T. C. Liu, W. Pell, B. Conway, S. Roberson, *J. Electrochem. Soc.* **1998**, *145*, 1882.
- [161] O. Crosnier, N. Goubard-Bretesché, G. Buvat, L. Athouel, C. Douard, P. Lannelongue, F. Favier, T. Brousse, *Curr. Opin. Electrochem.* **2018**, *9*, 87.
- [162] a) C. A. Castro Ruiz, D. Belanger, D. Rochefort, *J. Phys. Chem. C* **2013**, *117*, 20397; b) N. L. Nguyen, D. Rochefort, *Electrochim. Acta* **2014**, *147*, 96; c) S. Lindberg, S. Jeschke, P. Jankowski, M. Abdelhamid, T. Brousse, J. Le Bideau, P. Johansson, A. Matic, *J. Power Sources* **2020**, *460*, 228111; d) J. S. Seenath, D. Pech, D. Rochefort, *J. Power Sources* **2022**, *548*, 232040.
- [163] S. Trasatti, G. Lodi, in *Electrodes of Conductive Metallic Oxides* (Ed: S. Trasatti), Elsevier, Amsterdam **1980**, pp. 301–358.
- [164] A. Jronidi, G. Buvat, F. D. L. Pena, M. Marinova, M. Huvé, T. Brousse, P. Roussel, C. Lethien, *Adv. Energy Mater.* **2023**, *13*, 2203462.
- [165] a) C. Xu, C. Wei, B. Li, F. Kang, Z. Guan, *J. Power Sources* **2011**, *196*, 7854; b) W. Wei, X. Cui, W. Chen, D. G. Ivey, *Chem. Soc. Rev.* **2011**, *40*, 1697; c) S. Islam, M. M. Mia, S. S. Shah, S. Naher, M. N. Shaikh, M. A. Aziz, A. J. S. Ahammad, *Chem. Rec.* **2022**, *22*, e202200013.

- [166] a) N. Parveen, S. A. Ansari, M. Z. Ansari, M. O. Ansari, *Environ. Chem. Lett.* **2022**, *20*, 283; b) J. Yan, Q. Wang, T. Wei, Z. Fan, *Adv. Energy Mater.* **2014**, *4*, 1300816.
- [167] W. Sugimoto, K. Yokoshima, Y. Murakami, Y. Takasu, *Electrochim. Acta* **2006**, *52*, 1742.
- [168] a) Z. Sun, Y. Zhang, Y. Liu, J. Fu, S. Cheng, P. Cui, E. Xie, *J. Power Sources* **2019**, *436*, 226795; b) S. Cheng, L. Yang, D. Chen, X. Ji, Z.-j. Jiang, D. Ding, M. Liu, *Nano Energy* **2014**, *9*, 161; c) L. Si-Heng, L. Qing-He, Q. Li, L. Le-Hui, W. Hong-Yu, *Chin. J. Anal. Chem.* **2012**, *40*, 339.
- [169] J. Shin, J. K. Seo, R. Yaylian, A. Huang, Y. S. Meng, *Int. Mater. Rev.* **2020**, *65*, 356.
- [170] a) W. Wei, X. Cui, W. Chen, D. G. Ivey, *Electrochim. Acta* **2009**, *54*, 2271; b) W. Wei, X. Cui, W. Chen, D. G. Ivey, *J. Power Sources* **2009**, *186*, 543.
- [171] F. Ataherian, N.-L. Wu, *Electrochem. Commun.* **2011**, *13*, 1264.
- [172] H.-A. Pan, O. Ghodbane, Y.-T. Weng, H.-S. Sheu, J.-F. Lee, F. Favier, N.-L. Wu, *J. Electrochem. Soc.* **2015**, *162*, A5106.
- [173] a) L. Athouël, F. Moser, R. Dugas, O. Crosnier, D. Bélanger, T. Brousse, *J. Phys. Chem. C* **2008**, *112*, 7270; b) Y.-C. Hsieh, K.-T. Lee, Y.-P. Lin, N.-L. Wu, S. W. Donne, *J. Power Sources* **2008**, *177*, 660.
- [174] a) N.-L. Wu, S.-Y. Wang, C.-Y. Han, D.-S. Wu, L.-R. Shiue, *J. Power Sources* **2003**, *113*, 173; b) T. Cottineau, M. Toupin, T. Delahaye, T. Brousse, D. Bélanger, *Appl. Phys. A* **2006**, *82*, 599; c) T. Brousse, D. Bélanger, *Electrochem. Solid-State Lett.* **2003**, *6*, A244; d) M. B. Sassin, C. N. Chervin, D. R. Rolison, J. W. Long, *Acc. Chem. Res.* **2013**, *46*, 1062.
- [175] N. Goubard-Bretesché, O. Crosnier, C. Douard, A. Iadecola, R. Retoux, C. Payen, M. L. Doublet, K. Kisu, E. Iwama, K. Naoi, F. Favier, T. Brousse, *Small* **2020**, *16*, 2002855.
- [176] a) D. Choi, G. E. Blomgren, P. N. Kumta, *Adv. Mater.* **2006**, *18*, 1178; b) R. Lucio-Porto, S. Bouhtiyia, J.-F. Pierson, A. Morel, F. Capon, P. Boulet, T. Brousse, *Electrochim. Acta* **2014**, *141*, 203.
- [177] A. Morel, Y. Borjon-Piron, R. L. Porto, T. Brousse, D. Belanger, *J. Electrochem. Soc.* **2016**, *163*, A1077.
- [178] K. Robert, D. Stiévenard, D. Deresmes, C. Douard, A. Iadecola, D. Troadec, P. Simon, N. Nuns, M. Marinova, M. Huvé, P. Roussel, T. Brousse, C. Lethien, *Energy Environ. Sci.* **2020**, *13*, 949.
- [179] T. Brousse, M. Toupin, D. Belanger, *J. Electrochem. Soc.* **2004**, *151*, A614.
- [180] M. S. Hong, S. H. Lee, S. W. Kim, *Electrochem. Solid-State Lett.* **2002**, *5*, A227.
- [181] F. Ataherian, N.-L. Wu, *J. Electrochem. Soc.* **2011**, *158*, A422.
- [182] H. Mosqueda, O. Crosnier, L. Athouël, Y. Dandeville, Y. Scudeller, P. Guillemet, D. Schleich, T. Brousse, *Electrochim. Acta* **2010**, *55*, 7479.
- [183] K. S. Novoselov, A. K. Geim, S. V. Morozov, D.-e. Jiang, Y. Zhang, S. V. Dubonos, I. V. Grigorieva, A. A. Firsov, *Science* **2004**, *306*, 666.
- [184] a) M. Zeng, Y. Xiao, J. Liu, K. Yang, L. Fu, *Chem. Rev.* **2018**, *118*, 6236; b) J. Nan, X. Guo, J. Xiao, X. Li, W. Chen, W. Wu, H. Liu, Y. Wang, M. Wu, G. Wang, *Small* **2021**, *17*, 1902085; c) J. Zhang, S. Seyedin, Z. Gu, W. Yang, X. Wang, J. M. Razal, *Nanoscale* **2017**, *9*, 18604.
- [185] a) Z. Wang, Z. Xu, H. Huang, X. Chu, Y. Xie, D. Xiong, C. Yan, H. Zhao, H. Zhang, W. Yang, *ACS Nano* **2020**, *14*, 4916; b) J. Yang, W. Bao, P. Jaumaux, S. Zhang, C. Wang, G. Wang, *Adv Mater* **2019**, *6*, 1802004.
- [186] a) L. Lai, H. Yang, L. Wang, B. K. Teh, J. Zhong, H. Chou, L. Chen, W. Chen, Z. Shen, R. S. Ruoff, *ACS Nano* **2012**, *6*, 5941; b) C. Zhang, B. Zheng, C. Huang, Y. Li, J. Wang, S. Tang, M. Deng, Y. Du, *ACS Appl. Energy Mater.* **2019**, *2*, 5219.
- [187] M. D. Stoller, S. Park, Y. Zhu, J. An, R. S. Ruoff, *Nano Lett.* **2008**, *8*, 3498.
- [188] D. Chen, H. Feng, J. Li, *Chem. Rev.* **2012**, *112*, 6027.
- [189] J. Zhang, H. Zhang, Y. Cai, H. Zhang, *RSC Adv.* **2016**, *6*, 98010.
- [190] S. Manzeli, D. Ovchinnikov, D. Pasquier, O. V. Yazyev, A. Kis, *Nat. Rev. Mater.* **2017**, *2*, 17033.
- [191] C. Lee, H. Yan, L. E. Brus, T. F. Heinz, J. Hone, S. Ryu, *ACS Nano* **2010**, *4*, 2695.
- [192] a) K. S. Novoselov, A. Mishchenko, O. A. Carvalho, A. H. Castro Neto, *Science* **2016**, *353*, 6298; b) J. Zhang, W. Zhao, P. Yu, G. Yang, Z. Liu, *2D Mater.* **2020**, *7*, 042002.
- [193] a) A. Balati, A. Bazilio, A. Shahriar, K. Nash, H. J. Shipley, *Mater. Sci. Semicond. Process.* **2019**, *99*, 68; b) D. Deng, X. Pan, L. Yu, Y. Cui, Y. Jiang, J. Qi, W.-X. Li, Q. Fu, X. Ma, Q. Xue, *Chem. Mater.* **2011**, *23*, 1188; c) Z. Luo, J. Zhou, L. Wang, G. Fang, A. Pan, S. Liang, *J. Mater. Chem. A* **2016**, *4*, 15302; d) S. Yuan, S.-Y. Pang, J. Hao, *Appl. Phys. Rev.* **2020**, *7*, 021304.
- [194] a) G. P. Sharma, R. G. S. Pala, S. Sivakumar, *Electrochim. Acta* **2019**, *318*, 607; b) L. Wan, J. Liu, X. Li, Y. Zhang, J. Chen, C. Du, M. Xie, *Int. J. Hydrogen Energy* **2020**, *45*, 4521; c) F. Chen, S. Ji, Q. Liu, H. Wang, H. Liu, D. J. Brett, G. Wang, R. Wang, *Small* **2018**, *14*, 1800791.
- [195] S. J. Patil, D.-W. Lee, *J. Mater. Chem. A* **2018**, *6*, 9592.
- [196] a) R. N. Bulakhe, J.-J. Shim, *New J. Chem.* **2017**, *41*, 1473; b) J. Yan, S. Wang, Y. Chen, M. Yuan, Y. Huang, J. Lian, J. Qiu, J. Bao, M. Xie, H. Xu, *J. Alloys Compd.* **2019**, *811*, 151915; c) X. Xu, W. Zhong, X. Zhang, J. Dou, Z. Xiong, Y. Sun, T. Wang, Y. Du, *J. Colloid Interface Sci.* **2019**, *543*, 147; d) D. Guo, X. Song, L. Tan, H. Ma, H. Pang, X. Wang, L. Zhang, *ACS Sustainable Chem. Eng.* **2018**, *7*, 2803; e) P. Yang, W. Mai, *Nano Energy* **2014**, *8*, 274; f) X. Chang, W. Li, Y. Liu, M. He, X. Zheng, X. Lv, Z. Ren, *J. Alloys Compd.* **2019**, *784*, 293; g) K.-J. Huang, J.-Z. Zhang, Y. Fan, *Mater. Lett.* **2015**, *152*, 244; h) B. Kirubasankar, P. Palanisamy, S. Arunachalam, V. Murugadoss, S. Angaiah, *Chem. Eng. J.* **2019**, *355*, 881.
- [197] C. Lokhande, D. Dubal, O.-S. Joo, *Curr. Appl. Phys.* **2011**, *11*, 255.
- [198] L. Wang, D. Wang, X. Y. Dong, Z. J. Zhang, X. F. Pei, X. J. Chen, B. Chen, J. Jin, *Chem. Commun.* **2011**, *47*, 3556.
- [199] a) Y. Zhou, W. Guo, T. Li, *Ceram. Interfaces* **2019**, *45*, 21062; b) J. Shi, B. Jiang, C. Li, F. Yan, D. Wang, C. Yang, J. Wan, *Mater. Chem. Phys.* **2020**, *245*, 122533.
- [200] a) T. Lu, S. Dong, C. Zhang, L. Zhang, G. Cui, *Coord. Chem. Rev.* **2017**, *332*, 75; b) P. A. Shinde, N. R. Chodankar, M. A. Abdelkareem, S. J. Patil, Y. K. Han, K. Elsaid, A. G. Olabi, *Small* **2022**, *18*, 2200248.
- [201] J. Wang, Y. Wang, *SmartMat* **2022**, *4*, e1130.
- [202] M. Naguib, M. Kurtoglu, V. Presser, J. Lu, J. Niu, M. Heon, L. Hultman, Y. Gogotsi, M. W. Barsoum, *Adv. Mater.* **2011**, *23*, 4248.
- [203] K. R. G. Lim, M. Shekhirev, B. C. Wyatt, B. Anasori, Y. Gogotsi, Z. W. Seh, *Nat. Synth.* **2022**, *1*, 601.
- [204] M. K. Aslam, Y. Niu, M. Xu, *Adv. Energy Mater.* **2020**, *11*, 2000681.
- [205] M. A. Alkhadra, X. Su, M. E. Suss, H. Tian, E. N. Guyes, A. N. Shocron, K. M. Conforti, J. P. de Souza, N. Kim, M. Tedesco, K. Khoiruddin, I. G. Wenten, J. G. Santiago, T. A. Hatton, M. Z. Bazant, *Chem. Rev.* **2022**, *122*, 13547.
- [206] A. Gentile, S. Marchionna, M. Balordi, G. Pagot, C. Ferrara, V. Di Noto, R. Ruffo, *ChemElectroChem* **2022**, *9*, 202200891.
- [207] Q. Gao, W. Sun, P. Ilani-Kashkouli, A. Tselev, P. R. C. Kent, N. Kabengi, M. Naguib, M. Alhabeb, W.-Y. Tsai, A. P. Baddorf, J. Huang, S. Jesse, Y. Gogotsi, N. Balke, *Energy Environ. Sci.* **2020**, *13*, 2549.
- [208] a) X. Zhang, B. Shao, A. Guo, Z. Gao, Y. Qin, C. Zhang, F. Cui, X. Yang, *J. Alloys Compd.* **2021**, *862*, 158546; b) Y. Xu, B. Pan, W.-S. Li, L. Dong, X. Wang, F.-G. Zhao, *ACS Appl. Mater. Interfaces* **2021**, *13*, 41537; c) D. Zhang, M. Luo, K. Yang, P. Yang, C. Liu, W. Chen, X. Zhou, *Microporous Mesoporous Mater.* **2021**, *326*, 111389; d) Y. A. Dakka, J. Balamurugan, R. Balaji, N. H. Kim, J. H. Lee, *Chem. Eng. J.* **2020**, *385*, 123455; e) R. B. Rakhi, B. Ahmed, D. Anjum, H. N. Alshareef, *ACS Appl. Mater. Interfaces* **2016**, *8*, 18806; f) M. Cao, F. Wang, L. Wang, W. Wu, W. Lv, J. Zhu, *J. Electrochem. Soc.* **2017**, *164*, A3933; g) Z. Pan, F. Cao, X. Hu, X. Ji, *J. Mater. Chem. A* **2019**, *7*, 8984.



- [209] S. Fleischmann, J. B. Mitchell, R. Wang, C. Zhan, D.-e. Jiang, V. Presser, V. Augustyn, *Chem. Rev.* **2020**, *120*, 6738.
- [210] L. Sun, Q. Fu, C. Pan, *J. Hazard. Mater.* **2021**, *410*, 124565.
- [211] Z. Liu, L. Wang, Y. Xu, J. Guo, S. Zhang, Y. Lu, *J. Electroanal. Chem.* **2021**, *881*, 114958.
- [212] R. Liu, A. Zhang, J. Tang, J. Tian, W. Huang, J. Cai, C. Barrow, W. Yang, J. Liu, *Eur. J. Chem.* **2019**, *25*, 5547.
- [213] W. Liang, I. Zhitomirsky, *J. Mater. Chem. A* **2021**, *9*, 10335.
- [214] Q. Jiang, N. Kurra, M. Alhabeab, Y. Gogotsi, H. N. Alshareef, *Adv. Energy Mater.* **2018**, *8*, 1703043.
- [215] a) J. Miao, Q. Zhu, K. Li, P. Zhang, Q. Zhao, B. Xu, *J. Energy Chem* **2021**, *52*, 243; b) L. Wang, C. Lin, F. Zhang, J. Jin, *ACS Nano* **2014**, *8*, 3724; c) Y. Sun, D. Xu, S. Li, L. Cui, Y. Zhuang, W. Xing, W. Jing, *J. Membr. Sci.* **2021**, *623*, 119075; d) P. Zhang, Q. Zhu, R. A. Soomro, S. He, N. Sun, N. Qiao, B. Xu, *Adv. Funct. Mater.* **2020**, *30*, 2000922; e) M. Zhang, J. Zhou, J. Yu, L. Shi, M. Ji, H. Liu, D. Li, C. Zhu, J. Xu, *Chem. Eng. J.* **2020**, *387*, 123170; f) Z. Zhang, M. Guo, Y. Tang, C. Liu, J. Zhou, J. Yuan, J. Gu, *Nanotechnology* **2020**, *31*, 165403; g) L. Yang, F. Lin, F. Zabihi, S. Yang, M. Zhu, *Int. J. Biol. Macromol.* **2021**, *181*, 1063; h) W. Zhang, J. Ma, W. Zhang, P. Zhang, W. He, J. Chen, Z. Sun, *Nanoscale* **2020**, *12*, 6637; i) J. Zhang, S. Seyedin, S. Qin, Z. Wang, S. Moradi, F. Yang, P. A. Lynch, W. Yang, J. Liu, X. Wang, *Small* **2019**, *15*, 1804732; j) M. Zhang, F. Héraly, M. Yi, J. Yuan, *Cell Rep. Phys. Sci.* **2021**, *2*, 100449; k) J. Yan, Y. Ma, C. Zhang, X. Li, W. Liu, X. Yao, S. Yao, S. Luo, *RSC Adv.* **2018**, *8*, 39742; l) X. Li, H. Li, X. Fan, X. Shi, J. Liang, *Adv. Energy Mater.* **2020**, *10*, 1903794; m) H. Zhou, Y. Lu, F. Wu, L. Fang, H. Luo, Y. Zhang, M. Zhou, *J. Alloys Compd.* **2019**, *802*, 259; n) M. Mahmood, A. Rasheed, I. Ayman, T. Rasheed, S. Munir, S. Ajmal, P. O. Agboola, M. F. Warsi, M. Shahid, *Energy Fuels* **2021**, *35*, 3469; o) L. Wang, D. Shao, J. Guo, S. Zhang, Y. Lu, *Energy Technol.* **2020**, *8*, 1901003; p) C. Ma, W.-T. Cao, W. Xin, J. Bian, M.-G. Ma, *Ind. Eng. Chem. Res.* **2019**, *58*, 12018.
- [216] a) P. Jankowski, W. Wiecezorek, P. Johansson, *J. Mol. Modeling* **2017**, *23*, 6; b) A. Moretti, V. Sharova, D. V. Carvalho, A. Boulineau, W. Porcher, I. de Meazza, S. Passerini, *Batteries Supercaps* **2019**, *2*, 240.
- [217] Z. Zhu, S. Tang, J. Yuan, X. Qin, Y. Deng, R. Qu, G. M. Haarberg, *Int. J. Electrochem. Sci.* **2016**, *11*, 8270.
- [218] T. Cetinkaya, R. A. Dryfe, *J. Power Sources* **2018**, *408*, 91.
- [219] B. Song, F. Wu, Y. Zhu, Z. Hou, K.-s. Moon, C.-P. Wong, *Electrochim. Acta* **2018**, *267*, 213.
- [220] a) A. Daraghme, S. Hussain, L. Servera, E. Xuriguera, A. Cornet, A. Cirera, *Electrochim. Acta* **2017**, *245*, 531; b) M. Aslan, D. Weingarh, N. Jäckel, J. Atchison, I. Grobelsek, V. Presser, *J. Power Sources* **2014**, *266*, 374.
- [221] M. S. Javed, S. S. A. Shah, T. Najam, S. H. Siyal, S. Hussain, M. Saleem, Z. Zhao, W. Mai, *Nano Energy* **2020**, *77*, 105276.
- [222] S. Rajeevan, S. John, S. C. George, *J. Energy Storage* **2021**, *39*, 102654.
- [223] Q. Abbas, D. Pajak, E. Frackowiak, F. Béguin, *Electrochim. Acta* **2014**, *140*, 132.
- [224] a) J. Dong, Z. Wang, X. Kang, *Colloids Surf., A* **2016**, *489*, 282; b) S. Rajeevan, S. John, S. C. George, *J. Power Sources* **2021**, *504*, 230037.
- [225] M. Arunkumar, A. Paul, *ACS Omega* **2017**, *2*, 8039.
- [226] Z. Bai, H. Li, M. Li, C. Li, X. Wang, C. Qu, B. Yang, *Int. J. Hydrogen Energy* **2015**, *40*, 16306.
- [227] S. Sopčić, M. Kraljić Roković, Z. Mandić, *J. Electrochem. Sci. Eng.* **2012**, *2*, 41.
- [228] B. Xu, H. Wang, Q. Zhu, N. Sun, B. Anasori, L. Hu, F. Wang, Y. Guan, Y. Gogotsi, *Energy Storage Mater.* **2018**, *12*, 128.
- [229] M. Aslan, D. Weingarh, P. Herbeck-Engel, I. Grobelsek, V. Presser, *J. Power Sources* **2015**, *279*, 323.
- [230] B. Dyatkin, V. Presser, M. Heon, M. R. Lukatskaya, M. Beidaghi, Y. Gogotsi, *ChemSusChem* **2013**, *6*, 2269.
- [231] D. Kasprzak, I. Stępnik, M. Galiński, *J. Solid State Electrochem.* **2018**, *22*, 3035.
- [232] Q. F. Guan, Z. C. Ling, Z. M. Han, T. T. Luo, H. B. Yang, K. P. Yang, C. H. Yin, S. H. Yu, *Adv. Funct. Mater.* **2021**, *31*, 2105070.
- [233] a) S. Xu, G. Wei, J. Li, Y. Ji, N. Klyui, V. Izotov, W. Han, *Chem. Eng. J.* **2017**, *317*, 1026; b) H. Li, X. Chen, E. Zalnezhad, K. Hui, K. Hui, M. J. Ko, *J. Ind. Eng. Chem.* **2020**, *82*, 309; c) H. Hu, Z. Bai, B. Niu, M. Wu, T. Hua, *J. Mater. Chem. A* **2018**, *6*, 14876; d) S. Cho, D. Y. Kim, Y. Seo, *Adv. Mater.* **2020**, *7*, 2000750.
- [234] X. Zhao, K. Tao, L. Han, *Nanoscale* **2022**, *14*, 2155.
- [235] A. Tolosa, B. Krüner, N. Jäckel, M. Aslan, C. Vakifahmetoglu, V. Presser, *J. Power Sources* **2016**, *313*, 178.
- [236] B. Joshi, E. Samuel, Y.-i. Kim, A. L. Yarin, M. T. Swihart, S. S. Yoon, *Coord. Chem. Rev.* **2022**, *460*, 214466.
- [237] I. I. Salame, T. J. Bandoz, *J. Colloid Interface Sci.* **2001**, *240*, 252.
- [238] E. Frackowiak, *Phys. Chem. Chem. Phys.* **2007**, *9*, 1774.
- [239] a) C. Lamiel, I. Hussain, X. Ma, K. Zhang, *Mater. Today Chem.* **2022**, *26*, 101152; b) O. Petrii, I. Khomchenko, *J. Electroanal. Chem. Interfacial Electrochem.* **1980**, *106*, 277.
- [240] E. Krämer, T. Schedlbauer, B. Hoffmann, L. Terborg, S. Nowak, H. J. Gores, S. Passerini, M. Winter, *J. Electrochem. Soc.* **2012**, *160*, A356.
- [241] E. Wiberg, *Lehrbuch der anorganischen Chemie*, Walter de Gruyter, Berlin **2019**.
- [242] a) C. Bizot, M.-A. Blin, P. Guichard, J. Hamon, V. Fernandez, P. Soudan, J. Gaubicher, P. Poizat, *Electrochem. Commun.* **2021**, *126*, 107013; b) X. Wang, E. Yasukawa, S. Mori, *Electrochim. Acta* **2000**, *45*, 2677; c) K. Kanamura, T. Okagawa, Z.-i. Takehara, *J. Power Sources* **1995**, *57*, 119.
- [243] a) T. Nakajima, M. Mori, V. Gupta, Y. Ohzawa, H. Iwata, *Solid State Sci.* **2002**, *4*, 1385; b) M. Morita, T. Shibata, N. Yoshimoto, M. Ishikawa, *Electrochim. Acta* **2002**, *47*, 2787; c) H. Wu, Z. Song, X. Wang, W. Feng, Z. Zhou, H. Zhang, *Nano Res.* **2022**, *1*, <https://doi.org/10.1007/s12274-022-4669-8>.
- [244] A. Heckmann, M. Krott, B. Streipert, S. Uhlenbruck, M. Winter, T. Placke, *ChemPhysChem* **2017**, *18*, 156.
- [245] a) J. Krummacker, L. H. Heß, A. Balducci, *ChemSusChem* **2017**, *10*, 4178; b) J. Krummacker, A. Balducci, *Chem. Mater.* **2018**, *30*, 4857.
- [246] B. C. Sekhar, R. Hachicha, M. Maffre, C. Bodin, S. Le Vot, F. Favier, O. Fontaine, *J. Electrochem. Soc.* **2020**, *167*, 110508.
- [247] P. Meister, X. Qi, R. Kloepsch, E. Krämer, B. Streipert, M. Winter, T. Placke, *ChemSusChem* **2017**, *10*, 804.
- [248] E. Krämer, S. Passerini, M. Winter, *ECS Electrochem. Lett.* **2012**, *1*, C9.
- [249] D. G. Gromadskyi, Y. F. Fateev, Y. A. Maletin, *Corros. Sci.* **2013**, *69*, 191.
- [250] C. Krause, P. Röring, S. Röser, D. Diddens, J. Thienenkamp, I. Cekic-Laskovic, G. Brunklaus, M. Winter, *J. Chem. Phys.* **2020**, *152*, 174701.
- [251] R.-S. Kühnel, A. Balducci, *J. Power Sources* **2014**, *249*, 163.
- [252] a) L. H. Hess, L. Wittscher, A. Balducci, *Phys. Chem. Chem. Phys.* **2019**, *21*, 9089; b) J. Krummacker, C. Schütter, S. Passerini, A. Balducci, *ChemElectroChem* **2017**, *4*, 353.
- [253] S.-I. Pyun, S.-M. Moon, S.-H. Ahn, S.-S. Kim, *Corros. Sci.* **1999**, *41*, 653.
- [254] a) A. Gabryelczyk, S. Ivanov, A. Bund, G. Lota, *J. Energy Storage* **2021**, *43*, 103226; b) S.-T. Myung, Y. Hitoshi, Y.-K. Sun, *J. Mater. Chem.* **2011**, *21*, 9891.
- [255] L. Qiao, U. Oteo, M. Martinez-Ibañez, A. Santiago, R. Cid, E. Sanchez-Diez, E. Lobato, L. Meabe, M. Armand, H. Zhang, *Nat. Mater.* **2022**, *21*, 455.
- [256] a) B. Garcia, M. Armand, *J. Power Sources* **2004**, *132*, 206; b) R.-S. Kühnel, M. Lübke, M. Winter, S. Passerini, A. Balducci, *J. Power Sources* **2012**, *214*, 178; c) J. Krummacker, L. Hess, A. Balducci, *J. Electrochem. Soc.* **2019**, *166*, A1763; d) R.-S. Kühnel, J. Reiter, S. Jeong, S. Passerini, A. Balducci, *Electrochem. Commun.* **2014**, *38*, 117; e) S. Menne, R.-S. Kühnel, A. Balducci, *Electrochim. Acta* **2013**,

- 90, 641; f) T. Vogl, S. Menne, A. Balducci, *Phys. Chem. Chem. Phys.* **2014**, *16*, 25014.
- [257] a) T. Brousse, P.-L. Taberna, O. Crosnier, R. Dugas, P. Guillemet, Y. Scudeller, Y. Zhou, F. Favier, D. Bélanger, P. Simon, *J. Power Sources* **2007**, *173*, 633; b) D. Bélanger, T. Brousse, J. Long, *J. Electrochem. Soc.* **2008**, *17*, 49.
- [258] D. Landolt, *EPFL PRESS* **1993**, 260.
- [259] A. Abdisattar, M. Yeleuov, C. Daulbayev, K. Askaruly, A. Tolynbekov, A. Taurbekov, N. Prikhodko, *Electrochem. Commun.* **2022**, *142*, 107373.
- [260] a) J. Wojciechowski, Ł. Kolanowski, A. Bund, G. Lota, *J. Power Sources* **2017**, *368*, 18; b) H. Trivedi, K. D. Verma, P. Sinha, K. K. Kar, in *Handbook of Nanocomposite Supercapacitor Materials III* (Eds: Kamal K. Kar), Vol. 313, pp. 271–311, Springer, Berlin **2021**.
- [261] D. Momodu, M. Madito, F. Barzegar, A. Bello, A. Khaleed, O. Olaniyan, J. Dangbegnon, N. Manyala, *J. Solid State Electrochem.* **2017**, *21*, 859.
- [262] Q. Abbas, P. Ratajczak, P. Babuchowska, A. Le Comte, D. Bélanger, T. Brousse, F. Béguin, *J. Electrochem. Soc.* **2015**, *162*, A5148.
- [263] X. Yao, N. Huang, F. Han, Q. Zhang, H. Wan, J. P. Mwirerwa, C. Wang, X. Xu, *Adv. Energy Mater.* **2017**, *7*, 1602923.
- [264] G. P. Pandey, T. Liu, C. Hancock, Y. Li, X. S. Sun, J. Li, *J. Power Sources* **2016**, *328*, 510.
- [265] M. P. Chavhan, S. Ganguly, *Ionics* **2017**, *23*, 2037.
- [266] P. Galek, E. Frackowiak, K. Fic, *Electrochim. Acta* **2020**, *334*, 135572.
- [267] V. L. Martins, A. J. R. Rennie, N. Sanchez-Ramirez, R. M. Torresi, P. J. Hall, *ChemElectroChem* **2018**, *5*, 598.
- [268] X. Ma, X. Song, Z. Yu, S. Li, X. Wang, L. Zhao, L. Zhao, Z. Xiao, C. Qi, G. Ning, *Carbon* **2019**, *149*, 646.
- [269] J. Chmiola, G. Yushin, Y. Gogotsi, C. Portet, P. Simon, P.-L. Taberna, *Science* **2006**, *313*, 1760.
- [270] D. Gueon, J. H. Moon, *ACS Sustainable Chem. Eng.* **2017**, *5*, 2445.
- [271] M. Skunik-Nuckowska, S. Dyjak, K. Grzeszczuk, N. H. Wisnińska, F. Béguin, P. J. Kulesza, *Electrochim. Acta* **2018**, *282*, 533.
- [272] S.-L. Chou, J.-Z. Wang, S.-Y. Chew, H.-K. Liu, S.-X. Dou, *Electrochem. Commun.* **2008**, *10*, 1724.
- [273] Y. Wang, Z. Shi, Y. Huang, Y. Ma, C. Wang, M. Chen, Y. Chen, *J. Phys. Chem. C* **2009**, *113*, 13103.
- [274] Y. Gao, Y. S. Zhou, M. Qian, X. N. He, J. Redepenning, P. Goodman, H. M. Li, L. Jiang, Y. F. Lu, *Carbon* **2013**, *51*, 52.
- [275] B. Zhang, D. Wang, B. Yu, F. Zhou, W. Liu, *RSC Adv.* **2014**, *4*, 2586.
- [276] C. Zhang, H. Du, K. Ma, Z. Yuan, *Adv. Energy Mater.* **2020**, *10*, 2002132.
- [277] T. Li, X. Wang, P. Liu, B. Yang, S. Diao, Y. Gao, *J. Electroanal. Chem.* **2020**, *860*, 113908.
- [278] E. Pamaté, B. Gorska, P. Ratajczak, F. Béguin, *J. Mater. Chem. A* **2020**, *8*, 13548.
- [279] C. Ma, L. Wu, M. Dirican, H. Cheng, J. Li, Y. Song, J. Shi, X. Zhang, *Appl. Surf. Sci.* **2021**, *537*, 147914.
- [280] Y. Cao, X. Wang, Z. Gu, Q. Fan, W. Gibbons, V. Gadhamshetty, N. Ai, G. Zeng, *J. Power Sources* **2018**, *384*, 360.
- [281] J. Pokrzywinski, J. K. Keum, R. E. Ruther, E. C. Self, M. Chi, H. Meyer III, K. C. Littrell, D. Aulakh, S. Marble, J. Ding, *J. Mater. Chem. A* **2017**, *5*, 13511.
- [282] V. Quispe-Garrido, G. A. Cerron-Calle, A. Bazan-Aguilar, J. G. Ruiz-Montoya, E. O. López, A. M. Baena-Moncada, *Open Chem.* **2021**, *19*, 709.
- [283] Y. Wang, J. Guo, T. Wang, J. Shao, D. Wang, Y.-W. Yang, *Nanomaterials* **2015**, *5*, 1667.
- [284] L. Liu, J. Wang, C. Wang, G. Wang, *Appl. Surf. Sci.* **2016**, *390*, 303.
- [285] Y. Ma, X. Xie, W. Yang, Z. Yu, X. Sun, Y. Zhang, X. Yang, H. Kimura, C. Hou, Z. Guo, *Adv. Compos. Hybrid Mater.* **2021**, *4*, 906.
- [286] S. A. Kadam, Y.-R. Ma, Y.-R. Chen, Y. H. Navale, A. S. Salunkhe, V. B. Patil, S. D. Ralegankar, P. D. More, *Denki Zairyo Gijutsu Zasshi* **2023**, *52*, 500.
- [287] D. Majumdar, S. Ghosh, *J. Energy Storage* **2021**, *34*, 101995.
- [288] C. An, Y. Zhang, H. Guo, Y. Wang, *Nanoscale Adv.* **2019**, *1*, 4644.
- [289] P. Anandhi, V. J. Senthil Kumar, S. Harikrishnan, *Funct. Mater. Lett.* **2019**, *12*, 1950064.
- [290] S. Ouendi, K. Robert, D. Stievenard, T. Brousse, P. Roussel, C. Lethien, *Energy Storage Mater.* **2019**, *20*, 243.
- [291] X. Lu, T. Liu, T. Zhai, G. Wang, M. Yu, S. Xie, Y. Ling, C. Liang, Y. Tong, Y. Li, *Adv. Energy Mater.* **2014**, *4*, 1300994.
- [292] A. Salman, S. P. Sasikala, I. H. Kim, J. T. Kim, G. San Lee, J. G. Kim, S. O. Kim, *Nanoscale* **2020**, *12*, 20239.
- [293] C. Zhu, P. Yang, D. Chao, X. Wang, X. Zhang, S. Chen, B. K. Tay, H. Huang, H. Zhang, W. Mai, *Adv. Mater.* **2015**, *27*, 4566.
- [294] B. Wei, G. Mei, H. Liang, Z. Qi, D. Zhang, H. Shen, Z. Wang, *J. Power Sources* **2018**, *385*, 39.



**Emmanuel Pameté** has been a Humboldt fellow at the INM – Leibniz Institute for New Materials in Saarbrücken (Germany) since February 2023. Previously, he was a postdoc research scientist at the same institution after completing his Ph.D. in the Power Sources Group of Poznan University of Technology (Poland) in 2021. His current research activities include developing advanced energy materials and ecofriendly electrolytes for next-generation energy storage devices toward high energy, stable cyclability, and sustainability. His main topics of interest include supercapacitors, hybrid capacitors, and post-Li-ions batteries.



**Lukas Köps** is currently a Ph.D. student in the group of Prof. Andrea Balducci at the Institute for Technical Chemistry and Environmental Chemistry and the Center for Energy and Environmental Chemistry Jena (CEEC Jena) of the Friedrich-Schiller University Jena, Germany. He is working on the development of alternative electrolytes with reduced aging for electric double-layer capacitors, focusing in particular on aging at high voltages and high temperatures and automated data evaluation of electrochemical measurements.



**Fabian Alexander Kreth** is a member of the research group of Prof. Dr. Andrea Balducci at the Institute for Technical and Environmental Chemistry and at the Center for Energy and Environmental Chemistry of the Friedrich-Schiller University in Jena, Germany. His Ph.D. research focuses on the development of innovative electrolytes for supercapacitors and the development of advanced operando characterization techniques for the investigation of charge storage and aging mechanisms in electrochemical energy storage devices.



**Sebastian Pohlmann** works as vice president of Business Development at Skeleton Technologies. He received a Diploma in chemistry in 2012 and a Ph.D. in physical chemistry from the University of Münster in 2014. In early 2016, he started working for the Skeleton Technologies GmbH, leading its Cell Development team between 2018 and 2020. From 2020 he enabled Skeleton to win research and innovation grants worth over 60 MEUR in his position of VP of Innovation. Today he leads Skeleton's business development for its next generation Supercapacitors and its Superbattery technology.



**Alberto Varzi** studied chemistry of materials at University of Bologna (Italy) and received a Ph.D. in 2013 from Ulm University and the Center for Solar Energy and Hydrogen Research Baden-Württemberg (Germany). After a postdoctoral period at MEET battery research center – University of Münster, in 2014, he joined the Helmholtz Institute Ulm (HIU) of the Karlsruhe Institute for Technology (KIT). Since 2021, he is principal investigator and leads the group “Electrochemistry of Materials and Interfaces.” His current research interests span from solid state to aqueous batteries (including beyond-Li systems) as well as conventional and hybrid capacitors.



**Thierry Brousse** is a distinguished professor of materials chemistry at Polytech Nantes (Nantes Université, France) and a researcher at Institut des Matériaux de Nantes Jean Rouxel (IMN). He received his Ph.D. in 1991 from ISMRa Caen. He started working on oxide-based electrodes for supercapacitors in 2001-2002 at Prof. Bélanger’s lab (UQAM, Canada), and since then he triggered different research topics on innovative electrodes and designs for high-power energy storage devices. He organized the first ISEECap meeting in 2009 (International Symposium on Enhanced Electrochemical Capacitors) which is now taking place every two years in Europe.



**Andrea Balducci** is professor for applied electrochemistry at the Institute for Technical Chemistry and Environmental Chemistry and at the Center for Energy and Environmental Chemistry Jena (CEEC Jena) of the Friedrich-Schiller University Jena, Germany. He is working on the development and characterization of novel electrolytes and active/inactive materials suitable for the realization of safe and high-performance electrical capacitors and batteries.



**Volker Presser** is professor of energy materials at Saarland University, Program Division Leader at the INM – Leibniz Institute for New Materials, and managing co-director of the Saarland Center for Energy Materials and Sustainability (Saarene) in Saarbrücken (Germany). He obtained his Ph.D. from the Eberhard-Karls-University Tübingen (Germany) in 2009 and worked as a Humboldt fellow and research assistant professor in the team of Yury Gogotsi at Drexel University (2010-2012). His research focuses on next-generation materials (incl. MXene and hybrid materials) for energy storage and water remediation (esp. Lithium recovery and seawater desalination).